Structure and reactions of quantum halos

A. S. Jensen, K. Riisager, and D. V. Fedorov

Department of Physics and Astronomy, Aarhus University, DK-8000 Aarhus C, Denmark

E. Garrido

Instituto de Estructura de la Materia, CSIC, Serrano 123, E-28006 Madrid, Spain

(Published 5 February 2004)

This article provides an overview of the basic principles of the physics of quantum halo systems, defined as bound states of clusters of particles with a radius extending well into classically forbidden regions. Exploiting the consequences of this definition, the authors derive the conditions for occurrence in terms of the number of clusters, binding energy, angular momentum, cluster charges, and excitation energy. All these quantities must be small. The article discusses the transitions between different cluster divisions and the importance of thresholds for cluster or particle decay, with particular attention to the Efimov effect and the related exotic states. The pertinent properties can be described by the use of dimensionless variables. Then universal and specific properties can be distinguished, as shown in a series of examples selected from nuclear, atomic, and molecular systems. The neutron dripline is especially interesting for nuclei and negative ions for atoms. For molecules, in which the cluster division comes naturally, a wider range of possibilities exists. Halos in two dimensions have very different properties, and their states are easily spatially extended, whereas Borromean systems are unlikely and spatially confined. The Efimov effect and the Thomas collapse occur only for dimensions between 2.3 and 3.8 and thus not for 2. High-energy reactions directly probe the halo structure. The authors discuss the reaction mechanisms for high-energy nuclear few-body halo breakup on light, intermediate, and heavy nuclear targets. For light targets, the strong interaction dominates, while for heavy targets, the Coulomb interaction dominates. For intermediate targets these processes are of comparable magnitude. As in atomic and molecular physics, a geometric impact-parameter picture is very appropriate. Finally, the authors briefly consider the complementary processes involving electroweak probes available through beta decay, electromagnetic transitions, and capture reactions.

CONTENTS

I. INTRODUCTION

Many scientific disciplines speak of halos: meteorology, astrophysics, and accelerator physics, to name a few. In very general terms a halo is a diluted or less intense component surrounding a stronger or more massive central object. Quite a few quantum systems could fit this general description, but the way the term has been ap-

plied for the last 15 years on the quantum level has been more restrictive, namely, to denote systems in which a wave-function component has an unusually large spatial extension. If this were used as the sole criterion, many systems with widely differing properties could be counted as halos, e.g., Rydberg states in atoms, and the term would lose its scientific usefulness. The tradition has been to restrict the name to a more exclusive set of structures. We shall in Sec. II consider a more precise definition of the quantum halo; it suffices here to note that tunneling into a classically forbidden region should be a pronounced feature.

The interest in halo systems started with the study of light atomic nuclei, but the concept has now been extended to atomic and molecular physics. Several reviews of specific aspects of halos are available, but there has been no attempt to cover the basic principles of the physics of halo systems. Our aim is to provide such an overview and give a variety of examples of experimentally investigated and theoretically predicted halos. There is already a sizable literature in nuclear physics and one can expect the interest in halo systems to remain high with the help of the next generation of large-scale facilities for unstable nuclear beams and the contributions of other branches of physics. In this introductory section we shall recount briefly the history of the subject and some of the reasons for the interest in halo physics, offer perspectives, and present the goals of this review.

A. How the halo concept developed

The halo concept is quite simple and has appeared many times in the literature. An old example is the deuteron, in which the neutron and proton are more likely than not to be found outside the range of their interaction in the classically forbidden region. The energy needed for breakup into two nucleons is relatively small compared to nucleon separation energies. A necessary condition for halo formation is that the binding energy between clusters be small. In an overview paper Baz' *et al.* (1960) considered bound states close to such thresholds. They noted that the relative cluster motion can be described by a spatially extended Yukawa wave function and that this is most pronounced for *s*-wave neutrons due to the absence of centrifugal and Coulomb barriers. They also suggested that such systems of large radii should be easily detectable due to their high breakup probability. Soon after the work on nucleon halos, direct radiative proton capture was found to occur preferentially at distances several times the nuclear radius (Christy and Duck, 1961; Thomas and Tanner, 1963). The "leaking out" of the proton could thus be measured and the tail of the Coulomb wave function explicitly expressed as a function of the binding energy, e.g., in proton collisions with ^{7}Be (Riisager *et al.*, 1992). The first excited state in ^{17}F was by then already identified as an exceptional case and its proton halo nature was soon established (Rolfs, 1973). These examples emphasize the spatial structure of the wave function. Gamma decay offers a complementary way of probing the large extension of the wave function, as, for instance, in the case of the E1 transition in ^{11}Be (Millener *et al.*, 1983).

The cluster idea has often been used to describe light nuclei. For example, ^{6}He or ^{6}Li, may be treated as an alpha particle bound to a dineutron or a deuteron (Bayman *et al.*, 1985). This model explains the variation in the radius by the difference in the two-body binding energies as for these two nuclei; see also the early comment (Ellis and Tang, 1986) on the surprisingly large radius of ^{11}Li measured by Tanihata *et al.* (1985a, 1985b). The binding energy was also the main ingredient in the interpretation of the ^{11}Li structure in terms of a "dineutron" weakly bound to the ^{9}Li core (Hansen and Jonson, 1987).

The Faddeev equations (Faddeev, 1961), which provide the correct description of the large-distance asymptotic wave function of three interacting particles, were used by Efimov (1970) to show that three-body states of large spatial extension (Efimov states) exist when the unbound two-body subsystems are close to the binding threshold. At present, the best candidate for an Efimov state is that predicted in the atomic helium trimer by Cornelius and Glöckle (1986), but it still awaits an experimental confirmation. In a related development, Migdal (1972) has proved that a potential containing two interacting unbound particles allows many bound states if the particles are sufficiently close to the threshold. When this principle is applied to two neutrons loosely bound to a nucleus, the resulting states can be interpreted as dineutrons at the nuclear surface.

Extended states have also been discussed in atomic and molecular physics, where the interactions are rather well known and various power-law potentials arise at large distances. One class of weakly bound states is that of multipole-bound molecular negative ions. For instance, the potential associated with a charged particle in the field of a permanent electric dipole has a $1/r^2$ behavior. Mathematically such a potential produces infinitely many deeply bound states (see Landau and Lifshitz, 1958). Under physical conditions, the size of the dipole moment must exceed a critical lower limit to bind the charged particle (Fermi and Teller, 1947). Such bound states, although not necessarily classically forbidden, are spatially very extended.

B. How halos came into focus

On average nuclear radii increase as the 1/3 power of the nucleon number A. This behavior expresses the approximate incompressibility of nuclear matter and the saturation property of the nuclear interaction. It was therefore surprising that the measured interaction cross sections of Li isotopes colliding with ordinary nuclear targets displayed a very large increase for ^{11}Li (Tanihata *et al.*, 1985a, 1985b).

This discovery was soon followed by an interpretation of the structure of this nucleus in terms of a "neutron halo," a "dineutron" weakly bound in an *s* state to the

^{9}Li core (Hansen and Jonson, 1987). The large radius was explained by the weak binding of 295 ± 35 keV between ^{9}Li and the two neutrons (Young *et al.*, 1993). The effect is larger for ^{11}Li than for the deuteron due to the larger deuteron binding energy of 2.2 MeV. The nonstandard use of an unbound dineutron as a building block in this model is the only option leading to a two-body problem.

Soon after a narrow ^{9}Li momentum distribution was measured after breakup of ^{11}Li on a light target (Kobayashi *et al.*, 1988). The width, about an order of magnitude smaller than the Fermi momentum of 300 MeV/c found for ordinary fragmentation reactions, is consistent with the dineutron model, in which the large radius, through the uncertainty principle, is reflected in a narrow relative momentum distribution.

The same model implies that the two-neutron removal cross section is large because the nucleus can be easily broken by a distant, relatively small Coulomb push on the charged ^{9}Li core. Such a Coulomb dissociation may be viewed as an excitation to a dineutron-^{9}Li continuum state, followed by a decay into two components. This predicted cross-section enhancement was soon verified experimentally (Kobayashi *et al.*, 1989).

Traditional nuclear physics models fail to explain these observations. In fact, ^{11}Li turns out to be even more complicated than is suggested by the dineutron model. The three particles, two neutrons and ^{9}Li, form a Borromean system (Zhukov *et al.*, 1993), i.e., a bound three-body system in which each pair of particles, two neutrons and neutron ^{9}Li, is unbound. An extension of this description to the more appropriate three-body system with two neutrons and ^{9}Li (Johannsen *et al.*, 1990) accurately explains the bulk of the data involving this nucleus.

After the discovery of the new structure of ^{11}Li, the simpler two-body nuclear structures of both ground and excited states of ^{11}Be came into focus. Here also the neutron separation energy is small, the size is large, the momentum distributions after breakup are narrow, and the interaction and Coulomb dissociation cross sections are large. A number of other nuclei, in which the one- or two-neutron separation energies are small, are expected to exhibit similar halo features. Examples could be two-body (^{19}C), three-body (^{6}He,^{14}Be), and many-body (^{8}He) neutron halos. As heavy systems with small neutron separation energies are so far unexplored, more discoveries can be expected.

In atomic and molecular physics, experimental investigations of multipole-bound charged particles were initiated by Lykke *et al.* (1984). By now the stability of several systems has been established and the minimum dipole moment that ensures binding is rather accurately determined (Abdoul-Carime *et al.*, 2002). Another class of systems arises without any permanent multipoles of the particles. However, the accuracy needed for spatially extended systems is extremely high because the corresponding binding energy is extremely low. The prototype here is the atomic helium dimer ^{4}He$_2$, whose very existence was for a long time disputed due to its extremely small binding energy, now believed to be around 10^{-7} eV (Grisenti *et al.*, 2000). Only about ten years ago was experimental evidence provided for stability and a size of about $\langle r \rangle \approx 52$ Å (Schöllkopf and Toennies, 1994). These experiments are extremely difficult, and the stability of the predicted first (and only) excited Efimov state of the atomic helium trimer, ^{4}He$_3$, is not yet conclusively demonstrated.

An effect called quantum proximity resonances was discussed in theoretical work by Heller (1996). Peculiar scattering states may appear in scattering of a particle on two (or more) identical potentials separated by much less than one wavelength, provided the scattering length is much larger than the range of the potential. Then a broad *s*-wave resonance in one potential produces an extremely narrow *p*-wave proximity resonance for scattering on two potentials. Examples of analogous wave mechanical effects are sound waves incident on air bubbles in water, and resonant light scattering on identical molecular dipoles. Efimov states, the Thomas effect, and proximity resonances fall into a larger class of problems in which the "quantum size" is much larger than both potential range and distance between particles (Heller, 1996).

C. Perspectives

The most extended halo system experimentally known today is the atomic helium dimer (^{4}He$_2$), which is about 10 times larger than typical diatomic molecules. Both ^{4}He-^{3}He and ^{3}He$_2$ are unbound, but when sufficiently many atoms are added, even ^{3}He$_x$ becomes bound. Similar transitions occur for other more complicated molecular systems possibly with extreme properties but much less understood. Negative ions may also reveal some features related to halo physics like small binding energy, but possibly without the dominant nonclassical aspect. A small but growing number of multipole-bound negative ions exhibit universal scaling properties characteristic of halos. None of these systems is well studied.

An open question is the occurrence of the three-body giant halos called Efimov states. These states could play a role within many-body systems as generalized Efimov states, as static correlated substructures, or as mediators of dynamic processes. One example is the stability of Bose-Einstein condensates governed by decay into bound dimer or trimer structures. In the same vein, catalytic processes within media may involve three-body recombination processes in which one of the particles remains unchanged. Schematic examples are some of the following steps: $a+b+c \rightarrow (ab)* + c \rightarrow (abc)* + \gamma \rightarrow a + (bc)$, where the $*$ indicates excitation. When some of these states are spatially extended, the rates should be enhanced as in the case of radiative proton capture of ^{16}O. The involvement of three particles may increase the rates by as much as 10^{6} as in the course of antihydrogen production via the reaction of positronium with antiprotons rather than the capture of a positron.

In nuclear physics a comprehensive description of nuclei with small neutron separation energies requires a

full understanding of the structural evolution with respect to an increasing number of neutrons. Indeed, the structures are expected to range from the well-known ordinary stable nuclei, to those with excess neutrons at the surface, to neutron halo systems, to possibly quantum-stabilized systems developing beyond the neutron dripline where the neutron separation is zero, and eventually to neutron matter as encountered in neutron stars. Halos may also appear in ordinary nuclei as excited states.

Experimentally, the halo region of nuclei at small neutron separation energy has so far only been explored for the lightest nuclei. Theorists are working to incorporate continuum structures allowing more reliable predictions. Still, we are not yet assured that the relevant degrees of freedom have been identified for systems at the edge of stability. Many types of structures exist in nuclei, partly due to the strong interaction, partly due to the unique two-fermion structure of this mesoscopic system.

D. The goals of this review

This review aims at presenting the essential features that define a quantum halo system and at describing its properties in universal terms suitable for application in all subfields of physics. This assumes that our understanding has reached a level at which an overall picture can be painted that explains all the specific examples. It is fair to say that our subject has not yet fully developed beyond the stage of a phenomenological description. Still we believe that it is already possible to extract some universal features. Our representation will focus on qualitative features and physics content rather than on mathematical formulations and questions of experimental accuracy. In some parts of the exposition we make use of earlier overviews of parts of the field and in particular on the few available general reviews (Bertulani *et al.*, 1993; Riisager, 1994; Hansen *et al.*, 1995; Tanihata, 1996; Jonson and Riisager, 1998; Jensen and Zhukov, 2001).

The description of halos inevitably requires a separation of the (few) active degrees of freedom from the many which are essentially inactive. Then few-body techniques can be used to provide the main contributions to most observables. This is the starting point in our description. Of course, the precision which can be expected from a few-body description depends on the observable. Further improvement requires an understanding of the contributions from the neglected degrees of freedom. The selected examples provide testing grounds for both precision and contributing degrees of freedom. It is important to stress that many issues are not yet resolved, especially the contributions from the inactive degrees of freedom, few-body continuum structure, and reaction mechanisms (Glöckle *et al.*, 1996).

This review is divided into seven sections. In Sec. II we discuss the general structure of quantum halos, including conditions for their existence, characteristic properties, and quantities that establish whether a state is a quantum halo or not. In Sec. III we turn toward specific examples of halo systems. In Sec. IV we survey the properties of halos in two dimensions. These differ both qualitatively and quantitatively from those of three dimensions. High-energy breakup reactions, providing most of the information about halos, are discussed in Sec. V, where we focus mainly on three-body nuclear halos. We shall not discuss low-energy reactions, which are more sensitive to dynamical properties and are currently less exploited as probes of halo features. In Sec. VI we survey studies of halos using the electromagnetic and weak interactions, typically decay experiments. Finally, Sec. VII contains a summary and the conclusions.

II. ANATOMY OF QUANTUM HALOS

To describe halos merely as spatially extended objects is not very useful in a scientific context. A precise definition of the scale of the extension has to be made first. For this, the relevant degrees of freedom must be specified and halo characteristics formulated. Then quantitative analysis of spatial extension in connection with the binding energy and other quantum numbers of the states can be made. As we shall see, testing whether a state qualifies as a halo relies on the knowledge of a few decisive observables.

A. Characteristics

The analysis of a quantum system in terms of a halo structure begins with the identification of the important degrees of freedom and an understanding of their hierarchy. Quarks, gluons, and leptons are important at the subatomic level, nucleons and mesons form nuclei, nuclei and electrons are building blocks of atoms, which combine into molecules, which in large numbers in turn produce organic materials like proteins, etc. As an illustration of quantum halos and clusters, consider the three-body systems consisting of an electron (e^-) and the helium (He) and hydrogen (H) atoms, i.e., He+H $+e^-$ (Fig. 1). The two-body subsystems He+H and He $+e^-$ are unbound, while H+e^- has one weakly bound state, which can be crudely described as an effective two-body system although much better as a three-body system, i.e., $p+e^-+e^-$. The hydrogen and helium atoms are two- and three-body systems, i.e., $p+e^-$ and $\alpha+e^-+e^-$, where the α particle is a four-body system of $p+p+n+n$. The nucleons (n) and (p) are themselves in turn three-body systems made of three quarks. These structures are essentially completely uncoupled, and each of them may be studied without any knowledge of the substructures. A full and deep understanding, however, requires all degrees of freedom.

The prototypes of nuclear two- and three-body halos are often taken as ^{11}Be (^{10}Be+n), ^{8}Be ($\alpha+\alpha$), $^{3}_{\Lambda}$H ($\Lambda+d$) and ^{6}He ($\alpha+n+n$), ^{11}Li (^{9}Li+$n+n$), ^{9}Be ($\alpha+\alpha+n$), and $^{3}_{\Lambda}$H ($\Lambda+n+p$). Clearly further division of the individual cluster particles into nucleons and quarks is possible. Whether the hypertriton is most suitably de-

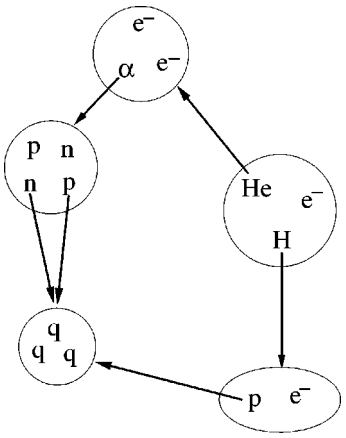

FIG. 1. The hierarchy of degrees of freedom illustrated by the three-body system $He+H+e^-$ (He and H atoms and an electron) and subdivisions first into an α particle and nucleons and eventually into quarks.

scribed by two or three clusters depends on the point of view and on the required accuracy.

Let us now introduce a general definition of quantum halo states. We must first specify the involved "particles" or clusters which in the combined system may form a bound state with an energy close to the threshold for breakup into its constituents. The corresponding cluster component in the many-body wave function may then dominate the structure as it eventually would above threshold for binding. However, the presence of a weakly bound cluster structure does not guarantee a spatially extended system. Furthermore, a length unit must be defined to measure whether a system is large or small. One approach would be to use the size of the clusters as this unit. Halo states would then be structures in which distances smaller than the combined cluster sizes occur with small probability in the relative wave function. This attempt fails miserably, as is evident from the hydrogen atom, whose electron is essentially always outside the proton radius. Hydrogen and all other atoms would also have to be classified as halos, and the definition would become meaningless.

Instead we choose to define halos as structures with large probability of configurations within classically forbidden regions of space. For two-body systems the classical turning point of the quantum state is then the measuring unit. This choice is such that halos are insensitive to details of the two-body effective interactions and owe their existence entirely to quantum mechanics. Because most of the probability is found outside these potentials, the only crucial ingredient is the large-distance tail behavior of the relative wave function. The implication is that halos now obey universal scaling laws independent of the potentials and the unit of length.

Our definition of a halo state thus combines the two conditions (Riisager *et al.*, 2000):

(i) There must be a large probability f_c for finding a cluster component in the total many-body wave function.

(ii) A large fraction f_h of the probability must be in the nonclassical region outside the cluster potentials.

The fractions f_c and f_h should both be substantial, for example, larger than 1/2. Other definitions can of course also be formulated, but the condition of a strong nonclassical wave-function component is a strong constraint. The present definition has only rather recently been proposed. Previous criteria based on light nuclei properties use the ratio of moments of the potentials (Fedorov *et al.*, 1993, 1994b). They have only qualitative significance, and extrapolations to heavier systems can be very misleading; see Vogt (2002). The universal scaling properties are lost because classical turning points do not scale in the same way as nuclear radii scale with nucleon number.

The above definition does not imply that cluster systems with $f_h<0.5$ are without interest. For instance, the astrophysical S factor for ^{8}B is determined by very-large-distance properties where the probability is very small (Riisager and Jensen, 1993; Grigorenko *et al.*, 1999; Davids *et al.*, 2001).

Our definitions imply that correlated structures combined into fewer "particles" than in the original many-body system give a way to form halos. Normally the importance of correlations can be ordered into two-body, three-body, etc. This is essentially also true for the present structures. However, one remarkable exception is provided by Borromean systems, in which the three-body correlations are responsible for the binding while the two-body correlations are too weak to bind any pair of particles.

Halos are threshold phenomena. To understand this, consider the various approaches to the limit for stability, e.g., adding more particles, increasing the energy, or changing the interaction. The initial structure could perhaps be reasonably well described by mean-field models without correlations. Moving closer to the edge of stability the system responds by rearranging into energetically more favorable structures. Correlations which far from the threshold contributed very little to the total binding become decisive for stability. The energy gain is first of all due to formation of few-body clusters and second to rearrangement of the intrinsic cluster structure, perhaps by excitation or polarization.

B. Size versus binding energy

Since our definition of quantum halos involves both spatial extension and clusterization, we must first choose the appropriate cluster division within the total many-body system. The lowest threshold for breaking into specific fragments usually indicates the dominating cluster structure. In principle there could be several close-lying thresholds, and details about the cluster-cluster coupling and the relative state would then determine the most important configuration. Equally important partition schemes introduce additional complications. Here we consider the usual case of one dominating cluster component.

For a given cluster structure we must now determine whether there is a substantial probability to be in the classically forbidden regions. For two-body systems with attractive potentials this implies evaluating the amount of density distribution located beyond the classical turning point. If the distance associated with this point is small compared to the size of the system, a halo is present. The radial moments characterize the density distribution, and when the second moment is somewhat larger than the square of the radius of the classical turning point, the system is a halo corresponding roughly to $f_h > 1/2$. The above definition assumes both that the size is strongly correlated with the binding energy and that universal scaling relations can be obtained independent of the details of the potential.

For many-body clusters, in order to extend the simple two-body measure of the classical forbidden regions, we shall use the second moment of an average size coordinate measured in terms of a similar average of classical two-body turning points. Measures other than the second radial moment could be designed and may be needed in some cases.

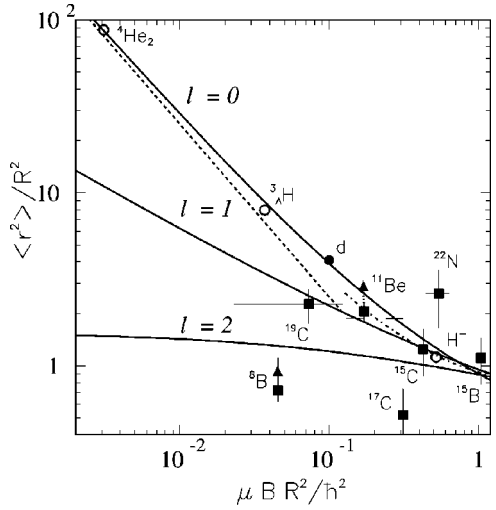

FIG. 2. Scaling plot for two-body halos. The ratio of the halo and the potential square radii as a function of the scaled separation energy. The dashed line corresponds to a pure *s*-wave Yukawa wave function. The solid and dash-dotted lines are results for square-well and r^{-2} potentials, respectively. The thin horizontal lines indicate where 50% of the wave function is outside the potential. Filled and open symbols are derived from experimental data or from theoretical calculations.

1. Two-body systems

The radial coordinate is the relative distance between the clusters. We assume spherically symmetric potentials, but the discussion is general and also valid for deformed potentials (Riisager *et al.*, 1992; Misu *et al.*, 1997). In the nonclassical region details of the potential become less unimportant, and the relevant tail properties of the wave function are determined mostly by the binding energy.

The probability distribution corresponding to the two-body wave function can be characterized by its radial moments. Often the second moment is assumed to be the most important. Let us first compare the spatial extension defined from different radial moments in the simplest case of a bound *s* state where the large-distance part of the radial wave function is used for all distances. For short-range interactions the *r* dependence of the tail is given by $\sqrt{2\kappa}\exp(-\kappa r)/r$, $B=\hbar^2\kappa^2/(2\mu)$, while we can use the exact wave function for the Coulomb potential. We then obtain for the nth radial moments

$$\langle r^n\rangle^{2/n}\frac{8\mu B}{\hbar^2}=\begin{cases}[n!]^{2/n} & \text{short},\\ [n!(1+n/2)(n+1)]^{2/n} & \text{Coul},\end{cases} \tag{1}$$

where μ is the reduced mass and B the binding energy. These moments are thus determined by $\mu B/\hbar^2$. Equation (1) is correct to the extent that the density distribution is found in the large-distance nonclassical region of the potential.

Let us first concentrate on short-range potentials and consider nonzero angular momenta ℓ. The nth nonnormalized moment diverges as $(\mu B)^{(2l-1-n)/2}$ for $n>2l-1$ and converges for $n<2l-1$ (Riisager *et al.*, 1992). When $n=2l-1$ the moment diverges as $\ln(\mu B)$. Thus the probability distribution itself ($n=0$) diverges only for $l\leqslant 1/2$, i.e., for *s* waves. The second moment ($n=2$) only diverges for $l\leqslant 3/2$, i.e., for *s* and *p* waves. The fourth moment ($n=4$) only diverges for *s*, *p*, and *d* waves, and so forth.

We can construct dimensionless measures of size and binding energy by the appropriate use of a scaling length R. We choose this radius as the classical turning point, in keeping with our definition of quantum halos. For square-well potentials R is well defined independent of energy. The nth moment must be larger than R^n if the nonclassical region dominates the probability distribution. Then the dimensionless measures of size and binding energy are related through universal angular-momentum-dependent functions.

In Fig. 2 we use the second radial moment for light nuclei to illustrate these scaling relations. When $\langle r^2\rangle/R^2>2$ the probability outside the classical turning point R is roughly 50% for *s* and *p* waves. For higher orbital angular momenta this probability never reaches 50% even for zero binding energy. Thus halos can only exist in *s* and *p* waves. Higher moments ($n>2$) could instead be used to define when the nonclassical contribution exceeds 50%. The criteria must then be changed accordingly.

For $n=2$ and $l=0$ the halo occurrence condition $\langle r^2/R^2\rangle>2$ is, through Eq. (1), equivalent to $\mu B R^2/\hbar^2<1/8$. However, a finite range of the square well increases the relative content outside R, especially for larger binding energy. Instead the condition $\langle r^2/R^2\rangle>2$ corresponds to $\mu B R^2/\hbar^2<0.27$ or 0.15 for *s* and *p* states, as indicated in Fig. 2. If both the dimensionless size and binding-energy combinations are measured with good accuracy, a necessary and sufficient condition for a halo state is then simply that $\langle r^2\rangle/R^2>2$ and that the binding-energy measure correspondingly be less than 0.2. In

principle one of these conditions is sufficient, but if both are fulfilled, the consistency of the assumed cluster division and the interpretation and accuracy of the corresponding measurements are simultaneously tested.

The classical turning point is, in general, dependent on the binding energy. This can be illustrated with a Woods-Saxon potential of strength $-U_0$ and radius and diffusivity parameter R_0 and a. When R is the corresponding classical turning point we obtain with $\langle r^2\rangle = \hbar^2/(4\mu B)$

$$\langle r^2/R^2\rangle \approx \frac{\hbar^2}{4\mu R_0^2 B}\frac{1}{[1+a\ln(U_0/B)/R_0]} < \frac{\hbar^2}{4\mu R_0^2 B}, \tag{2}$$

where the additional logarithmic binding-energy dependence increases the radius R. Compared to the square well of radius R_0 the nonclassical region is less populated but dependent on B and the Woods-Saxon parameters. Smaller binding energy is required to fulfill the halo condition and to obey the universal scaling relations.

The sloping edge of the Woods-Saxon potential permits states that have a high probability outside the radius R_0 but that are still inside the classical turning point (Vogt, 2002). Such states would lead to points in the lower right corner of Fig. 2, which would move upwards and to the left when R is changed into R_0, but would still not follow the scaling curve. Thus these states, which do not obey universal scaling relations (their properties depend on the characteristics of the Woods-Saxon potential), are not halo states.

For nuclei we estimate the classical turning point R of the appropriate square well from the mean-square radii of the constituent particles, i.e., $3/5R^2 = (\langle r^2\rangle_1 + \langle r^2\rangle_2 + 3.3\ \mathrm{fm}^2)$ where we used a Gaussian interaction range of 1.41 fm, resulting in the mean-square radius of 3.3 fm^2. This estimate does not change very much unless B is several orders of magnitude smaller than U_0.

Short-range power-law potentials, $r^{-\nu}$ ($\nu>2$), produce a classical turning point with even stronger energy dependence. The tendency is the same as for a Woods-Saxon potential, and the right-hand side of Eq. (2) should only be multiplied by a factor proportional to $B^{2/\nu}$. The effect becomes increasingly important as ν approaches 2.

Let us now consider attractive r^{-1} potentials. The effect of an energy-dependent turning point is well known from atomic states: $\langle r^2/R^2\rangle$ is always less than unity. The states reside mainly in the classical region even though their mean radii increase towards infinity. Not surprisingly the moments given in Eq. (1) are larger for Coulomb than for short-range potentials. The transition between these two types of moments was investigated with a potential alternating between attractive long-range and repulsive short-range behavior (Lombard and Volpe, 2002).

For a long-range repulsive potential, $\hbar^2 S/(2\mu r^\nu)$, $0<\nu<2$ combined with an attractive short-range potential, the wave function at intermediate distances behaves as $\exp[-(1-\nu/2)^{-1}S^{1/2}r^{1-\nu/2}]$. For a Coulomb potential ($\nu=1$) we have $\exp[-2\sqrt{Sr}]$ which is a slower falloff than at large distances, where the potentials are negligible compared to the energy and we get the usual exponential decrease, $\exp(-\kappa r)$. All moments remain finite for all binding energies for long-range potentials.

When the binding is provided by an attractive long-range Coulomb potential the mean-square radius is six times larger than for short-range potentials [see Eq. (1)], but the turning point is also at a large distance, resulting in points in the nonhalo region in the lower right corner of Fig. 2. In general, for any potential, the universal curve in Fig. 2 is either approximately followed or the points show up in the nonhalo region. If the classical turning points are changed, due to an inaccurate determination, the points would either slide along the curve or move into the strong-binding region where scaling does not apply.

The division between short and long range is the r^{-2} potential, with the same scaling properties as the kinetic-energy operator. The generic form is

$$V(r) = -\frac{\hbar^2}{2m}\frac{\nu^2+1/4}{r^2}, \tag{3}$$

which has infinitely many bound states at small distances without any lower energy bound; see Landau and Lifshitz (1958) for details. To avoid this divergence problem we assume an infinite wall at some short distance. Still, when $\nu^2>0$, infinitely many bound states labeled n are present at large distance, whose rms radius is given by

$$\langle r^2\rangle_n = \frac{2}{3}(\nu^2+1)\frac{\hbar^2}{2\mu B_n}, \tag{4}$$

can become arbitrarily large.

With R defined again as the classical turning point radius associated with state n, we get

$$\langle r^2/R^2\rangle_n \approx \frac{2}{3}\frac{\nu^2+1}{\nu^2+1/4} < \frac{8}{3} \tag{5}$$

independently of n. The halo condition $\langle r^2/R^2\rangle>2$ is then fulfilled only for $\nu^2<1/8$. For large ν^2 the classical turning point radius increases faster than $\langle r^2\rangle$ with decreasing binding energy, so that the structure cannot be classified as a quantum halo. Various scaling relations still exist as in Eq. (4) but they are specifically related to the r^{-2} behavior. Analogously the states located in the surface of a sloping short-range Woods-Saxon potential do not obey universal scaling laws unless they lie outside the classical turning point or, equivalently, unless the central expression in Eq. (2) is larger than 2.

The strong correlation between size and binding energy has been further extended for weakly bound two-body systems by Lassaut and Lombard (1997, 1999) and Lombard (2001a), who approximate the mean-square radius of an s wave as $\langle r^2\rangle = 3\hbar^2\varphi/(2\mu B)$, where $\varphi \approx (1+2\sqrt{\epsilon}+2\epsilon)/6 \in [1/6,1]$ is a universal function of $\epsilon = B/B_{\max}$. The lower limit 1/6 is obtained in the weak-binding limit when $B=0$. The maximum binding energy $B_{\max}$ occurs at the threshold for binding the second s state.

A peculiar behavior is found for the oscillating long-range von Neumann–Wigner potential (Stahlhofen, 1996; Lombard, 2001b) where one bound-state solution corresponds to a positive energy E_0. The terminology of positive-energy bound states is appropriate, since the wave function is an exponentially vanishing solution of the Schrödinger equation. This falloff is due to the infinitely many oscillations which confine the wave function to finite distances for one discrete positive energy. The mean-square radius of this state is given by $\langle r^2\rangle = 0.3376\hbar^2/(\mu E_0)$. The dependence on energy is of the same form as in Eq. (1), but the constant differs from 0.25. Thus the spatial properties of extended systems differ depending on the side from which the zero energy is approached. The same class of long-range potentials also produces positive-energy bound states of nonzero angular momenta (Lombard, 2001b). However, the mean-square radius for an $l=1$ state is inversely proportional to the energy in contrast to the square-root dependence for negative-energy bound states. Furthermore, an $l=1$ positive-energy bound state may exist even when there is no bound $l=0$ states.

2. Three-body systems

We now consider a three-cluster division and with individual masses, momenta, and coordinates denoted m_i, $\mathbf{p_i}$, and $\mathbf{r_i}$, respectively, describe the relative motion by means of hyperspherical coordinates ($i=1,2,3$). The total mass is $M=m_1+m_2+m_3$, while the average radial coordinate, the hyper-radius ρ, is given by

$$m\rho^2 \equiv \frac{1}{M}\sum_{i<k} m_i m_k (\mathbf{r_i}-\mathbf{r_k})^2, \tag{6}$$

where m is an arbitrary mass unit. The remaining five intrinsic coordinates are dimensionless angles (Zhukov *et al.*, 1993). The hyperspherical harmonics are the eigenfunctions of the angular part of the three-body kinetic-energy operator (excluding the center-of-mass motion). The eigenvalues are proportional to $K(K+4)$, where $K=0,1,2,\ldots$. In the hyper-radial equation there appears a diagonal generalized centrifugal barrier potential $\propto(K+3/2)(K+5/2)\rho^{-2}$, which never vanishes even for $K=0$ when all relative angular momenta are zero.

The large-distance asymptotic behavior of the wave function is $\rho^{-5/2}\exp(-\kappa\rho)$ where κ is related to the binding energy by $B=\hbar^2\kappa^2/(2m)$ (Merkuriev, 1974). It is possible to compute the radial moments $\langle\rho^n\rangle$ for short-range interactions in the limit where only the large-distance behavior is important. Although for interacting particles. K is not conserved, the components in an expansion in hyperspherical harmonics are still characterized by K. Using the two-body results with the substitution $l\to K+3/2$ we find that the non-normalized nth moment of ρ diverges for $B\to 0$ as $B^{(2K+2-n)/2}$ when $n>2K+2$ and as $\ln B$ when $n=2K+2$. Even for $K=0$ the probability distribution remains at finite distances due to the finite centrifugal barrier. The second moment only diverges for $K=0$ and then only logarithmically as $\ln B$.

Let us include an additional long-range repulsive potential which depends on the hyper-radius as $\hbar^2 S/(2\mu\rho^\nu)$ with $0<\nu<2$. Again asymptotic behavior, $\exp(-\kappa\rho)$, is reached at large distances where the potential can be neglected. At intermediate distances beyond the short-range attraction, as for two-body systems, the wave function behaves as $\exp[-(1-\nu/2)^{-1}S^{1/2}\rho^{1-\nu/2}]$. All moments of the hyper-radius remain finite for any binding energy.

In order to formulate existence conditions for three-body quantum halos we must determine the quantum probability in the nonclassical region of the phase space, where the energy is smaller than the sum of all potential energies. We note first that this region is not determined by the classical turning points of the diagonal hyper-radial potential. Indeed, it is entirely possible to have classical motion in the hyper-radial coordinate while the system is nonclassical. To scale hyper-radial moments we thus need a unit of length related to the two-body forbidden regions. Therefore we generalize the scaling considerations from two- to three-body systems by defining a scaling parameter ρ_0 as suggested from Eq. (6), i.e.,

$$m\rho_0^2 \equiv \frac{1}{M}\sum_{i<k} m_i m_k R_{ik}^2, \tag{7}$$

where R_{ik} is the two-body scaling length of the system i and k. To appreciate the content of Eq. (7) let us assume that particle 1 is far from identical particles 2 and 3. If $(R_{23}/R_{12})^2 \ll 2m_1m_2$ we obtain $\langle r_{12}^2\rangle/R_{12}^2 \approx \langle\rho^2\rangle/\rho_0^2$ as for three identical bosons. Thus in this case the classical two-body regions can be measured in hyper-radial space with ρ_0 as the unit.

Compressing the information on the nonclassical region into just one length is a simplification that can at best be expected to provide a good average for the three two-body subsystems. In addition, we face the same problem of energy dependence as for isolated two-body systems when it comes to defining the quantities R_{ik}. The choice we make remains the same, i.e., define R_{ik} for an appropriate square well when short-range interactions produce most of the two-body binding. When only long-range interactions are present we can use the two-body bound-state energy to define R_{ik} for attractive potentials and R_{ik} equal to zero for repulsive potentials.

The definition of three-body quantum halos can now be formulated in terms of two-body quantities and of the classical turning points. The definition of ρ_0 in Eq. (7) differs by the mass weights from that used by Fedorov *et al.* (1994c). Using Eq. (7) facilitates comparisons between two- and three-body systems, since their binding energies then are the main difference.

The energy scaling variable is then analogously defined as $Bm\rho_0^2/\hbar^2$ independent of m. The resulting three-body plot is shown in Fig. 3. The condition for a halo is now $\langle\rho^2\rangle/\rho_0^2>2$, corresponding to the two-body criterion of $\langle r_{12}^2\rangle/R_{12}^2>2$, which was given by Fedorov

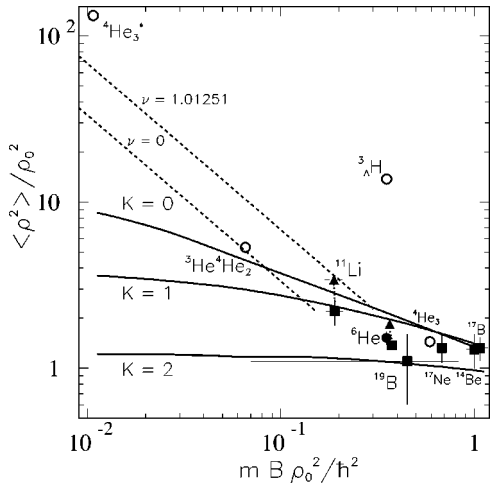

FIG. 3. Scaling plot for three-body halos. The ratio of the halo and effective-potential square radii is plotted vs the scaled separation energy. The solid lines are theoretical, scaled curves for different hypermomentum K. The dashed lines show the Efimov states for a symmetric system, $\nu=1.012\,51$, and for minimum attraction, $\nu=0$. Filled symbols are derived from experimental data and open symbols are from theoretical calculations.

et al. (1993). Clearly only structures with dominating configurations of $K=0$ and 1 can classify as halo states.

The three-body binding energy B in Fig. 3 can be divided into contributions from the different two-body subsystems. If one or more of these contribute significantly compared to the total B due to a bound subsystem, the system is most likely not a three-body halo. If one subsystem dominates, the main structure is probably one particle bound to the pair and together perhaps forming a two-body halo. There is a strong tendency for three-body systems to be either predominantly two-body systems or without bound states in any subsystem.

In states with one and only one bound subsystem the bound particles move in phase and were therefore named tango states by Robicheaux (1999); see also Li and Lin (1999) and Vallet *et al.* (2001). The states in the other limit in which none of the three subsystems is bound are named Borromean systems; see Zhukov *et al.* (1993). They provide the best examples of three-body correlation as two-body halos are excluded by definition.

The existence of Borromean systems formed by three pointlike particles can be related to kinetic and potential effects. Let us assume that the relative two-body states between all pairs of particles remain unchanged. Then a comparison of reduced masses shows that the (positive) kinetic energy is smaller for the three-body than for the free two-body systems. The additional potential energy of one pair in the three-body system may be sufficient to bind this system when the subsystems are only marginally unbound.

Borromean systems exist only when the strength g of the attractive two-body potential for a symmetric (boson) system belongs to the interval $[g_3,g_2]$ determined by the threshold strengths for binding the three- and two-body systems. For ordinary radial shapes, the ratio of the strengths is $g_3/g_2\approx 0.8$. The lower limit of 2/3 is almost reached when a repulsive barrier is added, whereas a repulsive core increases this ratio towards the upper limit 1 (Richard and Fleck, 1994; Goy *et al.*, 1995; Moszkowski *et al.*, 2000). This interval $[g_3,g_2]$ tends to become larger when the constituents have an intrinsic structure, since rearrangements provide additional binding energy for the three-body system.

A Borromean system in which one subsystem is bound ($g>g_2$) becomes a tango state. When two or three subsystems simultaneously approach their respective thresholds for binding in relative s states, a new class of (Efimov) states appears. This can be understood from the behavior of the hyper-radial potential. For zero-range two-body potentials the only energy available through combination of parameters is $\hbar^2/(2\mu\rho^2)$, where μ is a combination of reduced masses. The potential must then have the intermediate (between short and long ranges) ρ^{-2} form given in Eq. (3).

The strength determines the number of solutions from none, for $\nu^2<0$, to infinitely many, for $\nu^2>0$. For three identical bosons with s states at zero energy, $\nu=1.012\,51$ and infinitely many Efimov states are present, although none of the subsystems have even one bound state (Efimov, 1970, 1990). The total angular momentum should be low, preferably zero; higher values allow the Efimov effect but decrease the possible mass combinations (Nielsen *et al.*, 2001).

The finite-range interactions provide additional length parameters. Then the hyper-radial potentials approach zero faster than ρ^{-2} at hyper-radii larger than a mass weighted average of the two-body scattering lengths. The number of Efimov states is therefore finite unless at least two scattering lengths are infinitely large. Another essential exception preventing infinitely many states is the presence of a long-range attractive interaction in at least one of the two subsystems (or two out of three) with a zero-energy s state. In general infinitely many states appear for a symmetric system in which the ratio of the two-body scattering length (a) and the effective range (R_e) is infinitely large. This occurs both for $R_e=0$ (the Thomas effect) and when $a=\infty$ (the Efimov effect; Adhikari *et al.*, 1995; Amorim *et al.*, 1997; Nielsen *et al.*, 2001).

At the threshold ($g=g_2$) of binding in two-body systems, for ordinary short-range attractive potentials, the three-body ground state is relatively well bound, i.e., about 1 MeV for nuclei (Fedorov *et al.*, 1994a). Then the Efimov states appear (Efimov, 1970) as excited states with size and energy related as in Eq. (4), i.e.,

$$B_n=B_0\exp[-2\pi n/\nu],\quad \langle\rho^2\rangle_n=\langle\rho^2\rangle_0\exp[2\pi n/\nu], \tag{8}$$

where the scaling parameter is obtained from the strength of the effective radial potential of the form in Eq. (3). Even for very low n the states are broadly extended and very weakly bound.

These states then appear parallel to the lines labeled by ν in Fig. 3. For nuclei in which the neutron-core mass ratio is less than 1, the states must be in the region be-

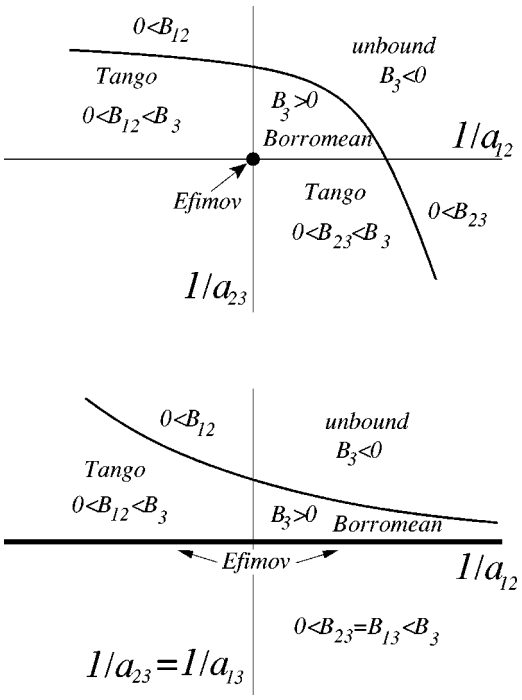

FIG. 4. Sketch of the different regions of stability for a three-body system as a function of the inverse *s*-wave two-body scattering lengths a_{ik}. The central point corresponds to $a_{ik}=\infty$, which is the threshold for binding of the first state. All potentials are attractive or vanishing. The upper part assumes no interaction between particles 1 and 3 and the lower part assumes the same interaction between 1–3 and 2–3.

tween the two dashed lines. For molecules, the states would most likely be above the upper dashed line. The ground state would be an ordinary nonhalo state, whereas the excited states would be giant halos. The ground state can only be a halo when the ratio $g_3/g_2 \approx 1$, which only happens with a repulsive core and a sharp attractive pocket (Moszkowski *et al.*, 2000).

3. Transitions from two- to three-body systems

For a two-body system the scattering length a measures the interaction sphere, i.e., the cross section is $\propto a^2$. Furthermore, zero *s*-state binding energy is equivalent to infinite a, and this threshold is then determined by $1/a=0$. Weakly bound or slightly unbound systems are then parametrized by small values of $1/|a|$, where $a>0$ corresponds to unbound states and $a<0$ to bound states.

The different structures are schematically shown in Fig. 4 for weakly bound systems with at most one bound state in each two-body subsystem. For sufficiently weak potentials no bound states are possible. For decreasing $1/|a|$ the Borromean region appears before any subsystem is bound. Moving horizontally to the left on the figure we cross the threshold for binding subsystem 1–2 and enter the region of one and only one bound subsystem. This region is divided into regions of bound and unbound three-body systems with respect to the two-body system and particle 3.

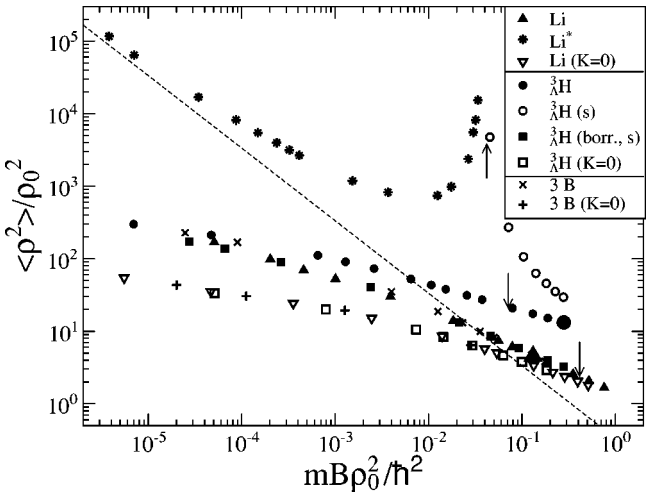

FIG. 5. Scaling plot for three-body halos as in Fig. 3: dashed line, the Efimov curve for $\nu=0$ [see Eq. (8)]; ▽, ▲, ∗, masses corresponding to ^{11}Li (^{9}Li$+n+n$); □, ■, ○, ●, $^3_\Lambda$H ($\Lambda+n+p$); realistic points are indicated by a large closed triangle and circle; +, ×, three different particles with two fixed scattering lengths while the third is varied. The arrows indicate transitions between Borromean, tango, and bound-state regions. We used ρ_0 from Eq. (10). See text for further discussion.

The definition of ρ_0 in Eq. (7) allows a direct explanation of the lone point corresponding to the tango state of the hypertriton in Fig. 3. The point belongs to the lower part of Fig. 4 well into the tango region. The three-body binding energy consists of about 2.2 MeV from the deuteron plus about 137 keV from the deuteron-Λ binding. In the corresponding two-body scaling plot in Fig. 2 the binding energy of the deuteron-Λ particle would be only 137 keV, which would bring this point back to the $l=0$ curve. The hypertriton is a two-body halo and not a three-body halo in spite of the rather suggestive number of three particles.

In Fig. 5 we follow the hypertriton point as we vary the neutron-proton interactions corresponding to a change from the tango to the Borromean region in Fig. 4. This is first achieved for a model including only neutron-proton relative *s* waves (○). Then Λ becomes unbound before the deuteron (we do not reach the Borromean region), and the size of this Λ-deuteron effective two-body system increases as the binding approaches the threshold. Another path is followed in Fig. 5 by maintaining the tensor term in the complicated, but realistic, neutron-proton interaction and only reducing the central *s*-wave attraction (●). Then the Borromean region is reached and the path merges at small binding energies with the curve (■) obtained by using *s* waves and varying the λ-nucleon (not binding) attraction.

The transition from the Borromean to the Efimov region is also illustrated in Fig. 5 by using ^{11}Li with increasing *s*-wave neutron-^{9}Li attraction (▲). The interactions are varied vertically from the Borromean region in Fig. 4 across the Efimov strip. Approaching infinite scattering length increases the three-body binding energy and the bound state moves into the lower right corner in

the nonhalo region of Fig. 5. As this n-^{9}Li s-wave attraction is decreased, the points (▲) follow a curve like that of three bosons (×), eventually merging with the previously defined universal curve (×, ▲, ■).

In Fig. 5 we also show calculations for three bosons, ^{11}Li and $^{3}_{\Lambda}$H including only $K=0$ components in the wave functions (+, □, ▽). They basically follow a universal curve determined by the hyper-radial potential at large distance (Jensen *et al.*, 2003)

$$V(\rho)=-\frac{\hbar^2}{2m\rho^2}\pi\sqrt{8}\frac{\rho_0}{\rho}, \tag{9}$$

where the scaling parameter is given by

$$\rho_0\equiv\frac{\sqrt{2}}{3}\sum_{i<k}R_{ik}\sqrt{\frac{m_i m_k}{m(m_i+m_k)}} \tag{10}$$

as a linear average of classical turning points comparable to Eq. (7). This $K=0$ curve is in the asymptotic weak-binding region almost an order of magnitude below a similar but realistic curve obtained without the $K=0$ restriction. Both curves clearly converge for small binding towards a similar universal behavior, i.e., depend logarithmically on binding energy, but with different proportionality factors. The $K=0$ approximation severely underestimates the sizes of halos.

The realistic curve corresponds for Borromean systems to hyper-radial potentials at large distance behaving as $-\hbar^2 48 a_{av}/(2m\pi\rho^3\sqrt{2})$, where a_{av} is a weighted average of the scattering lengths a_{ik} (Jensen *et al.*, 1997),

$$a_{av}\equiv\frac{\sqrt{2}}{3}\sum_{i<k}a_{ik}\sqrt{\frac{m_i m_k}{m(m_i+m_k)}}. \tag{11}$$

This radial potential is approximately obtained numerically from Eq. (9) by substituting a_{av} for ρ_0. Unfortunately, the three-body binding energy cannot be found from the large-distance behavior alone. Some knowledge of the short-distance properties is also necessary (Amorim *et al.*, 1997; Frederico *et al.*, 1999; Fedorov and Jensen, 2001a, 2001b). The simplest prescription is to use a renormalized unit of length as in Fig. 5, where ρ_0 is this length.

Then a_{av}/ρ_0 should determine a universal behavior reached for small binding. Such a simple dependence is not very precise in all cases, but a value of $a_{av}/\rho_0\approx 3.0$ seems to be correct within 20% in the validity region where all two-body scattering lengths are substantially larger than the effective ranges. These criteria are not easily fulfilled for all three subsystems simultaneously, since this basically means that the individual terms in a_{av} and ρ_0 must obey $a_{ik}\gg R_{ik}$, while the averages are only allowed to differ by a factor of about 3. Thus universal scaling is only present when the subsystems are rather similar.

When the attraction is increased until the neutron-^{9}Li system has an s state at zero energy, infinitely many Efimov states appear. They are equally spaced along the dashed (Efimov) line in Fig. 5, but unfortunately separated by a huge distance as obtained from Eq. (8) with the appropriate value of $\nu\approx 0.074$. Thus only the first of these is seen in the figure close to the Efimov line in the upper left corner (∗). With larger binding energy (B_2) of the two n-^{9}Li subsystems the size of this excited state at first decreases and then turns around to increase as B_2 approaches and overtakes the three-body binding energy (Efimov, 1970, 1990; Fedorov *et al.*, 1994a). This implies that non-Borromean three-body systems could have such spatially extended, excited states with energies close to the two-body threshold.

The position in the scaling plot in Fig. 3 indicates halo structure, Efimov states, or two- or three-body scaling properties. Also strong rearrangement effects may be seen to result in nonstandard scaling parameters and positions in the plot. The qualitative behavior of the scaling results are intuitively easy to understand (Fedorov *et al.*, 1994c). For example, in the vicinity of the Borromean-tango border the system approaches a two-body system with a loosely bound third particle. The size and the scaling properties are then necessarily determined by the third particle relative to the two-body entity, i.e., two-body scaling.

Crossing the different thresholds in Fig. 4 does not cause any computational problem provided the Faddeev equations are used. The three Faddeev components described in different Jacobi coordinates efficiently account for the proper asymptotic behavior of the wave function (Fedorov and Jensen, 1993; Fedorov *et al.*, 1994c). Use of only one component is insufficient to describe the structure.

4. Many-body systems

The relative motion of a system of N particles may be described by hyperspherical coordinates derived from a set of $N-1$ Jacobi vectors (Barnea, 1999a, 1999b). In analogy to Eq. (6), the hyper-radius is defined by $m\rho^2=\Sigma_{i<k}m_i m_k \mathbf{r}_{ik}^2/M$, where M is the total mass. The remaining $3(N-1)-1$ coordinates are dimensionless. The wave function Ψ is multiplied by $\rho^{(3N-4)/2}$ and the kinetic-energy operator for the new Schrödinger equation has the form

$$\frac{\hbar^2}{2m}\left(-\frac{\partial^2}{\partial\rho^2}+\frac{(f-1)(f-3)}{4\rho^2}+\frac{1}{\rho^2}D(\text{angles})\right), \tag{12}$$

where $f=3(N-1)$ is the number of degrees of freedom and $D(\text{angles})$ is a function containing first- and second-order derivatives with respect to the angles. The generalized centrifugal barrier term may be rewritten as

$$\frac{\hbar^2}{2\mu}\frac{(f-1)(f-3)}{4\rho^2}\equiv\frac{\hbar^2}{2\mu}\frac{l^*(l^*+1)}{\rho^2}, \tag{13}$$

where $l^*\equiv(f-3)/2$ is a generalized angular momentum quantum number, which, however, is only conserved for two particles in spherical potentials.

Let us now first consider an isotropic wave function without any angular dependence or equivalently only consisting of s waves in all relative partial waves. Then no clusterization of groups of particles takes place. The

contribution from the function D in Eq. (12) is then zero and we have effectively a two-body system with a centrifugal barrier corresponding to l^*. Halo formation defined in terms of the moments of ρ is therefore only possible for $l^* \leqslant 3/2$. This in turn implies $f \leqslant 6$ and $N \leqslant 3$, which under these assumptions is the maximum number of clusters possible in a halo.

For a halo to exist with more than three particles the severe constraint imposed by the spatially confining centrifugal barrier must be circumvented. This requires higher partial waves for the relative motion between some particles or groups of particles. However, the states are then necessarily correlated in the angular space and some clusterization must take place. If the angular dependence becomes too strong, the resulting pronounced correlations effectively reduce the number of clusters below N. This is analogous to the reduction from three-body to two-body structure observed in the hypertriton. This reduced number of clusters would then be more isotropic, and we can repeat the argument of halo occurrence demanding either a low centrifugal barrier or a correlated structure attempting to avoid this barrier. Clearly the number of independent halo particles has to be relatively small.

The potential energy gained as a consequence of correlations could be an advantage. Let us use the example of identical particles outside a core. The core plus one particle is unbound by the resonance energy ε. The additional energy associated with $N-1$ particles is $\varepsilon(N-1)+v(N-1)(N-2)/2$, where v is the (negative) average potential gain from the interaction. This energy is negative when $\varepsilon < -v(N-2)/2$, which becomes possible for large N if v remains constant. This simple estimate illustrates that contributions may be combined from many individually insufficient particles. Reaching an N-body bound state then seems easy, but the opposite effect of the kinetic energy should also be included.

Assume now that two identical fermions and a core form a Borromean system. Adding more pairs of these fermions often leads to unbound systems due to the Pauli principle. However, specific numbers of these pairs may form configurations of special stability, in analogy to the magic numbers in atoms and nuclei. Such additional quantum stabilization, due to generalized shell structure, may produce fragile but bound states owing their existence to correlations. Magic numbers corresponding to new cluster combinations could arise. Even if these correlations did not lead to positive binding they might still produce relatively stable continuum structures (Jensen and Riisager, 1991, 1992).

In a simple intuitive picture the stable configurations of a system approaching a threshold of instability should exploit correlations in an optimal way. The gain in correlation energy might be relatively small, and for strongly bound states hardly visible, but at the edge of stability this marginal energy difference could result in a bound state. The rearranged bound structure might be rather exotic although still made out of the same constituent particles. Quantum halos stabilized by shell structure are an interesting possibility.

5. Transitions between mean field and clusters

The mean field is the simplest approximation to the structure of a many-body system, but correlations that are treated most easily in the cluster model may be important. These two opposite starting points are not easily combined without undertaking the enormous task of a full-scale treatment of the many-body problem. A mean-field approximation is by definition accurate when the correlations are negligible, whereas cluster models are accurate when the intrinsic cluster structure can be neglected. The intrinsic and relative degrees of freedom cannot be separated when the relative cluster configurations have significant spatial overlap, resulting in comparable interactions between clusters and between particles within the clusters.

The self-consistent mean-field Hartree-Fock approximation is a good starting point for stable nuclei, atoms, and electrons in solids. The full spectrum of structure and difficulties can be illustrated by moving from beta stability to zero neutron separation energy (dripline) in the nuclear chart. At first, mean-field computations are successful when modified to include pairing correlations and deformations. The neutron skin develops as the neutron excess increases (Mizutori *et al.*, 2000). As the dripline is approached, the system responds by developing correlations to postpone decay. Other thresholds of instability than the neutron dripline also favor corresponding clusterization.

These rearrangements are not easy to predict, but pronounced cluster structure may appear and eventually develop into a halo or even into an Efimov state. The new low-lying structures in unstable systems may then be linked to excited states of exotic structure in ordinary stable systems.

The transition from a mean-field to a cluster description, or equivalently how clusters develop in a many-body system, has been investigated in many different ways. Let us first note that a Hartree-Fock solution can exhibit strong two-body halo features whenever an occupied state has sufficiently small binding energy and orbital angular momentum equal to 0 or 1 (Bertsch *et al.*, 1988). The corresponding cluster division is into a particle and a core consisting of the remaining particles in the total system. The only difference from our two-body description is the antisymmetrization (if required) and the self-consistent origin of the potential.

The correlations needed for many-body halos and in particular for three-body halos are not available in the space of Slater determinants. However, a mean-field solution with a doubly degenerate highest-lying occupied (s or p) state close to the threshold could be spatially very extended (Bertsch *et al.*, 1988), while the correlation between two nucleons and the remaining core cannot be a stable three-body halo configuration. The space is insufficient.

The structure changes when nucleons are added and the nuclear dripline is approached. Staying within the (relativistic) mean-field model and moving from stability to the neutron dripline in the nuclear chart, we find that

three overlapping regions appear, normal, neutron skin, and halo regions (Meng and Ring, 1998; Mizutori *et al.*, 2000). In the first, for ordinary stable systems, the neutron and proton densities have similar radii. In the second region, the neutrons extend beyond the protons, revealing a neutron skin with nuclear-matter-like high density and a rapid falloff outside the neutron radius. Finally a neutron halo may appear with an exponentially decreasing density distribution outside the bulk density region. A quantitative measure of the corresponding structure can be designed as differences of specific radii, i.e., the root-mean-square radius and the so-called Helm radius defined as the radius corresponding to the first zero point of the Fourier transform of the density (see Mizutori *et al.*, 2000). The Helm radius is very similar to the sharp cutoff radius of Myers and Swiatecki (1969, 1974) describing the extension of the bulk density.

The pairing correlations are included by the BCS approximation or by full (relativistic) Hartree-Fock-Bogoliubov computations. These correlations do not prevent diverging radii for odd-N nuclei, whereas even-N radii, although they can become large, remain finite even for s states of zero energy (Bennaceur *et al.*, 2000). Furthermore, the coupling to other states spreads this unusually large radius to the neighboring nuclei, and halos seem to appear more often. These phenomena occur because the asymptotic behavior of the two-neutron wave function, being determined by the nonvanishing quasiparticle energy, is roughly equal to the pairing gap for the state closest to the Fermi energy (Bennaceur *et al.*, 2000; Mizutori *et al.*, 2000).

In a Borromean system where the two-body threshold is above the three-body threshold, the correct asymptotic description cannot be given by the quasiparticle energy. The two-particle plus core large-distance behavior of the three-body asymptotics is obtained from the Faddeev equations. The corresponding logarithmic divergence of the mean-square radius could then easily be destroyed by a small change of the available Hilbert space. The limitation imposed by the Cooper pairs in the Bogoliubov computation is sufficient to remove the divergence but still allows large sizes.

The relativistic Hartree-Bogoliubov mean-field computations (Ring, 1996) reported by Meng and Ring (1996, 1998) show halo structures of even numbers of neutrons. The calculated extended wave function for two loosely bound particles is understandable within the mean field as explained above, even without the proper asymptotic three-body behavior. The many-particle halos obtained for zirconium isotopes (Meng and Ring, 1998) are more surprising. They arise because the highest occupied single-particle states ($p_{3/2}$, $p_{1/2}$, $f_{7/2}$, and $f_{5/2}$) for a number of isotopes simultaneously appear very close to threshold. The Cooper pairs are then distributed within these orbits. In a sufficiently large Hilbert space allowing the proper asymptotic behavior, the valence particles would redistribute into spatially more confined structures and reduce the number of particles in the halo.

The origin of the stability of a Borromean nucleus like ^{11}Li is attributed by Barranco *et al.* (1999, 2001) to an enhanced pairing interaction obtained through couplings to low-lying surface vibrations. The single-particle $s_{1/2}$ and $p_{1/2}$ states are, respectively, shifted down and up from their mean-field positions. This then allows the strong correlation found between $s_{1/2}^2$ and $p_{1/2}^2$ configurations. The particle-vibrational coupling generates a density-dependent pairing interaction essentially only active outside the ^{9}Li core. This supports the use of a renormalized effective neutron-neutron interaction as done by Bertsch and Esbensen (1991). On the other hand, most models use the free neutron-neutron interaction, since the spatial extension is large and the influence of any surrounding nuclear matter is very small. The two interactions could then in principle agree outside the core, but in practice the renormalization must be significant to account for the binding of ^{11}Li.

The validity of the cluster description can be extended by adjusting the interaction parameters to experimental two-body scattering properties. Subsequent smaller parameter changes reproducing specific observables could then be acceptable, while other computed observables are left as independent tests or predictions. Such renormalizations are assumed to account for the effects of the missing degrees of freedom, i.e., excitations of the intrinsic clusters, polarization beyond that of the free two-body effective interaction, contributions from other cluster configurations, off-shell effects, (anti)symmetrization between particles in different clusters, and perhaps other contributions. The cluster description then requires that only small effects be allowed from these degrees of freedom.

Low-energy scattering properties are identical for phase-equivalent potentials that only differ by the number of bound states (Baye, 1987). This mathematical fact can be used to account rather well for the exclusion of fermionic clusters from states already occupied by identical fermions within the clusters. For example, the two valence neutrons in ^{11}Li are not allowed in the occupied neutron states within ^{9}Li (Garrido *et al.*, 1999a).

Only Pauli and pairing correlations can be investigated with the zero-range Skyrme force often used in mean-field calculations (Bennaceur *et al.*, 2000; Mizutori *et al.*, 2000). The reason is that zero-range attractive potentials introduce an instability with infinitely many bound states of arbitrary low energy at small distances. This collapse of the many-body wave function is not prevented by the repulsive density-dependent term in the Skyrme interaction (Fedorov and Jensen, 2001a, 2001b). This corresponding regularization problem is well known in field theory (see, for example, Amorim *et al.*, 1997 and Bedaque *et al.*, 1999).

Direct inclusion of additional degrees of freedom has been attempted, but to be efficient the choice must be very dependent on the system. Cluster configurations like two tritons, on top of two neutrons and an α particle, are significant in the ^{6}He structure (Csótó, 1993; Arai *et al.*, 1999). Excitation of the cluster particles can also make significant contributions, as in nuclear drip-

line systems (Nunes *et al.*, 1996; Arai *et al.*, 1999) and for the hypertriton (Miyagawa and Glöckle, 1993, 1995).

An elaborate microscopic multicluster model has been successfully applied to halo nuclei (Descouvemont, 1995). It is based on one or more cluster divisions, parameters chosen as generator coordinates, full antisymmetrization, conserved quantum numbers, and use of basic two-particle interactions. Bound and excited states as well as scattering states have been investigated, despite the heavy numerical tasks involved.

The antisymmetrized molecular-dynamics model has provided a good description of the structure of light nuclei (Kanada-En'yo *et al.*, 1995; Kanada-En'yo and Horiuchi, 2001; Sugawa *et al.*, 2001). The method is variational and based on Slater determinants built from single-particle Gaussian wave packets distributed at various points in space. The cluster structure is then followed as it develops as a function of neutron number. The Gaussian wave function is a severe limitation on the halo description.

Mean-field and cluster models can be combined by treating the intrinsic cluster motion in the mean-field approximation and the valence particles as in the shell model (Bertsch *et al.*, 1988) or placed in cluster configurations (Tosaka and Suzuki, 1990; Tosaka, Suzuki, and Ikeda, 1990; Itagaki *et al.*, 2001). To allow different mean fields for core and valence particles, the variational shell model was formulated (Otsuka *et al.*, 1993). The quantum Monte Carlo method deals accurately with the valence particles (Koonin *et al.*, 1997; Otsuka *et al.*, 2001) while leaving the inert core to produce the energies of the single-particle states in which the correlations are allowed. The full many-body solution is possible for relatively few particles (Carlson and Schiavilla, 1998; Wiringa *et al.*, 2000; Arai *et al.*, 2001; Mezei *et al.*, 2001; Pieper, 2002). All these methods provide a variety of structures including excited states. Unfortunately they are not good enough at describing the large-distance behavior of loosely bound systems such as quantum halos.

C. Halo occurrence

We shall accept a state as a quantum halo if the two conditions specified in Sec. II.A are fulfilled, i.e., there is a sufficiently large cluster configuration with a sufficiently large spatial extension.

Halo occurrence depends of course on the definition adopted. This is worth emphasizing, since the selection of appropriate observables may be strongly influenced by the definition. It would be better if different observables contained the same information about halo properties, but this can hardly be expected. For example, the fourth radial moment emphasizes tail properties more than the probability distribution. A small component of halo character in a nonhalo state could therefore still produce a very strong signal if the observable is sufficiently sensitive.

An observable strongly sensitive to tail properties or to halo features, while ignoring the main parts of the wave function, could be used to detect the occurrence of halo states. Such a magnifying glass effect must be related to the halo definition. This is not a question of subjective judgment concerning interesting physics content, but simply a matter of specifying the notation. Different definitions could be considered as correct if they are consistent and serve the purpose.

The recent results of relatively small spectroscopic factors obtained by analyzing nucleon knockout reactions (Brown, 2001; Enders *et al.*, 2002) are interesting in this context. Such factors imply small single-particle components in the many-body wave function. Since our first condition for single-particle halos requires that the spectroscopic factors be larger than 0.5, halo candidates are expected to have large spectroscopic factors, as measured for ^{8}B (Brown *et al.*, 2002).

Turning to molecular systems, the mean-field is not very useful for describing the relative motion of parts of the system. Instead mean-field models are good approximations for the much more mobile valence electrons. Here again halo formation is favored for few-body systems (small molecules). However, the electron motion must be approximately decoupled from the cluster motion to allow sufficiently large cluster components.

Addition of an electron to an atom or a small molecule may produce halo structure. The distinction between intrinsic and halo degrees of freedom is now less obvious and may not be possible at all. One electron and one or two molecules form a halo; the added electron may strongly couple to the other electrons; another molecular cluster division may provide a better description.

Small binding energy in an s state favors two-body halo occurrence. An intuitive conclusion is then that a three-body halo is formed if we add another particle identical to one of the constituents. However, then the three-body system is probably rather well bound with a small radius. On the other hand, the Efimov states may appear as one or more excited states. To form a three-body ground-state halo the initial two-body system should be unbound, since zero binding results in a normal ground state and the Efimov (excited) states, and even more binding excludes halo formation.

1. Excitation energy dependence

A many-body system may have a finite excitation energy E^*. The binding energy B of the cluster is the separation energy required to move the clusters in their ground states infinitely far apart from each other. The total excitation energy can essentially all be deposited in the relative cluster motion, i.e., $B \approx E^*$, but other quantum states of the same energy may exist with $B \ll E^*$. This corresponds to intrinsic excitations of the clusters. It is still possible to define halos, Borromean systems, and tango states in terms of the degrees of freedom of the relative cluster as long as they remain independent of intrinsic structure.

Quantum halos are not characterized by a conserved quantum number. Strong coupling to other more complicated states dilute the component of the halo and

might effectively prevent its occurrence. To investigate this we construct a model in which the many-body states are spanned by the direct product of the two Hilbert spaces built by the halo and all other degrees of freedom. This separation is reflected in a Hamiltonian consisting of three terms, two acting only within their respective spaces and one coupling $V^{(c)}$. We choose a basis in which the Hamiltonian is diagonal when $V^{(c)}=0$. We furthermore assume only one state $|h\rangle$ of energy E_h in the halo space. We denote the many-body basis states spanning the other space by $|\alpha\rangle$ and their energy by E_α.

The full Hamiltonian in the space spanned by the product basis is then diagonal except for the row and the column of the halo basis containing the coupling terms denoted $V_{h\alpha}$. Diagonalization of this Hamiltonian matrix gives the eigenvalue equation (Bohr and Mottelson, 1969)

$$E_h - E_i = \sum_\alpha \frac{V_{h\alpha}^2}{E_\alpha - E_i}, \tag{14}$$

where E_i is the energy of the eigenstate $|i\rangle$. The probability $c_h^2(i)$ of finding the halo state $|h\rangle$ in $|i\rangle$ is

$$c_h^2(i) = \left(1 + \sum_\alpha \frac{V_{h\alpha}^2}{(E_\alpha - E_i)^2}\right)^{-1}. \tag{15}$$

There is one solution E_i of Eq. (14) between each pair of the successive (ordered) energies E_α. One state $|i\rangle$ exhibits halo character provided $c_h^2(i)$ is larger than 0.5, requiring that each of the terms in the sum in Eq. (15) be smaller than one. Thus all interaction matrix elements $V_{h\alpha}$ must be smaller than the difference between E_α and E_i.

In the schematic model, with equidistant level spacing D between the ordered E_α energies and constant matrix elements $V \equiv V_{h\alpha}$, the condition for halo occurrence is $D > \pi V$ (Bohr and Mottelson, 1969; Jensen and Riisager, 2000). In other words, the distance between nonhalolike many-body states must be larger than the coupling to the halo state.

The coupling of a halo state to a large number of other states can often be described by an optical potential having real and imaginary parts. Then only halo degrees of freedom are treated explicitly.

An explicit relation between the matrix elements of the coupling and the imaginary potential W can be found in Satchler (1983),

$$W_{hh}^2 \approx \pi \sum_\alpha \frac{V_{h\alpha}^2}{D}, \tag{16}$$

where D is the average level spacing of the many-body states. Using the approximation $|E_\alpha - E_i| \approx D/2$ and the definition in Eq. (16) we obtain from Eq. (15) that $c_h^{-2}(i) \approx 1 + 4W_{hh}/(\pi D)$ and $c_h^2(i)$ then exceeds 0.5 roughly when $D > W_{hh}$.

The condition is now expressed in terms of phenomenological optical potentials and level distances. Only states coupling to the halo basis state contribute to the optical potential in Eq. (16), and D is the average distance between those levels. The coupling could as well be explained as proceeding via doorway or hallway states of special structure (Gadioli and Hodgson, 1992), for example, two-particle/one-hole states which in turn couple to more complicated states. This description eliminates many of the coupling matrix elements in Eq. (16), but a consistent counting of levels leading to D must be introduced. The condition, $D > W_{hh}$, is expected to remain valid with both sides of the inequality redefined. However, fewer levels and detailed knowledge of the couplings could reduce the uncertainties, especially those related to shell structure.

2. Nuclear ground-state halos

Well-defined single-particle states imply spectroscopic factors close to unity. At the lowest limit of 0.5, where halo formation may occur, other components in the many-body wave function are as important. Still the single-particle s and p states close to threshold are essential for the occurrence of two- and three-body halos. The general properties are most easily illustrated by using the square-well potential with realistic depth and radius parameters appropriate for neutrons, i.e., $V \approx V_0[1 - (N-Z)/(2A)]$, $R \approx r_0 A^{1/3}$, where $r_0 \approx 1.35$ fm, $V_0 \approx -50$ MeV, N and Z are neutron and proton numbers, and $A = N + Z$. The wave numbers inside and outside the well, respectively, are $K^2 = 2m(V_0 + E)/\hbar^2$ and $\kappa^2 = -2mE/\hbar^2$. The wave function inside is the spherical Bessel function $j_l(r)$ while that outside is the related outgoing Hankel function $h_l^{(+)}(i\kappa r)$. The conditions for zero-energy solutions for given l then become $j_{l-1}(KR) = 0$, which reduces to $\cos(KR) = 0$ and $\sin(KR) = 0$ for $l = 0$, 1, respectively. The solutions for s waves are

$$\left(1 - \frac{N-Z}{2A}\right) A^{2/3} = \frac{\hbar^2 \pi^2 (n - 1/2)^2}{2m r_0^2 (-V_0)} \tag{17}$$

and p waves are analogously obtained by replacing $n - 1/2$ by n, where $n = 1,2,3,...$ is a nonzero integer.

The solutions of Eq. (17) appear as curves in the $N - Z$ nuclear chart. Along the beta stability line we find $A_0 \approx 0.4$, 11, 55, 164 for s states and $A_1 \approx 4$, 31, 112 for p waves. The spin-orbit interaction would affect the p-wave results. From Siemens and Jensen (1987) it is numerically found that $A_1 = 2$, 28, 105 and $A_1 = 4$, 34, 116 for $p_{3/2}$ and $p_{1/2}$ states, respectively. The square-well results agree fairly well with the weighted p-wave averages obtained from these values. The numbers change as the neutron dripline is approached, i.e., $A_0 \approx 1$, 14, 69, 196 and $A_1 \approx 5$, 39, 136 for the s and p waves, respectively. These extrapolations are in fair agreement with Hartree-Fock-Bogoliubov computations using the SKM* interaction (Dobaczewski *et al.*, 1994) while deviating substantially from relativistic mean-field computations (Sharma *et al.*, 1994).

The possible halos for beta-stable nuclei must occur as excited states with energies close to the neutron separation energy. Otherwise the halo binding energy would be too large. Moving towards the dripline, halos may occur

as low-lying excitations or as the nuclear ground state. The square-well estimates reveal the overall behavior but cannot be correct in detail for several reasons, e.g., bad radial shape, lack of self-consistency, large extrapolations in nucleon numbers, and possible strong configuration mixing.

The approach to the threshold of zero *s*-state energy is interesting since halos would occur before the extreme limit. The behavior with energy and nucleon number along the beta stability line can be found in many textbooks (Bohr and Mottelson, 1975; Siemens and Jensen, 1987) for realistic potentials. The first observation is that the single-particle levels cross each other. This implies a change of shell structure, as the chemical potential increases or as the dripline is approached (Dobaczewski *et al.*, 1996; Utsuno *et al.*, 1999). Furthermore, the *s* states approach zero energy with changing nucleon number much more slowly than the higher angular momenta. Thus occupation of an *s* state close to zero energy becomes possible for more nuclei than expected from just counting *s* states crossing -7 MeV as a function of A along the beta stability line (Hamamoto, 2001). The same tendency, though less pronounced, is also seen for *p* states, but almost absent for higher l values.

These observations imply that nuclear halos may occur in heavy as well as light nuclei. The distribution of single-particle energies as a function of *N, Z*, and energy remains crucial for localizing halo candidates. These are the same pieces of information needed to study the special stability arising for some nucleon numbers away from the well-known beta stability line (Utsuno *et al.*, 1999).

Detailed study of the configuration interactions in the shell model are necessary to determine whether halos in heavy nuclei are likely to be seen. If the energy of, for example, a *p* state remained close to zero as its neutron occupation increased, then many-body halos would seem possible, as suggested by Meng and Ring (1998). However, the particles would not remain uncorrelated as assumed in the mean-field approximation. Clusters would be formed and halo features would disappear when all correlations were allowed between many valence particles.

The total single-particle level density g increases linearly with the volume and the nucleon number A. The *s* and *p* single-particle level density $g_{s,p}$ increases on average only as $A^{1/3}$. The number of halos as a function of nucleon numbers is then equal to $g_{s,p}$ measured at the Fermi energy times the size s_w of the window allowing halos. This window size probably decreases in inverse proportion to the square of the nuclear radius, which usually increases as $A^{2/3}$, and the number of halos, $g_{s,p}s_w$, would vary as $A^{-1/3}$. However, this scaling of radii is not valid for very unstable nuclei, and in addition the slow variation of *s* and *p* single-particle energies close to the threshold must increase the window size. The number of halos would then on average be more abundant than indicated by this estimate, which in any case is unreliable due both to specific shell structure and to large fluctuations of the number of low-lying single-particle levels.

3. Nuclear halos in excited states

The single-particle *s* or *p* components of a given state determine the halo properties. The coupling to other many-body states due to the finite excitation energy E^* can be estimated from the imaginary part of the optical potential W (Siemens and Jensen, 1987),

$$W(r)=\left(W_0-4W_1a_W\frac{\partial}{\partial r}\right)\frac{1}{1+\exp[(r-R_w)/a_w]}, \quad (18)$$

where $R_w=r_wA^{1/3}$, $r_w\approx 1.25$ fm, $a_w\approx 0.5$ fm, and

$$W_0\approx\frac{(B+E_F)^2+\pi^2T^2}{60\ \text{MeV}}, \quad (19)$$

$$W_1\approx W_s\left(1\pm\frac{N-Z}{A}\right). \quad (20)$$

Here $+$ refers to protons and $-$ to neutrons, $E_F(<0)$ is the Fermi energy, T is the effective temperature related to $E^*\approx aT^2$, and the level-density parameter $a\approx A/(7.5\,\text{MeV})$. The expression for W_0 is taken from Baym and Pethick (1978) and Jeukenne *et al.* (1976), and its numerical value is negligibly small for small E^*.

The expectation value for the radial wave function ϕ of the single-particle state is then

$$W_{hh}=\int|\phi(r)|^2W(r)r^2dr\approx 2\kappa(R_wW_0+2.4a_wW_1), \quad (21)$$

where the approximation assumes an *s*-wave halo state with $r^2|\phi(r)|^2\approx 2\kappa\exp(-2\kappa r)$ valid for negligible Coulomb contribution (Jensen and Riisager, 2000). The condition $D>W_{hh}$ with $D\approx D_0\exp(-2\sqrt{aE^*})$ for neutrons then becomes

$$\frac{Z}{A}\sqrt{B}\exp(2\sqrt{aE^*})<0.1\frac{D_0}{W_s}\sqrt{\frac{\hbar^2}{2\mu a_w^2}}\approx\frac{1}{2}\sqrt{\text{MeV}}, \quad (22)$$

where we used $D_0\approx 7$ MeV from Jensen and Riisager (2000) and $W_0\ll W_s\approx 12$ MeV from Siemens and Jensen (1987). If the particle is a proton we should replace Z by the number of neutrons N.

For a *p*-wave neutron halo state we assume $3\kappa R<1$ MeV and obtain analogously the condition

$$\frac{Z}{A^{4/3}}\exp(2\sqrt{aE^*})<0.3\frac{D_0}{W_s}\frac{r_w}{a_w}\approx 0.5, \quad (23)$$

which is independent of binding energy, reflecting that the *p*-wave probability remains at finite distance even for $B=0$, in contrast to the diverging *s* waves (Riisager *et al.*, 1992; Hamamoto *et al.*, 2001). The condition in Eq. (23) is always fulfilled for dripline nuclei for $E^*=0$, but finite excitations quickly prevent *p*-wave halo formation. For protons N is replaced by Z.

In Eqs. (22) and (23), the only somewhat less well known parameter is D_0/W_s, which enters linearly in contrast to the exponential excitation energy dependence. Although for small E^* the precise value can be important, it hardly matters for finite E^*. Rewriting Eqs. (22) and (23) we find

$$B < 250\ \mathrm{keV}\frac{A^2}{Z^2}\exp(-4\sqrt{aE^*}) \quad \text{for } s \text{ states}, \quad (24)$$

$$Z < 0.5\ A^{4/3}\exp(-2\sqrt{aE^*}) \quad \text{for } p \text{ states}. \quad (25)$$

The replacement $Z \leftrightarrow N$ for protons is valid only when the tail of the wave function is unaffected by the Coulomb interaction. The upper limit of B decreases exponentially with E^* from 1 MeV at $E^*=0$ to fractions of an eV at high E^*. The chances of seeing excited-state halos close to stability are negligible, in agreement with the comprehensive information about neutron s states close to threshold coming from low-energy neutron scattering experiments (Lynn, 1968; Allen and Musgrove, 1978).

The neutron single-particle s-wave strength is large for $A \approx 55$ and $A \approx 164$, but this does not imply that halo structures exist. The corresponding largest measured s-wave neutron-scattering lengths a_{nc} are 15 and 47 fm (Koester *et al.*, 1991). The energy of the virtual state is then about $\hbar^2/(2ma_{nc}^2) \approx 92$ and 9.4 keV, which is at least ten orders of magnitude larger than the upper limits obtained from Eq. (24) with an excitation energy of around the neutron separation energy of 7 MeV. The virtual-state energy measures the energy distance from the threshold of the possible halo state and as such it is compared with the estimate of the upper binding-energy limit. Although these are the most favorable cases among stable nuclei (apart from very light nuclei), they do not appear very promising; only low-lying states can be expected to have s-wave halo features.

The two-body halo occurrence condition is equivalent to a large a_{nc}. Adding another neutron would produce a smaller nonhalolike three-body ground state, but with the help of the already large a_{nn} the first excited Efimov state is now possible. It must occur when the neutron-core halos are extremely pronounced. Large scattering lengths are the conditions for both two- and three-body halos, and in general they must therefore appear in the same regions of the nuclear chart.

Below the breakup threshold the fragmentation of the halo state into many-body states is already substantial for a relatively low excitation energy. Above the breakup threshold when the states start to overlap, i.e., when the average width is comparable to the level spacing and only a single decay channel is open, width collectivization occurs (Rotter, 1991; Zelevinsky, 1996). One state couples strongly to the continuum and thus regains single-particle character, whereas the others essentially decouple. This regime is reached about 1 MeV above the channel threshold. Large (n,γ) radiative capture cross sections could arise due to enhanced single-particle strength both below the threshold reached after γ emission and above the threshold populated before γ emission. These possibilities are not yet explored, but most likely the properties of halos are not directly involved.

As emphasized by Vogt (2002) one might expect that the behavior of strength functions close to a (single-neutron) threshold would be related to halo occurrence. The cluster fraction may be too small to allow halo formation, but the small single-particle halolike components in each many-body state would still be influenced by proximity to the threshold. Such collective effects might then be visible in appropriate strength functions. However, as far as halos are concerned, qualitatively new phenomena cannot be expected, since neutron strength functions at the single-neutron threshold are well described in detail from standard points of view (see, for example, Lynn, 1968).

Establishing a connection would of course still be valuable, and one could look for enhancements of specific effects, e.g., parity mixing in heavy nuclei (Mitchell *et al.*, 1999, 2001). Such an effect might be present for halo states effectively due to a lower energy spacing between opposite parity states (Feshbach *et al.*, 2000). Explicit calculations have so far only been done for ^{11}Be with low-lying bound $1/2^+$ and $1/2^-$ states, but other halo states could also be affected through mixing with low-lying continuum states. More calculations are needed before a final picture can be drawn.

III. EXAMPLES OF HALO STRUCTURE

The general structures described in the previous section can be illustrated by examples of two-, three-, and many-body halos from nuclear, atomic, and molecular physics. Dividing the many-body system degrees of freedom into (few) active and (many) frozen variables is the first task. The accuracy of this approximation depends on which observable is considered. On the other hand, the frozen intrinsic degrees of freedom begin to contribute substantially to the value of any relevant observable, the halo structure has most likely disappeared.

A. Common features

The deviation from the asymptotic s-wave two-body relation between size and binding energy can be quantified by φ defined as $\langle r^2\rangle = 3\hbar^2\varphi/(2\mu B)$. The quantity φ can be approximated by a universal function of $\epsilon = B/B_{\max}$ (see Lombard, 2001a), which varies in the interval [1/6, 1]. The interactions may vary from Coulomb-like via power-law potentials to short-range potentials. The radius decreases as a function of binding energy from infinity for $B=0$ or $\epsilon=0$. This improved scaling relation is valid independently of the details of the potential only when the bulk of the wave function is in the nonclassical region.

Some diatomic molecules almost reach the lowest possible value $\varphi(0)=1/6$, reflecting that these molecules are in the nonclassical region and therefore also have pronounced halo states. The decoupling from other degrees of freedom is often much better verified for molecules that clusterize in a natural way without overlap of their individual density distributions. Halos could then be very pronounced although their structure is relatively simple.

Known halo nuclei correspond to values of φ between 0.27 and 0.53. Even the zero binding limit is influenced

by many-body effects from coupling of the different degrees of freedom. The density overlap is larger than for molecules, and configuration mixing limits halo appearance via the second occurrence condition. Molecular halos should thus be more abundant. In nuclei where a natural clusterization does not exist *a priori* halos should be fewer and possibly have a more complicated structure.

1. Basic ingredients

The cluster division and the corresponding interactions are first chosen. At this stage, some care must be exercised. To illustrate, we consider a two-body system with reduced mass μ with a spherical Gaussian potential $\hbar^2/(2\mu r_e^2)(-v_0)\exp(-r^2/r_e^2)$. We use a normalized Gaussian wave function $\propto\exp[-r^2/(2b^2)]$ as the trial s state with b as a variational parameter. The energy is then $E=\hbar^2/(2\mu r_e^2)[3/(2x)-v_0(1+x)^{-3/2}]$, where $x\equiv(b/r_e)^2$. The derivative of E vanishes for $(1+x)^5=v_0^2x^4$, determining b and $E=\hbar^2/(2\mu r_e^2)[3/(2x)-(v_0^2/x)^{1/5}]$. The solution $E=0$ is obtained for $x=2$ corresponding to the critical value $v_0=3^{5/2}/4$. The mean-square radius is then also finite, $\langle r^2\rangle=3r_e^2$, in contrast to the correct diverging result in Eq. (1). Thus the *a priori* selected Hilbert space does not even allow the qualitative divergent behavior.

The same analysis with an exponential wave function instead of the Gaussian leads to a diverging mean-square radius when the energy approaches zero. The exponential is thus more appropriate and gives the correct asymptotic behavior. Extending to three-body systems, we find that the Jacobi coordinates are the natural choice, i.e., the relative coordinates between one pair of particles (x) and between their center of mass and the third particle (y). Parametrized wave functions with Gaussians in x and y again produce a qualitatively wrong behavior. Use of exponentials improves the asymptotic behavior but mostly for the two-body subsystem related to the x coordinate. For the remaining two-body subsystems the asymptotically correct relative motion cannot be simultaneously reproduced. This is only achieved through the Faddeev decomposition of the wave function, in which the two-body components are explicitly introduced in their corresponding Jacobi coordinates. Then the qualitatively correct energy-size behavior is reproduced, even for the delicate structures arising from the Efimov effect.

The lesson to be drawn is that the size of the basis is less important than the shape of the functions. For halos the large-distance asymptotics of a bound state are crucial, and the space must allow the correct behavior. In particular, Gaussians are in general not at all suited. This explains why the elaborate cluster models based on linear combinations of Gaussians do not reproduce well-pronounced halo structures (Kanada-En'yo *et al.*, 1995). Increasing the number of basis functions alleviates this problem, and a good accuracy may be obtained with a sufficiently large basis. However, the correct divergent behavior possible for extreme cases requires bases with the asymptotically correct shapes. Models like the interacting shell model often use harmonic-oscillator basis functions (Koonin *et al.*, 1997; Brown, 2001; Langanke and Martínez-Pinedo, 2003). Because the primary goal of these models is to explain the energies and transitions many oscillator shells of moderate length parameter are much more efficient at this than those required to reproduce the spatial extension of halos. Thus interacting shell models are also not well suited for halo computations.

By definition the asymptotic behavior corresponds to distances beyond the short-range interactions. It is independent of the detailed structure of the potential and can therefore be determined by using zero-range interactions (Demkov and Ostrovskii, 1988). However, this simplification requires a renormalization to avoid the collapse of the ground state, an effect known as the Thomas collapse (Thomas, 1935). Several techniques using various physical parameters are now available (Bertsch and Esbensen, 1991; Adhikari *et al.*, 1995; Esbensen *et al.*, 1997; Bedaque *et al.*, 1999; Fedorov and Jensen, 2002).

The reduction of the available space associated with the division into inert and active degrees of freedom also requires a renormalization of the interaction. This is a major concern in shell-model theory where the interaction is adjusted to the basis. The correct energy of the state can be reproduced while the wave function is constrained within a smaller space. The operators corresponding to observables also have to be renormalized.

For halos we want both the energy and the radial extension to be correct. It seems best to first select the effective two-body interactions in agreement with the available low-energy scattering data which determine the large-distance behavior. A few parameters like scattering length, effective range, and shape parameter, or alternatively, resonance energies may be sufficient. When known they can be used directly as input parameters. The active degrees of freedom must then be treated to the accuracy required. No operator renormalization should be used, reflecting the assumption that halo properties can be fully described by these degrees of freedom. Corrections from the neglected degrees of freedom are treated at a later stage, providing a test of the initial assumption.

Significant corrections may arise from the mixing of configurations corresponding to several cluster divisions when their thresholds are close. Such cases are rare. One component usually dominates, and the effective interactions can be adjusted to account for the remaining pieces. Direct inclusion of several clusters may be necessary at some level of accuracy or to provide a deeper understanding (Csoto, 1993; Arai *et al.*, 1999, 2001).

2. Lessons to be learned

For weakly bound systems the low-energy two-body scattering properties account for the main part of the structure. One example is the deuteron, in which widely differing nucleon-nucleon potentials reproduce the principal properties. Effective-range theory explains this

fact. It also shows that the overall properties (binding and radius) of the deuteron provide little information about the details of the interaction. Only scattering length and effective range are important. To learn more it is necessary to have either more details or higher accuracy.

Getting useful information about the nucleon-nucleon interaction relevant to halos from dilute nuclear matter properties is not straightforward. Matter so dilute that only two particles can interact is found only in the free nucleon-nucleon interactions. From matter at nuclear saturation density, we learn about the effective nuclear interaction within the nucleus. For intermediate densities there are most likely significant contributions from the frozen degrees of freedom.

For few-body structure to be applicable, as in the case of neutrons surrounding a core, the overlap of the constituent particles must be relatively small. This is not far from the limit where the free interaction is appropriate. Deviations arising from the neutron probability at the surface region of the core can be accounted for by density-dependent effective interactions. However, this goes against the few-body model assumptions by involving the intrinsic degrees of freedom. The cluster occurrence criterion is relevant in this connection. There may be only a small window open for halo occurrence. How small can be answered by understanding the transition from ordinary nuclei via clusters to halos.

Since halos in s and p states necessarily have an overlap with the core, excitation of the core degrees of freedom is likely. At the two-body level this can be accounted for by means of effective two-body potentials reproducing two-body scattering. Polarization effects beyond these two-body interactions must be included in another way, e.g., three-body potentials or by directly including excitations of the constituents.

Still the starting point has to be the completely decoupled approximation, providing a reference for improvements beyond the few-body structure. However, the inescapable effects of the intrinsic degrees of freedom have to be mocked up, for instance, by effective potentials or direct couplings to selected states.

The situation is thus that of a nearly decoupled halo structure, influenced to some degree by the substructure of its constituents. Systems, in which a dominant structure is weakly perturbed by couplings to the intrinsic structure of its building blocks, although not abundant within nuclear physics, occur often, e.g., in the combinations of degrees of freedom associated with atomic-nuclear, nuclear-nucleonic, and atomic–solid-state degrees of freedom. An exotic example of possible mixing of molecular and nuclear degrees of freedom is burning water, in which the water molecule H_2O within the measured accuracies has the same energy as a nuclear resonance level in ^{18}Ne (Belyaev *et al.*, 2001).

From a decoupled approximation we can first of all expect to learn about the properties of the systems, i.e., whether they are of halo structure or not. We can classify the states in groups with various universal features, e.g., Borromean, tango, Efimov, s- or p-wave dominated, ground or excited states. We can characterize states in neighboring systems as isobaric analogs or transitional states between halos and other ordinary structures. The characterization is conveniently found by using the scaling plots for two- and three-body systems. The properties of these classes then allow predictions and conceptual connections between subfields.

The classification we propose is independent of the details of the interactions. The necessary effective interactions can sometimes be extracted from the results of *ab initio* calculations, e.g., for atomic-molecular systems. For nuclear systems this possibility is still more remote. We can instead rely on phenomenology to learn about the in-medium nucleon-nucleon or nucleon-nucleus interactions and develop methods to bridge the gap from zero to nuclear matter densities and the gap between few-body and many-body problems.

B. Two-body systems

We shall concentrate on bound states below thresholds for decays into other structures. States above such thresholds are interesting but outside the scope of this section.

1. Nuclei

The combined requirements of low excitation energy and low Coulomb and centrifugal barriers strongly suggest we look at the nucleon driplines. Thresholds for simultaneous emission of several neutrons are above the one-neutron binding energy although they become close for increasing nucleon numbers. Thresholds for emission of several charged particles could be lower than one-proton emission but now the Coulomb barrier prevents both decay and halo formation. An example of such a cluster threshold could be ^{8}Be, which is only 92 keV above the energy of two free α particles. The α decay width is about 10 eV, indicating that the Coulomb barrier is substantial. This decay could also be called spontaneous fission, which otherwise is the dominating decay mode only for stable nuclei heavier than uranium. This illustrates that the division into binary fission fragments does not allow significant halo structure even close to or above the threshold. Rare-earth nuclei, in which fission is energetically favored and only prevented by a large barrier, do not form halos. This is not even possible for the actinides, in which the fission barrier or cluster threshold is relatively small. The decoupling of the corresponding degrees of freedom cannot be taken as a good approximation. Thus the existence of close- or low-lying thresholds is not a sufficient condition for formation of a halo.

We therefore return to the regions along the nucleon driplines. The ground-state two-body candidates (neutron plus core) are the heaviest isotopes with positive neutron separation energy S_n. The tail of the radial wave function is $\exp(-\kappa r)$ where $\kappa^{-1} \sim 5-10$ fm for halos and $\sim$1.5–2.0 fm for ordinary nuclei. We have collected in Table I a number of established or suggested one-nucleon halo candidates. The deuteron, $^2_1$H$_1$, with a

TABLE I. Two-body halo candidates. The columns give cluster division of the system, excitation energy E^* (MeV), separation energy S (MeV), orbital angular momentum quantum number l of the dominating components and references.

System	E^*	S	l	References
$^{2}_{1}H_{1}$ $(n+p)$	0.0	2.2	0	Audi and Wapstra, 1995
$^{11}_{4}Be_{7}$ $(^{10}_{4}Be_{6}+n)$	0.0	0.50	0	Audi and Wapstra, 1995
$^{14}_{5}B_{9}$ $(^{13}_{5}B_{8}+n)$	0.0	0.97	0	Ajzenberg-Selove, 1991
$^{15}_{6}C_{11}$ $(^{16}_{6}C_{10}+n)$	0.0	1.22	0	Ajzenberg Selove, 1991
$^{19}_{6}C_{13}$ $(^{18}_{6}C_{12}+n)$	0.0	0.53	0,2	Nakamura *et al.*, 1999
$^{31}_{10}Ne_{21}$ $(^{30}_{10}Ne_{20}+n)$	0.0	>0	1,3	Sakurai, 2002
$^{34}_{11}Na_{23}$ $(^{33}_{11}Na_{22}+n)$	0.0	?	1,3	Audi and Wapstra, 1995
$^{35}_{12}Mg_{23}$ $(^{34}_{12}Mg_{22}+n)$	0.0	?	1,3	Audi and Wapstra, 1995
$^{40}_{13}Al_{27}$ $(^{39}_{13}Al_{26}+n)$	0.0	>0	1,3	Sakurai, 2002
$^{43}_{14}Si_{29}$ $(^{42}_{14}Si_{28}+n)$	0.0	>0	1,3	Notani *et al.*, 2002
$^{4}_{2}He_{2}$ $(^{3}_{2}He_{1}+n)$	20.21	0.36	0	Tilley *et al.*, 1992
$^{10}_{4}Be_{6}$ $(^{9}_{4}Be_{5}+n)$	6.26	0.55	0	Ajzenberg-Selove, 1990
$^{10}_{4}Be_{6}$ $(^{9}_{4}Be_{5}+n)$	5.96	0.85	0	Ajzenberg-Selove, 1990
$^{11}_{4}Be_{7}$ $(^{10}_{4}Be_{6}+n)$	0.32	0.18	1	Endt, 1990
$^{12}_{5}B_{7}$ $(^{11}_{5}B_{6}+n)$	2.62	0.65	0	Ajzenberg-Selove, 1990
$^{12}_{5}B_{7}$ $(^{11}_{5}B_{6}+n)$	2.72	0.55	1	Ajzenberg-Selove, 1990
$^{14}_{5}B_{9}$ $(^{13}_{5}B_{8}+n)$	0.74	0.23	1	Ajzenberg-Selove, 1991
$^{17}_{6}C_{11}$ $(^{16}_{6}C_{10}+n)$	0.29	0.44	0,2	Tilley *et al.*, 1993
$^{18}_{7}N_{11}$ $(^{17}_{7}N_{10}+n)$	2.61	0.22	1	Tilley *et al.*, 1995
$^{21}_{8}O_{13}$ $(^{20}_{8}O_{12}+n)$	3.08	0.73	?	Endt, 1990
$^{25}_{10}Ne_{15}$ $(^{24}_{10}Ne_{14}+n)$	3.32	0.96	?	Endt, 1990
$^{25}_{10}Ne_{15}$ $(^{24}_{10}Ne_{14}+n)$	4.07	0.11	?	Endt, 1990
$^{2}_{1}H_{1}$ $(n+p)$	0.0	2.2	0	Audi and Wapstra, 1995
$^{8}_{5}B_{3}$ $(^{7}_{4}Be_{3}+p)$	0.0	0.138	1	Audi and Wapstra, 1995
$^{12}_{7}N_{5}$ $(^{11}_{6}C_{5}+p)$	0.0	0.60	1	Audi and Wapstra, 1995
$^{22}_{13}Al_{9}$ $(^{21}_{12}Mg_{9}+p)$	0.0	≈0.02	0,2	Audi and Wapstra, 1995
$^{23}_{13}Al_{10}$ $(^{22}_{12}Mg_{10}+p)$	0.0	0.13	0,2	Audi and Wapstra, 1995
$^{21}_{14}Si_{7}$ $(^{20}_{13}Al_{7}+p)$	0.0	?	0,2	
$^{26}_{15}P_{11}$ $(^{25}_{14}Si_{11}+p)$	0.0	≈0.1	0,2	Audi and Wapstra, 1995
$^{27}_{15}P_{12}$ $(^{26}_{14}Si_{12}+p)$	0.0	0.90	0,2	Audi and Wapstra, 1995
$^{31}_{17}Cl_{14}$ $(^{30}_{16}S_{14}+p)$	0.0	0.29	0,2	Audi and Wapstra, 1995
$^{35}_{19}K_{16}$ $(^{34}_{18}Ar_{16}+p)$	0.0	0.078	0,2	Audi and Wapstra, 1995
$^{4}_{2}He_{2}$ $(^{3}_{1}H_{2}+p)$	20.21	−0.40	0	Tilley *et al.*, 1992
$^{17}_{9}Fe_{8}$ $(^{16}_{8}O_{8}+p)$	0.50	0.105	0	Ajzenberg-Selove, 1991
$^{21}_{11}Na_{10}$ $(^{20}_{10}Ne_{10}+p)$	2.42	0.007	0	Endt, 1990
$^{3}_{\Lambda}H_{1}$ $(d+\Lambda)$	0.0	0.14	0	Gibson, 2001
$^{6}_{\Lambda}He_{2}$ $(^{5}_{\Lambda}He_{2}+n)$	0.0	0.17	1	Hiyama *et al.*, 1996 and 2001
$^{8}_{4}Be_{4}$ $(^{4}_{2}He_{2}+^{4}_{2}He_{2})$	0.0	−0.092	0	Audi and Wapstra, 1995

binding energy of 2.2 MeV can be classified as a (proton and neutron) halo state (Hansen *et al.*, 1995). Neglecting the intrinsic nucleon structure, the system is a genuine two-body system, and the only bound state is a relative s state with a small d admixture caused by the tensor interaction.

The helium isotopes display a very pronounced odd-even mass variation. All odd isotopes heavier than $^{4}_{2}He_{2}$ are neutron unstable, whereas all known even isotopes are one-neutron bound. The heaviest, $^{10}_{2}He_{8}$, with $S_n \approx 2.2$ MeV is the first to be unbound with respect to two-neutron emission, with $S_{2n} \approx 1.1$ MeV (Korsheninnikov *et al.*, 1994; Ostrowski *et al.*, 1994). Thus two-body halos are prevented by a particle unstable core, since S_n is larger than the two-neutron separation energy S_{2n} of these even isotopes.

This odd-even behavior is systematic along the dripline. Therefore in two-body neutron ground-state halos the neutron number N should be odd, with $0 < S_n(N) < 1$ MeV and $S_n(N+2) < 0$. If the last positive neutron separation energy is larger than 1 MeV the halo is insufficiently developed as for $^{8}_{3}Li_{5}$, $^{22}_{6}N_{15}$, $^{23}_{8}O_{15}$, $^{26}_{9}F_{17}$,

$^{29}_{10}Ne_{19}$, and $^{41}_{14}Si_{27}$. For $^{34}_{11}Na_{23}$ ($S_n \approx 1.1$ MeV) and $^{35}_{12}Mg_{23}$ ($S_n \approx 0.23$ MeV) the bindings are obtained by extrapolation. Uncertainties are generally of the order of the values themselves.

The neutron dripline is currently not known with certainty above Ne. Possible halos with low S_n are specified in Table I. The valence neutron in $^{11}_{4}Be_7$ is an *s*-state halo, as seen in Fig. 2. The relatively large S_n for $^{14}_{5}B_9$ indicates that even for the expected *s* state the halo should not be much extended. In contrast, $^{19}_{6}C_{13}$ satisfies the halo criterion of Fig. 2 while $^{17}_{6}C_{11}$ is too small, indicating a dominating $l=2$ component. Other candidates are $^{31}_{10}Ne_{21}$ and $^{40}_{13}Al_{27}$, in which the neutron bindings are unknown but positive and probably very small.

The low binding energies in Table I must be accompanied by low orbital angular momentum. The ground-state structures of carbon isotopes certainly include admixtures of $l=0$ and 2 through couplings to core excited 2^+ states. These nuclei are only halos if *s*-state configurations dominate. The stability of $^{34}_{11}Na_{23}$ and $^{35}_{12}Mg_{23}$ are not known, but the neutron separation energies could be very low or negative. These nuclei are thus potentially good candidates, since $l=1$ also might be the dominating structure.

In Fig. 2, $^{22}_{7}N_{15}$ appears above the $l=0$ curve at relatively large binding with large radius. This does not indicate a halo system, but rather signals either inconsistency between core density and classical turning point R or, as suggested by Kanungo *et al.* (2001), core modification due to the presence of the last neutron.

Excited one-neutron halo states may also occur. To find these we have to search for isotopes with excitation energies below S_n by at most 1 MeV. If these are not surrounded by many other excited states, they could represent halos provided the quantum numbers and the structure in general are correct. We list a number of possibilities in Table I.

The first possibility is the 0^+ excited state of the α particle at 20.21 MeV. It is not known whether a significant component of $n+^3_2He_1$ is present or whether a more collective behavior like a breathing mode might be a more suitable description. The *p* state in $^{11}_{4}Be_7$ is usually referred to as a halo state. The first excited state in $^{15}_{6}C_9$ would be a candidate if the *d* configuration in this $5/2^+$ state had been less dominating. The nuclei $^{17}_{6}C_{11}$, $^{18}_{7}N_{11}$, $^{21}_{8}O_{13}$, and $^{25}_{10}Ne_{15}$ also have excited states close to the neutron-emission threshold, but again the structure is not established and the *d* components may be too large.

The proton dripline could also support halo states, although the Coulomb barrier tends to confine the charge-density distribution. The odd-proton isotopes are again most likely to form one-proton halo states, though in this case the repulsive Coulomb interaction now rather favors even numbers. We have collected in Table I the cases along the dripline with $S_p<1$ MeV. The proton dripline is roughly known for all elements below uranium. It is likely the Coulomb potential prohibits proton halos above $^{35}_{19}K_{16}$.

The weakly bound $^{8}_{5}B_3$, with the proton in a *p* state, well studied in connection with the solar neutrino problem (Riisager and Jensen, 1993; Grigorenko *et al.*, 1999) has recently been analyzed more carefully with few-body techniques. The centrifugal and Coulomb barriers together confine the spatial extension to almost normal size, as expected for $^{12}_{7}N_5$. The binding energies of $^{17}_{9}F_8$, $^{22}_{13}Al_9$, $^{23}_{13}Al_{10}$, $^{26}_{15}P_{11}$, $^{27}_{15}P_{12}$, $^{31}_{17}Cl_{14}$, and $^{35}_{19}K_{16}$ are all rather small, as also expected for $^{21}_{14}Si_7$. The *s* components must dominate over the *d* component to overcome Coulomb confinement. We would also include $^{21}_{14}Si_7$, which is not yet known but quite possibly could have a very small proton binding energy.

Excited states below a few MeV and close to the proton separation energy are rather few for these light nuclei. Table I presents the two halo candidates in $^{17}_{9}F_8$ and $^{21}_{11}Na_{10}$. Furthermore, it is perhaps interesting to note that the excited state of the α particle is 0.40 MeV above the proton threshold and 0.36 MeV below the neutron threshold. Thus the possible halo could be a mixture of neutron and proton halos, even though the proton is unbound but held back by the Coulomb barrier.

In general many excited states exist above the proton threshold. They are resonances in the continuum, although their decay width may be so small that in practice they behave as bound states. However, halos may result from tunneling far into the barrier. This clearly becomes easier as the top of the Coulomb barrier is approached. However, simultaneously the width increases, the structure deviates more and more from that of a bound state, and the nonclassical region disappears. In short the halo picture is no longer valid. Closer to the threshold, tunneling is more difficult, the width is smaller, and the states are more similar to bound states. One example is provided by the different cluster divisions of two α particles in $^{8}_{4}Be_4$.

The isobaric analog states (Bohr and Mottelson, 1969) of a halo could be candidates for excited halo states, since they have the same structure as the original state except for the exchange of neutrons and protons. Thus a one-neutron halo could transform into a one-proton halo, which might be an excited state. In this case we must consider the Coulomb energy shift ΔE_C arising from the charge of the added proton. An estimate is $\Delta E_C \approx Ze^2/R$, where Z is the charge of the core and R is the radius of the halo particle. Using the *s*-state estimate $[R^2=\hbar^2/(4\mu B)]$ in Eq. (1) for the radius of a well-pronounced one-neutron halo, we then get

$$\Delta E_C \approx \frac{Z}{3}\sqrt{B\ \ 1\ \ \mathrm{MeV}} < 1\ \ \mathrm{MeV}\ \ \text{or}\ \ BZ^2 \leqslant 9\ \ \mathrm{MeV}. \tag{26}$$

Since the binding energy of a halo state is less than about 1 MeV, we conclude that $Z \leqslant 3$. Thus for $Z>3$ the analog of a neutron halo state would be above the threshold for proton binding, or if the proton is close to the threshold the initial state would not be a halo.

These considerations apply only for zero core isospin. For finite core isospin the analog state has two compo-

nents (Bohr and Mottelson, 1969), one similar to the neutron core state and one equal to the analog of the core and a neutron in the initial halo state. Both components correspond to excited states in the frozen single-particle basis. For halos to exist not only should the threshold for both analog states be at the right energy but the coupling between states should also not act destructively. Thus, except for the very lightest systems, these states are not very likely halos.

Another class of two-body states are the hypernuclei, in which the Λ particle is bound to a nucleus. The simplest of these strange nuclei is the hypertriton ${}^{3}_{\Lambda}\mathrm{H}_1$ consisting of a deuteron weakly bound to the Λ particle in a pronounced *s*-state halo (Cobis *et al.*, 1997; Gibson, 2001). The Λ-nucleus binding increases with the nuclear mass, and strange two-body ground-state halos are not possible, e.g., ${}^{5}_{\Lambda}\mathrm{He}_2$ in Table I. On the other hand, excited strange halo states may still occur.

More than one Λ particle can bind to an ordinary nucleus and give a sequence of possible strange two-body halos if the last Λ is in a sufficiently weakly bound low-angular-momentum state. Then the core also has finite strangeness, but the general principles for occurrence and structure remain unchanged. Since the Λ particle binds strongly to nuclei above hydrogen, another type of halo appears with nucleons surrounding a strange core, as in ${}^{6}_{\Lambda}\mathrm{He}_2$, with a very small neutron binding energy.

2. Atoms and molecules

The nuclear strong interaction falls off exponentially with distance. For atoms and molecular systems power-law potentials r^{-m} are the typical long-distance behavior. The exponent m is then an integer arising from corresponding electromagnetic multipole-multipole interactions. The larger the value of m, the shorter the range, and $m=2$ is the threshold dividing short- from long-range potentials.

The order of magnitude of the masses is given either by the electron mass m_e or by the nucleon mass m_N. The space dimensions are in the range of Å. For a halo the energies should therefore be smaller than typical values $B \approx 0.1\hbar^2/(\mu R^2)$, i.e., with $R=10$ Å in the two cases given by $B \approx 7$ meV or 4 μeV. These estimates must be quadratically rescaled if the classical turning point is very different from the value used for R.

The pure Coulomb case corresponding to electrons in atoms is $m=1$. An $m=1$ system could be very loosely bound and very large, like an atomic Rydberg state, for example. However, it is also well established that the largest parts of the wave functions reside in the classically allowed region, and semiclassical descriptions are rather accurate. Thus the wave functions may extend to larger and larger distances but in complete harmony remain proportional to the increasing extension of the potentials. These structures are excluded as halos by our second condition.

The generic case producing Efimov states is $m=2$. It is realized in nature for a charged particle interacting with neutral molecules with permanent electric dipole moments. The dipole moment introduces a directional dependence, and angular momentum is not conserved in the body-fixed system. Still the strength of such potentials must exceed a minimum value to allow binding, as we learned in the discussion of the Efimov effect. This strength corresponds to a critical value of $0.64ea_0$ (electron charge times Bohr radius), as already noted by Fermi and Teller (1947). The finite size of the molecule producing the dipole moment increases the critical value to about $0.8ea_0$ (Abdoul-Carime *et al.*, 2002). An efficient computational method has been introduced by Clary (1988) and recent *ab initio* calculations by Gutowski *et al.* (1998) and Skurski *et al.* (2000).

Experimentally information has been accumulating about electrons in such dipole bound states (Desfrancois, 1995; Abdoul-Carime *et al.*, 2002). The energies typically vary between 1 and 100 meV. The halo features could therefore be prominent. However, with decreasing energy the classical turning point in the $1/r^2$ potential increases dramatically and the mean-square radius of the state cannot be substantially larger, as seen in Fig. 2, where the scaled mean-square radius is always smaller than about 3. Thus, in the weak-binding limit, the dominance of the Yukawa tail prevents scaling, although r^{-2} potentials have (different) scaling properties. The systems may be extremely large and the appropriate length scale far exceeds 10 Å. As a consequence, binding energies much smaller than 7 meV are needed. The best halo candidates are propanal and formaldehyde very close to the limiting dipole moment for binding (Abdoul-Carime *et al.*, 2002).

The $1/r^2$ potential with sufficient attractive strength produces infinitely many bound states with energies predicted by Eq. (8). With a dipole moment $5\times 0.64\, ea_0$ ($\nu \approx 1$) the second state should then appear at a binding energy about three orders of magnitude smaller than that of the first, i.e., in the range of μeV. Dipole moments closer to the critical value decrease this estimate to dramatically smaller energies far outside the range of any experiment. However, an infinite series is not physical. The molecular deformation and the additional electron are coupled in their rotational motion in at least a two-channel problem. This coupling effectively changes the large distance of the potential and thereby rules out the theoretically possible infinitely many one-channel states of large spatial extension. To understand this effect one can imagine an electron far away for which one is not able to distinguish details like its orientation. Then the average over directions produces an interaction like the long-distance tail for a spherical, neutral molecule, i.e., $1/r^4$.

An increasing dipole moment increases the binding and an electron added to an excited molecular rotational state could then, after suitable couplings to other states, give an energy closer to the threshold. This seems like a mechanism that would produce a halo state, but then the ground state would be of normal size and would not explore the large-distance tail of the potential. The required binding energy of the excited state should be a

fraction of a meV, and the coupling changing the potential tail should be very small. These systems obtained by adding an electron to molecules with finite dipole moment provide interesting spatially extended structures, although most of them are not halos.

In the case of $m=3$, the large-distance behavior arises from the interaction between neutral systems with permanent dipole moments (LeRoy and Bernstein, 1969; Gao, 1999). At large distance the directional average leads to an effective $1/r^6$ behavior of the potential. Scaling properties can be formulated and exploited to predict energies of high-lying molecular vibrational states near the threshold from energies of a few other such states. Even more, the difference between the sixth root of the energies of such levels is a universal constant multiplied by a specific function of reduced mass and potential strength. However, this prediction, based on semiclassical assumptions, breaks down close to threshold, where the halos could be formed. Many atomic dimers as well as more complicated molecular systems have vibrationally excited states close to threshold (Gao, 1999). For molecules the binding energies must be in the range of μeV.

Another origin of $1/r^3$ behavior could be a charged particle interacting with a molecule with no dipole but a permanent electric quadrupole moment (Gutowski and Skurski, 1999; Abdoul-Carime *et al.*, 2002). The long-distance behavior is shifted to $1/r^4$ as for a negative ion due to the effective directional average. Now the above estimate of the limit of about 7 meV is appropriate, since the potential tail vanishes much faster. A few candidates like the succinonitrile molecule and the formamide dimer are described by Abdoul-Carime *et al.* (2002) together with the related uncertainties. Measurements have found them to be too bound to form a halo, whereas the calculations in some cases would allow it. The difference is thought to arise from correlation effects between valence electrons and molecular electrons.

The $m=4$ behavior appears in two neutral systems, one with a permanent dipole moment and the other with a permanent quadrupole moment. Another less exotic combination is a charged particle interacting with a neutral system.

Negative atomic ions present the most obvious examples. Their binding energies should not exceed about 10 meV. The H^- system has too large an electron binding energy, 0.75 eV, and a size comparable to the neutral atom. This implies existence of strong dynamic correlations between the two electrons beyond those caused by the Pauli principle. They repel each other and are most likely found on opposite sides of the charged proton core. This altogether excludes H^- from being a two-body halo state. We know that H^- has no excited bound states but a number of low-lying resonances (Balling *et al.*, 2000).

The binding energies of heavier negative atomic ions are easily smaller, as can be seen for Ca^- with 24.6 meV (Andersen *et al.*, 1997). However, even in this extreme case of small binding, the two-body structure is inappropriate. The correlations with the electrons in the neutral atom are very strong and the size is compatible with the size of Ca. Thus Ca^- is not a two-body halo state. All other known ground states are also excluded, but this simultaneously opens the possibility of excited-state halos.

For an electron bound to a neutral molecule, most structures would consist of a spatially localized electron either bound to one of the atoms or used as glue between two atoms. A truly ground-state electron-molecule two-body system is not very likely. However, in excited states an electron may be pushed to distances outside the atoms, where only the molecule as a whole is important. The binding energy should then be below a few meV.

A two-body system consisting of a neutral and a negatively charged molecule corresponds to a halo binding energy of at most a few μeV. The structure of such systems could as well be a (more complicated) molecule and an attached electron. An illustration is found in HeH^-, i.e., helium bound to the negative hydrogen atom (Li and Lin, 1999; Robicheaux, 1999). The electron binding of about 50 μeV is too large for halo formation. This case clearly favors the suggested negative molecule-molecule structure, since He^- is unbound. Combining H^- with other closed-shell atoms leads to stronger binding. Again this opens the door for excited-state halos. Which structure prevails cannot in general be decided *a priori*.

The $m=5$ behavior appears for two neutral systems, both with permanent electric quadrupole moments, for which all lower moments are zero. The large-distance behavior is shifted to $1/r^6$ due to the inevitable coupled-channel effects and direction averaging. For halos the binding energies have to be below a few μeV. Such systems have not yet been studied.

The case of $m=6$ is the induced dipole-dipole interaction, always present at large distances for neutral polarizable systems and in particular for two neutral atoms. The most prominent example is the atomic helium dimer $^4He_2$, with a binding energy of about 0.13 μeV and a size of about 50 Å (Schollkopf and Toennies, 1996; Nielsen *et al.*, 1998b). This is a beautiful two-body halo, the largest known, as seen in Fig. 2.

The critical stability of the helium dimer can be contrasted with the instability of $^4He^3He$, in which the mass of one of the nuclei is changed from four to three nucleons, while the molecular interaction is left completely unchanged. The corresponding increase in kinetic energy (the reduced mass is lowered by a factor 6/7) is sufficient to decrease the binding beyond the threshold of stability.

Another combination of helium isotopes, $^3He^6He$, maintains the reduced mass and therefore the binding energy of about 0.13 μeV, whereas $^4He^6He$ increases the reduced mass and consequently also the binding. The lightest elements in the Periodic Table are most affected by isotopic variations, which can be very important for such fragile structures.

A series of calculations of alkali-helium pairs resulted in a number of very weakly bound states (Yuan and Lin,

1998; Kleinekathofer *et al.*, 1999). The system ^{4}He^{6}Li is bound by about 0.13 μeV and ^{4}He^{7}Li by 0.49 μeV. The isotopes ^{4}He^{A}K ($A=39,40,41$) are bound by about 1.0 μeV, ^{4}He^{A}Rb ($A=85,87$) by 0.88 μeV, and ^{4}He^{133}Cs by 0.41 μeV. They are all very good examples of halo systems. Furthermore, ^{4}He^{23}Na is bound by 2.5 μeV, leaving enough room also to bind ^{3}He^{23}Na by 0.090 μeV. Both are halos. All the other examples come out as unbound when ^{4}He is replaced by ^{3}He.

C. Three-body systems

Using two-body effective potentials reproducing low-energy scattering properties (phase shifts) one can compute the three-body structure. If the three-body binding energy is not precisely reproduced, it is necessary to fine-tune, for example, by using a three-body interaction to account for contributions from the intrinsic particle degrees of freedom. This defines a basic model for analyzing the structure and reactions of three-body systems.

For attractive, short-range, two-body interactions the three-body system is more bound than the subsystems. Therefore a halo state arises only when the two-body subsystems are unbound or very weakly bound. The two-body systems could all be unbound (a Borromean system) or perhaps only one subsystem might be bound (a tango state). The Efimov effect is then close on the ordinary scale of binding, although perhaps far on the scale of the weak binding of these delicate structures.

Two-body subsystems must be either very weakly bound or low-lying resonances, or virtual states must be present, in order to support a halo state. There is a definite connection between the structure of the subsystems and for the three-body system properties. This includes the continuum spectrum of the three-body system (Glöckle *et al.*, 1996), which contains traces of some of the Efimov states when the Efimov conditions are approximately fulfilled. Thus the continuum structure could be very interesting even though not yet fully understood in terms of the structure of the two-body subsystem (Cobis *et al.*, 1998; Garrido *et al.*, 2002).

1. Nuclei

The most obvious three-body halo candidates are dripline nuclei with even numbers of neutrons or protons, in which the nucleus with one less neutron or proton is unbound or perhaps very weakly bound. We include in Table II Borromean systems with two neutrons, two protons, and some exotic divisions of Borromean and tango structure. The binding of non-Borromean two-neutron systems being generally larger than 2 MeV, we do not include them here as halo candidates. When the neutron-core system has a two-body bound state with zero energy, an additional neutron increases the binding energy by 1–2 MeV for light nuclei. Thus a few MeV is therefore an estimate of the smallest binding energy of non-Borromean two-neutron systems.

The two nuclei $^6_2$He$_4$ and $^{11}_3$Li$_8$ are prototypes of nuclear three-body halos. For $^6_2$He$_4$ the two-body interactions are well known, and the $p_{3/2}$ neutron core component is dominant in the n-$^4_2$He$_2$ subsystem, which is unbound, with a resonance energy at about 0.77 MeV. Still the measured three-body binding energy is about 1 MeV. Favorable circumstances for a halo are a small core radius and a repulsive s-wave interaction enlarging the system. Moving the resonance down from 0.77 MeV to zero would roughly add 1.5 MeV and produce a binding of about 2.5 MeV.

For $^{11}_3$Li$_8$ the s- and p-wave probabilities in the neutron core subsystem are roughly equal. The binding would increase from 0.3 MeV to about 1 MeV if the virtual s states and the p resonances were moved from their average values of about 0.4 MeV to zero energy. Spin splittings, conceptually of a hyperfine nature, arise from the 3/2 spin of the core coupled to the neutron angular momentum. These splittings appear to be relatively small for p waves but substantial for s waves (Garrido *et al.*, 2002). Only the statistical average of the positions is important for most observables like the energy, since the Pauli principle dictates corresponding population of both these spin-split states.

Substantial spin-splitting effects can occur when only one of the partners is occupied. This can be seen in 1^- excitations of $^{11}_3$Li$_8$, where the two neutrons may occupy the lowest of the spin-split s and p states, leaving the two highest unoccupied. Then the 1^- spectrum is lowered compared to any zero-core-spin model prediction.

An effect of spin splitting is that the neutron core states are different even for s states. Therefore if one of these two-body states has zero energy the other energy is different from zero. Thus the Efimov condition of two simultaneous zero-energy s states is highly unlikely for such systems with finite core spin (Fedorov *et al.*, 1995). The Coulomb interaction prevents the appearance of Efimov states, and only two-neutron halo systems are then possible. Candidates for Efimov states should therefore be sought among systems where two neutrons surround a spin-zero core, which automatically ensures two identical subsystems. Then the ground state is most likely bound by at least 1 MeV and the Efimov states should appear as a sequence of excited states close to the threshold energy.

The heaviest stable helium isotope is $^8_2$He$_6$, which, like $^6_2$He$_4$, is Borromean and which has an even stronger two-neutron binding. The stronger binding is enhanced by the closed-shell structure for helium, but such Borromean pairs are quite common, as can be seen in Table II, e.g., ($^{17}_5$B$_{12}$, $^{19}_5$B$_{14}$), ($^{29}_9$F$_{20}$, $^{31}_9$F$_{22}$), and ($^{35}_{11}$Na$_{24}$, $^{37}_{11}$Na$_{26}$). Another pair could be ($^{44}_{14}$Si$_{30}$, $^{46}_{14}$Si$_{32}$) if $^{45}_{14}$Si$_{31}$ were established as unbound. The pair ($^{41}_{13}$Al$_{28}$, $^{43}_{13}$Al$_{30}$) illustrates the discrete nature, since $^{40}_{13}$Al$_{27}$ is just neutron bound whereas $^{42}_{13}$Al$_{29}$ is probably unstable. The heaviest of such pairs very likely have admixtures of more complicated states arising from the intrinsic structure of the Borromean constituent.

The other examples in Table II show the established Borromean systems $^{14}_4$Be$_{10}$ and $^{38}_{12}$Mg$_{26}$, the almost certainly Borromean $^{22}_6$C$_{16}$, and the established non-

TABLE II. Three-body halo candidates. The columns give division of the system, separation energy $S=S_{2n}$ in MeV, orbital angular momentum l of the dominating nucleon-core components, remarks (B for Borromean, T for tango) and references as in Table I. Excited states are indicated by a star on the separation energy.

System	S	l	R	References
${}^{6}_{2}\mathrm{He}_4$ (${}^{4}_{2}\mathrm{He}_2+n+n$)	0.97	1	B	Audi and Wapstra, 1995
${}^{8}_{2}\mathrm{He}_6$ (${}^{6}_{2}\mathrm{He}_4+n+n$)	2.13	1	B	Audi and Wapstra, 1995
${}^{11}_{3}\mathrm{Li}_8$ (${}^{9}_{3}\mathrm{Li}_6+n+n$)	0.30	0,1	B	Audi and Wapstra, 1995
${}^{14}_{4}\mathrm{Be}_{10}$ (${}^{12}_{4}\mathrm{Be}_8+n+n$)	1.33	0,2	B	Audi and Wapstra, 1995
${}^{17}_{5}\mathrm{B}_{12}$ (${}^{15}_{5}\mathrm{B}_{10}+n+n$)	1.4	0,2	B	Audi and Wapstra, 1995
${}^{19}_{5}\mathrm{B}_{14}$ (${}^{17}_{5}\mathrm{B}_{12}+n+n$)	≈0.5	0,2	B	Audi and Wapstra, 1995
${}^{22}_{6}\mathrm{C}_{16}$ (${}^{20}_{6}\mathrm{C}_{14}+n+n$)	≈1	0,2	B	Audi and Wapstra, 1995; Sakurai *et al.*, 1999
${}^{29}_{9}\mathrm{F}_{20}$ (${}^{27}_{9}\mathrm{F}_{18}+n+n$)	≈0.9	0,1,2	B	Audi and Wapstra, 1995
${}^{31}_{9}\mathrm{F}_{22}$ (${}^{29}_{9}\mathrm{F}_{20}+n+n$)	>0	0,1,2,3	B	Sakurai, 2002
${}^{32}_{10}\mathrm{Ne}_{22}$ (${}^{30}_{10}\mathrm{Ne}_{20}+n+n$)	≈1	0,1,2,3	T	Audi and Wapstra, 1995
${}^{34}_{10}\mathrm{Ne}_{24}$ (${}^{32}_{10}\mathrm{Ne}_{22}+n+n$)	>0	0,1,2,3	B	Notani *et al.*, 2002
${}^{35}_{11}\mathrm{Na}_{24}$ (${}^{33}_{11}\mathrm{Na}_{22}+n+n$)	≈0.5	0,1,2,3	B	Audi and Wapstra, 1995
${}^{37}_{11}\mathrm{Na}_{26}$ (${}^{35}_{11}\mathrm{Na}_{24}+n+n$)	>0	0,1,2,3	B	Notani, 2002
${}^{38}_{12}\mathrm{Mg}_{26}$ (${}^{36}_{12}\mathrm{Mg}_{24}+n+n$)	≈1	0,1,2,3	B	Audi and Wapstra, 1995; Sakurai *et al.*, 1997
${}^{41}_{13}\mathrm{Al}_{28}$ (${}^{39}_{13}\mathrm{Al}_{26}+n+n$)	>0	0,1,2,3	T	Sakurai, 2002
${}^{43}_{13}\mathrm{Al}_{30}$ (${}^{41}_{13}\mathrm{Al}_{28}+n+n$)	?	0,1,2,3	B	
${}^{44}_{14}\mathrm{Si}_{30}$ (${}^{42}_{14}\mathrm{Si}_{28}+n+n$)	?	0,1,2,3	?	
${}^{46}_{14}\mathrm{Si}_{32}$ (${}^{44}_{14}\mathrm{Si}_{30}+n+n$)	?	0,1,2,3	?	
${}^{10}_{6}\mathrm{C}_4$ (${}^{8}_{4}\mathrm{Be}_4+p+p$)	3.821	1	B	Audi and Wapstra, 1995
${}^{17}_{10}\mathrm{Ne}_7$ (${}^{15}_{8}\mathrm{O}_7+p+p$)	0.950	0	B	Audi and Wapstra, 1995
${}^{20}_{12}\mathrm{Mg}_8$ (${}^{18}_{10}\mathrm{Ne}_8+p+p$)	2.325	0,2	B	Audi and Wapstra, 1995
${}^{22}_{14}\mathrm{Si}_8$ (${}^{20}_{12}\mathrm{M}_8+p+p$)	≈−0.2	0,2	B	Audi and Wapstra, 1995
${}^{24}_{15}\mathrm{P}_9$ (${}^{22}_{13}\mathrm{Al}_9+p+p$)	≈0.76	0,2	T	Audi and Wapstra, 1995
${}^{27}_{16}\mathrm{S}_{11}$ (${}^{25}_{14}\mathrm{Si}_{11}+p+p$)	≈0.90	0,2	B	Audi and Wapstra, 1995
${}^{29}_{17}\mathrm{Cl}_{12}$ (${}^{27}_{15}\mathrm{P}_{12}+p+p$)	≈0.68	0,2	T	Audi and Wapstra, 1995
${}^{31}_{18}\mathrm{Ar}_{13}$ (${}^{29}_{16}\mathrm{S}_{13}+p+p$)	≈0.1	0,2	B	Audi and Wapstra, 1995
${}^{33}_{19}\mathrm{K}_{14}$ (${}^{31}_{17}\mathrm{Cl}_{14}+p+p$)	≈0.8	0,2	T	Audi and Wapstra, 1995
${}^{35}_{20}\mathrm{Ca}_{15}$ (${}^{33}_{18}\mathrm{Ar}_{15}+p+p$)	≈0.76	0,2	B	Audi and Wapstra, 1995
${}^{6}_{3}\mathrm{Li}_3$ (${}^{4}_{2}\mathrm{He}_2+n+p$)	3.70	1	T	Audi and Wapstra, 1995
${}^{6}_{3}\mathrm{Li}_3$ (${}^{4}_{2}\mathrm{He}_2+n+p$)	0.14*	1	T	Audi and Wapstra, 1995
${}^{8}_{5}\mathrm{B}_3$ (${}^{4}_{2}\mathrm{He}_2+{}^{3}_{2}\mathrm{He}_1+p$)	1.725	1	T	Audi and Wapstra, 1995
${}^{9}_{4}\mathrm{Be}_4$ (${}^{4}_{2}\mathrm{He}_2+{}^{4}_{2}\mathrm{He}_2+n$)	1.757	1	B	Audi and Wapstra, 1995
${}^{3}_{\Lambda}\mathrm{H}_1$ ($\Lambda+n+p$)	2.34	0	T	Gibson, 2001
${}^{6}_{\Lambda}\mathrm{He}_3$ (${}^{4}_{2}\mathrm{He}_2+\Lambda+n$)	4.26	0,1	T	Hiyama *et al.*, 1996, 2001

Borromean (although very close) system ${}^{32}_{10}\mathrm{Ne}_{22}+n+n$. Although the present estimate is that ${}^{25}_{8}\mathrm{O}_{17}$ is neutron unstable by only 0.1 ± 0.48 MeV, leading one to hope that ${}^{24}_{8}\mathrm{O}_{16}+n+n$ should be a Borromean system, this is contradicted by the established instability of ${}^{26}_{8}\mathrm{O}_{18}$.

Borromean two-proton halos are fewer due to the confining Coulomb potential; see Table II for examples lighter than calcium. Unlike the two-neutron cases the three-body binding for an even-proton system is not necessarily larger than the two-body p-core binding because now the repulsive Coulomb interaction also contributes. The p-core system may even be more stable than the p-p-core, depending on how far apart the two protons are spatially in the total system. In fact, the three-body binding energy can be arbitrarily close to zero. The even-proton systems listed in Table II are Borromean, in contrast to the weakly bound odd-proton systems, of which we include a few with estimated negative binding energy.

The few-body structure may be an appropriate approximation in some cases, even when the system is of ordinary size. The core of ${}^{10}_{6}\mathrm{C}_4$ is the α-unstable ${}^{8}_{4}\mathrm{Be}_4$. However, the Coulomb barrier also stabilizes this state in the continuum, allowing structure and reaction studies of the combined system. Actually, many properties are known for nuclei beyond the proton dripline, since

they have sufficiently long lifetimes to be studied.

A few examples of less straightforward cluster divisions are listed at the end of Table II. Two α particles are only bound by 92 keV; using one neutron as glue leads to the Borromean ${}^{9}_{4}\mathrm{Be}_4$ nucleus. The spatial extension is confined by the Coulomb and centrifugal barriers, although the additional neutron allows a larger size than ${}^{8}_{4}\mathrm{Be}_4$. This nucleus could be considered the first in a series of a number of α particles held together by an appropriate number of neutrons (Wilkinson, 1986; Kanada-En'yo *et al.*, 1995; von Oertzen, 1997; Kanada-En'yo and Horiuchi, 2001; Sugawa *et al.*, 2001). Such states may appear not only as ground states but as structures of specific excited states.

Both ${}^{8}_{5}\mathrm{B}_3$ and ${}^{3}_{\Lambda}\mathrm{H}_1$ are tango states in which one bound subsystem, ${}^{7}_{4}\mathrm{Be}_3$, and the deuteron form a relatively tight entity compared with distance and binding to the third particle, proton, and Λ. The qualitatively dominating structure and the scaling properties are then of two-body nature. This is especially pronounced for the hypertriton, as seen and explained in connection with Figs. 3 and 5. For ${}^{8}_{5}\mathrm{B}_3$ the proton binding of 0.14 MeV is small compared to the 1.59-MeV binding of the two helium isotopes. Still the underlying three-body structure is necessary for accurate computations.

The two-body scaling is also recovered for ${}^{6}_{\Lambda}\mathrm{He}_3$, but in contrast to the hypertriton the Λ particle is now closely attached to the α particle as a strange skin while the remaining neutron forms a halo weakly bound to this strange two-layer core (Hiyama, 1996, 2001). This strong binding of the Λ particle to ordinary nuclei extends the nucleon dripline, as witnessed by the weak binding of a neutron to the bound ${}^{5}_{\Lambda}\mathrm{He}_2$ system. Adding one more neutron produces a rather strongly particle-bound ${}^{7}_{\Lambda}\mathrm{He}_4$ system. In the same way ${}^{7}_{\Lambda}\mathrm{Be}_4$ $({}^{5}_{\Lambda}\mathrm{He}_2+p+p)$ constitutes a Borromean system beyond the non-strange proton dripline. It should be emphasized that the two-body nature of these strange halos does not imply that the systems effectively are two-body structures.

The structure of ${}^{7}_{\Lambda}\mathrm{Li}_3$ $({}^{4}_{2}\mathrm{He}_2+\Lambda+d)$ reveals an interesting effect. The deuteron size is reduced substantially due to the presence of the Λ particle. This is analogous to the effect of impurities in solids which sometimes drastically change the properties of the material (Tamura, 2002). The corresponding gain in energy allows strange excited states with halo properties (Hiyama, 1996, 2001).

Another tango system is ${}^{6}_{3}\mathrm{Li}_3$, in which the 3.7-MeV binding energy seems to be too large for a halo state. The deuteron alone is responsible for 2.2 MeV and the remaining 1.5 MeV is also too large to allow a two-body halo of α and deuteron. The special tight structure of the α particle could, however, extend the halo region, as we noted for ${}^{6}_{2}\mathrm{He}_4$, but now both the deuteron charge and the larger binding prevent a large radius.

The nuclei ${}^{6}_{2}\mathrm{He}_4$ and ${}^{6}_{3}\mathrm{Li}_3$ could have isobaric analog halo states, since $Z\leqslant 3$, as required by Eq. (26) if the binding energy is sufficiently small. The known halo state of ${}^{6}_{2}\mathrm{He}_4$ should then have an analog in ${}^{6}_{3}\mathrm{Li}_3$ which has a similar structure when one of the protons is changed into a neutron in the same relative state (Zhukov *et al.*, 1995; Li *et al.*, 2002). This is indeed possible and appears as the 0^+ state with $E^*=3.563$ MeV, i.e., 0.14 MeV from the threshold; see Table II. The state is less bound than its analog in ${}^{6}_{2}\mathrm{He}_4$ due to the repulsive Coulomb potential's amounting to about 0.83 MeV.

Strange halo analog states may also exist. For example, the $T=1/2$, $J^{\pi}=1^{-}$ state in ${}^{6}_{\Lambda}\mathrm{He}_4$ $({}^{4}_{2}\mathrm{He}_3+\Lambda+n)$ has an analog in ${}^{6}_{\Lambda}\mathrm{Li}_2$ $({}^{4}_{2}\mathrm{He}_2+\Lambda+p)$. However, this state is proton unbound due to the higher energy from the additional Coulomb repulsion. Halo formation would require more binding in the initial analog state.

The notion of halo analog states makes sense for systems in which the total isospin is carried by the two nucleons, i.e., when the core has zero isospin. Generalization to a finite core isospin was attempted for ${}^{11}_{3}\mathrm{Li}_8$ and ${}^{11}_{4}\mathrm{Be}_7$ by Zhukov *et al.* (1995), who defined a halo analog state as the replacement of one valence neutron by a proton in the same valence state. This definition is in conflict with the definition of isospin, which implies that in any decoupled two-component system, like a halo and core, both parts must contribute coherently to the analog state, as explained in detail by Bohr and Mottelson (1969). Including only one of these components is in contradiction to the isospin analogy. Extending the notion of halo analog states even further, to states of deuteron core structure, is even more misleading, first because the state is not an isobaric analog and second because it is not analogous to any two-neutron halo state.

The structure of an isobaric analog state is by definition similar to the original state. The small differences are due to the Coulomb potential's breaking the symmetry, i.e., the energy of the state is changed by the difference in Coulomb repulsion (diagonal part), while its structure is modified by the admixture of different isospins (nondiagonal part). For halos these effects are enhanced by the presence of the binding threshold. One more proton increases the energy and the binding threshold is approached or exceeded. Then, the dimensions of the state increase to minimize the additional p core Coulomb repulsion. The relative weights of nucleon core configurations are also shifted from p to s waves to reduce the centrifugal barrier repulsion of the spatially larger state (Millener, 1997).

These effects are analogous to the well-known Thomas-Ehrmann shifts (Bohr and Mottelson, 1969). For the weakly bound halo states the isospin mixing of the isobaric-analog states may be substantially larger than for the ordinary nuclei. This was investigated for one-neutron halos (Hansen *et al.*, 1993) but has so far been studied only for specific examples of two-neutron halos (Arai *et al.*, 1995).

Other excited states may have interesting properties as well. The two-proton Borromean states, and in general cluster states in which the Coulomb interaction contributes, already start with a disadvantage. The excitation energy would further hinder formation of quantum halos. The two-neutron Borromean nuclei are more

likely to have excited states of halo character. If the excited states arise from core excitations they are clearly not predictable from the original three-cluster structure. The frozen degrees of freedom must be activated.

Also of interest are the three-body states built on a ground-state cluster configuration. Since the binding energy for Borromean nuclear systems can be several MeV, there may be room for an excited state. Such states, including the ground state, could be the first in the series of Efimov states. The sequence is terminated when the effective radial potential falls off faster than the second power of the size coordinate. This happens when the hyper-radius is a few times the average of the three *s*-wave scattering lengths; see Eq. (11).

An Efimov state would, according to Eq. (8), be $\exp(\pi/\nu)$ larger than the size of the previous state, and its energy would correspondingly be reduced by a factor of $\exp(-2\pi/\nu)$. The value of ν is 0.074 when two masses are nine times smaller than the third mass and only two subsystems have *s* states at zero energy, which is the case for $^{11}_{3}\mathrm{Li}_8$ (Jensen and Fedorov, 2003). The radius then increases from one state to the next by a factor of 3×10^{18}. Since two-neutron halos are the only candidates, it is therefore extremely unlikely to find a second Efimov state in nuclei.

We want to emphasize that the first, in contrast to the second, Efimov state is not excluded in nuclei. We can illustrate this by increasing the *n* core scattering length for $^{11}_{3}\mathrm{Li}_8$ to about 18 000 fm, where the first excited state appears (Fedorov *et al.*, 1994a). This is about 14 orders of magnitude smaller than the estimate obtained if the first excited state is 3×10^{18} larger than the ground state. This state is therefore not localized at distances where the hyper-radial potential behaves as $1/\rho^2$ ($a_{av}<\rho$). The characteristic scaling features require at least two Efimov states, but the first could also be the last.

2. Atoms and molecules

The combination of electrons (charged particles) and molecules to form bound three-body systems can be achieved in three different ways, each of which contains as many possibilities as combinations of the number of molecules. We do not here distinguish between molecules and neutral atoms. If the system is effectively a two-body system with an electron as one of the particles, the energy scale is a few meV. In genuine three-body halo systems the energy scale is rather a few μeV, corresponding to 10 mK. Experimental investigations are therefore very demanding and only a few results are available. In some of these combinations a large number of halos is possible, especially when excited states are included. In contrast to nuclei, excited states are probably less mixed with other configurations and the halo features could then survive to larger excitation energies. We shall only give examples for illustration.

The first three-body system on the atomic level is the neutral helium atom ($\alpha+e+e$). This is a well-bound Coulombic system far from any halo structure. Another similar system is the negative hydrogen atom H^- ($p+e+e$), also too strongly bound to form a halo. A similar system is the positive hydrogen molecule H_2^+ with two protons and one electron, which is even more bound than H^-. Here accurate computations are available for the binding as a function of the screening parameter for a statistically screened Coulomb potential (Bressanini *et al.*, 2002). At some point the threshold for binding the hydrogen atom is reached. Bressanini *et al.* are able to simulate the manipulation of systems either by the external fields created by thermal ionization in plasmas or by the effective potentials acting on electrons in metals. Close to threshold, halos may arise.

The next type is two electrons and a neutral atom, corresponding to doubly charged negative ions. These particles are probably all unbound, although this has not been proved rigorously to date. This does not necessarily imply the absence of structure in the continuum, although no low-lying resonances in electron scattering on H^- and D^- are found (Andersen *et al.*, 1995). Such doubly charged negative atomic ions probably do not form halos.

Two electrons added to a neutral molecule could form bound states, for example, when the molecule is large and two well-separated atoms each bind one electron. This could very easily happen when the molecule consisted of many atoms. In smaller molecules with few atoms, the two additional electrons repel each other, and therefore lead to a more likely formation of halos. Recently the stability of the doubly charged small molecules BeF_4^{2-} (BeF_4+e+e) and MgF_4^{2-} (MgF_4+e+e) was established (Middleton and Klein, 1999). Such systems, however, cannot be classified as three-body systems. Indeed restructuring and many-body effects due to the presence of the two electrons involve the intrinsic degrees of freedom (Weikert and Cederbaum, 1993). For example, the division of BeF_4^{2-} into $BeF_4^- + F^-$ could be more advantageous to form a two-body halo. The two-electron plus molecular or atomic systems are either unbound, very likely not forming halos, or restructure into a different clusterization.

Two molecules (or atoms) combined with a negatively charged particle can form weakly bound states. The charged particle could be a muon or an antiproton, but we shall here only consider the electron. Examples are the negative hydrogen atom plus closed-shell atoms. The lightest are $^{A_1}\mathrm{H}+e+^{A_2}\mathrm{He}$ with different isotopic combinations corresponding to $A_1=1, 2$ and $A_2=3, 4$. These tango systems become unbound by removal of the electron that can bind to H but not to He.

The potential between H and He decreases as $1/r^6$ at large distance, while addition of the electron changes the effective radial potential to $1/r^4$, corresponding to the dipole-induced potential of He by the bound H^- system. The pocket in the effective potential becomes much wider and appears at a larger distance (Li and Lin, 1999). Two bound states are established theoretically for each isotopic combination. The angular momenta are $J=0, 1$ and the energies vary in the range between 1 and 100 μeV. The sizes are about 10–20 Å. They are prom-

ising halo candidates, especially the weakest bound $J=1$ state in $^1H+e+^3He$ (Bendazzoli *et al.*, 1997).

Using the hydrogen molecule instead of He we also get a system, $H+e+H_2$, with a few bound, but potentially rather extended, states (Robicheaux, 1999). Replacing He with other noble gases, e.g., $H+e+Ne$, leads to many more bound states, in which excited states might be close to threshold and exhibit halo features. The stronger bindings between the noble gas and H, as well as between the noble gas and the electron, are responsible. If one used, instead, two helium atoms in $^4He+e+^4He$, the three-body system would be unbound with respect to $^4He_2$. A number of tango states involving two atoms and an electron have been proposed (Robicheaux, 1999). Examples containing Mg are Mg_2^-, $Mg+e+Ne$, $Mg+e+Ar$, $Mg+e+Kr$, and $Mg+e+Xe$, where any of these systems could form a halo state.

Combining three atoms or molecules can produce very weakly bound systems. The best known is the symmetric helium trimer $^4He_3$ with a bound ground state of almost normal size and one excited state, often referred to as a good candidate for an Efimov state with binding of about 0.18 μeV and size around 52 Å. The only bound asymmetric helium trimer, $^3He^4He_2$, has one pronounced halo state with binding and radius around 1 μeV and 13 Å (Nielsen *et al.*, 1998b; Yuan and Lin, 1998).

Two-body properties suggest that the replacement of one helium atom by an alkali atom produces halo candidates (Yuan and Lin, 1998; Kleinekathofer *et al.*, 1999). A few examples of molecular three-body halos are $^7Li^4He^3He$ and $^{23}Na^3He_2$, with binding energies and radii around (0.18 μeV, 68 Å) and (0.5 μeV, 50 Å), respectively. Furthermore, $^6Li^4He^3He$ could in the end prove to be even more weakly bound. Other combinations with heavier alkali atoms can also be envisaged. $^3He_2$ or $^3He^4He$ could be combined with an alkali atom to achieve pronounced halo structure.

Excited states with an Efimov structure would appear along the dashed line in Fig. 3. However, if the interaction only allowed one Efimov state, it could appear anywhere above the Efimov line. This can be understood if we imagine decreasing the scattering length from infinity until only the ground state and one Efimov state are left, as for the atomic helium trimer system (Nielsen *et al.*, 1998b, 2001). Continuing even further, we would find that the size of the excited state kept increasing and at some point moved into the nonclassical region in hyperradius, where the potential no longer would behave as $1/\rho^2$. The state would then be a halo state in hyperradius, which is only possible for the last Efimov state. When the second excited state disappears, the energy of the first moves towards zero from a value strongly dependent on the shape of the two-body potential and completely independent of the Efimov scaling condition.

Efimov states could appear as the result of an appropriate combination of particles. The smallest factors relating neighboring states are found for the largest values of ν [see Eq. (8)]. Three examples illustrate this behavior (Jensen and Fedorov, 2003), i.e., 1.01 for three identical bosons, 0.499 for three equal masses with only two subsystems with *s* states at zero energy, and 0.074 when two masses are nine times smaller than the third mass and only two subsystems have *s* states at zero energy ($^{11}_3Li_8$). From one state to the next radii increase by factors of $\exp(\pi/\nu)=22$, 542, and 3×10^{18}, respectively.

The most favorable condition is obtained when one mass is much smaller than the other two. For example, $^3He^{23}Na_2$ and $^4He^{133}Cs_2$ give $\nu\approx1.2$, 2.4 corresponding to radii increasing by about 20 and 4.5, respectively. An even more favorable case is that of an electron and two identical molecules or atoms (Pen'kov, 1999). Then ν could be as large as 100 (electron-molecule mass ratio $\approx10^{-5}$) and the number of Efimov states within practical reach would increase substantially. However, this requires a large electron-atom scattering length or equivalently a binding energy very close to zero. The needed match may be difficult to find but, on the other hand, it does not have to be precise due to the large ν. The most difficult part is probably to find systems in which the three-body structure is maintained.

One interesting possibility, the tuning of effective interactions by magnetic fields, has been exploited to manipulate Bose-Einstein condensates (Cornish *et al.*, 2000; Roberts *et al.*, 2001). Another suggestion, to use an external electric field, was discussed in connection with the Efimov effect for helium trimers (Nielsen *et al.*, 1998a). Sweeping across such resonances would allow the formation and subsequent investigation of these giant halos (Nielsen *et al.*, 2002).

D. Multibody systems

Halo formation seems to be strongly favored for two- and three-body clusterization. However, multibody halos are not excluded altogether, especially if they are enhanced by quantum shell effects or a particularly stable configuration, for example, of macroscopic geometric origin. The question of which degrees of freedom are active is again decisive.

1. Nuclei

The low cluster charge in a halo state suggests combinations of neutrons, protons, and α particles as sources of halo structure. The most favored is several neutrons surrounding a core, and here most likely four neutrons plus a core would be preferred, since three neutrons lose out due to the odd-even effect. If six or a larger even number of neutrons plus a core could form a halo, a special quantum-mechanical shell effect stabilizing such systems would have to be rather strong. This is unlikely. Good candidates for five-body halos seems to be the Borromean nuclei, in which removal of two neutrons also produces a Borromean system.

We list in Table III pairs of such neighboring Borromean systems located earlier. Their possible halo structure is not well established, although all systems seem to be more complicated than the two-neutron Borromean structure suggested in Table II. These cases show the importance of a good selection of the degrees

TABLE III. Multibody halo candidates. The columns give division of the system, four- and two-neutron separation energies (in MeV) S_{4n}, S_{2n}, indication with B if Borromean property is known, and references as in Tables I and II.

System	S_{4n}	S_{2n}	B?	References
$^{8}_{2}\mathrm{He}_6$ ($^{4}_{2}\mathrm{He}_2+4n$)	3.10	2.13	B	Audi and Wapstra, 1995
$^{14}_{4}\mathrm{Be}_{10}$ ($^{10}_{4}\mathrm{Be}_6+4n$)	4.00	1.33	B	Audi and Wapstra, 1995
$^{19}_{5}\mathrm{B}_{14}$ ($^{15}_{5}\mathrm{B}_{10}+4n$)	≈1.9	≈0.5	B	Audi and Wapstra, 1995
$^{22}_{6}\mathrm{C}_{16}$ ($^{18}_{6}\mathrm{C}_{12}+4n$)	≈4.7	≈1	B	Sakurai *et al.*, 1999
$^{31}_{9}\mathrm{F}_{22}$ ($^{27}_{9}\mathrm{F}_{18}+4n$)	>0	>0	B	Sakurai, 2002
$^{34}_{10}\mathrm{Ne}_{24}$ ($^{30}_{10}\mathrm{Ne}_{20}+4n$)	>0	>0	?	Lukyanov *et al.*, 2002; Notani *et al.*, 2002
$^{37}_{11}\mathrm{Na}_{26}$ ($^{34}_{11}\mathrm{Na}_{22}+4n$)	>0	>0	?	Lukyanov *et al.*, 2002; Notani *et al.*, 2002
$^{43}_{13}\mathrm{Al}_{30}$ ($^{39}_{13}\mathrm{Al}_{26}+4n$)	?	?	?	
$^{46}_{14}\mathrm{Si}_{32}$ ($^{42}_{14}\mathrm{Si}_{28}+4n$)	?	?	?	

of freedom, i.e., two or four valence neutrons and the corresponding (different) Borromean cores.

The next type of system necessarily contains two charged components. Replacing one or more neutrons with protons immediately allows deuteron substructures that are rather loosely bound, but sufficiently bound to prevent such halos. The quantum gain from additional shell effects is probably not sufficient to bind several deuteron clusters (Jensen and Riisager, 1991, 1992).

Using α particles as building blocks is a step up in charge but the tight structure of large binding and small radius is an advantage. Furthermore, both the α particles and the neutron-α system are unbound. Possibilities are nuclei such as $^{4x+y}_{2x}\mathrm{X}^{2x+y}$ with x α particles bound by the y neutrons, which decrease the Coulomb repulsion by keeping the positive charges apart and which simultaneously provide additional attraction. The Borromean nucleus $^{9}_{4}\mathrm{Be}_5$, in its ground state or an excited state, could be considered the simplest example of such a system.

At the dripline α-neutron clusters are more favored than at beta stability because at the edge of stability the stablest such structures must be exploited optimally to obtain a stable solution. The absolute energy gain, achieved in this way, although small, makes the difference between stability or decay. These cluster states may then even become the ground state.

The stability of $^{24}_{8}\mathrm{O}_{16}$ matches full $d_{5/2}$ and $s_{1/2}$ shells and an empty $d_{3/2}$ shell. Two more neutrons make the system unstable. However, adding one proton instead supplies binding for six additional neutrons, i.e., two more than the $d_{3/2}$ shell can hold. The first four of these neutrons are naturally accounted for since the $d_{3/2}$ level is slightly unbound in $^{25}_{8}\mathrm{O}_{17}$ while slightly bound in $^{26}_{9}\mathrm{F}_{17}$. In the shell-model description the last two neutrons require occupation of higher-lying levels. The change of stability or the occurrence of new magic numbers as the dripline is approached has been investigated in shell-model computations (Otsuka *et al.*, 2001).

It is tempting to attribute the surprisingly different number of neutrons at the dripline for $^{24}_{8}\mathrm{O}_{16}$ and $^{31}_{9}\mathrm{F}_{22}$ to a different cluster structure. The nucleus $^{24}_{8}\mathrm{O}_{16}$ would then be explained as four $^{6}_{2}\mathrm{He}_4$ clusters. Furthermore, the following neutron dripline nuclei with even proton numbers, $^{32}_{10}\mathrm{Ne}_{22}$, $^{38}_{12}\mathrm{Mg}_{26}$, and $^{44}_{14}\mathrm{Si}_{30}$, would be obtained from each other by adding $^{6}_{2}\mathrm{He}_4$, whereas the first, $^{32}_{10}\mathrm{Ne}_{22}$, is constructed with $^{24}_{8}\mathrm{O}_{16}$ plus $^{8}_{2}\mathrm{He}_6$. These may be cluster components providing extra stability and perhaps eventually producing halos.

Clusters with higher charges are less likely, although exotic structures like two $^{6}_{2}\mathrm{He}_4$ or $^{11}_{3}\mathrm{Li}_8$ bound into $^{12}_{4}\mathrm{Be}_8$ or $^{22}_{6}\mathrm{C}_{16}$ have been suggested as possible bound states. Such cluster states and related phenomena have been intensively studied (see, for example, Kanada-En'yo and Horiuchi, 2001; Sugawa *et al.*, 2001).

2. Atoms and molecules

Unlike nuclei in which odd-even effects are strong, four-body halos are favored for electrons combined with molecules. The decoupling of different degrees of freedom is more pronounced for molecules. This is demonstrated by the long series of collective rotational and vibrational states, providing a larger number of possible excited states close to the threshold of binding.

Combining neutral molecules with electrons in general allows each molecule or atom to bind the electron and therefore prohibit the cluster structure necessary for halo formation. An even simpler example of this effect is seen for Ca^-, in which the electron binding energy of 24.6 meV is rather small (Andersen *et al.*, 1997), but the radius is also expected to be small because the electron is rather strongly correlated with both valence and closed-shell electrons. This is a problem relevant for many-body physics not halo physics.

The most attractive combinations are the neutral molecules. We have already discussed atomic helium trimers and concluded that $^4\mathrm{He}_3$ has an Efimov excited state and $^3\mathrm{He}^4\mathrm{He}_2$ is a halo. The system of mixed atoms $^4\mathrm{He}_n$ $^3\mathrm{He}_2$ is unbound for $n=1$ and bound for $n\geq 2$ (Bressanini *et al.*, 2002). When one ^{3}He atom is added to the system, $^4\mathrm{He}_n$ $^3\mathrm{He}_3$ is unbound for $n<4$ in the calculations while bound for $n\geq 32$. For any given number of ^{3}He atoms the complex can be bound by some number n of ^{4}He. Deciding whether some of these systems qualify as halos requires more than such a global analysis, but systems with the lowest number of atoms are certainly the most likely candidates, i.e., $^4\mathrm{He}_2$ $^3\mathrm{He}_2$.

The addition of a ^{3}He atom always has two effects. On the one hand, it reduces the stability due to the weaker two-body binding and the Pauli exclusion principle. On the other hand, it provides more pair binding. It has been predicted theoretically that $^3\mathrm{He}_n$ is stable at least for $n>35$ (Guardiola and Navarro, 2000). Other combinations with alkali atoms can be readily drawn from the results reported by Kleinekathöfer *et al.* (1999), e.g., $^3\mathrm{He}_n$ with alkali atoms, where stability may be achieved for $n=2$.

Excited states allow a completely new class of multibody halo states, as recently suggested in connection with Bose-Einstein condensates (Sørensen *et al.*, 2002a, 2002b). A description in terms of effective two-body potentials and a Faddeev-type wave-function decomposition leads to a number of spatially extended bound many-body states. These appear for very large two-body scattering length within the size of the external ion trap. They are metastable and would decay by recombination into lower-lying dimer and trimer states. They are also to a large extent independent of the specific two-body potential and carry all the characteristics of Efimov states as given in Eq. (8). Their large size, extending far beyond the range of the two-body interaction, indicates a strong decoupling. While these molecules may not appear directly in nature, the two-body scattering length can be tuned by use of external fields. The existence conditions for such states can in principle be controlled, allowing an easier study of their properties.

IV. TWO-DIMENSIONAL STRUCTURE

Many physical phenomena depend on the spatial dimension d. Beyond the case $d=3$ (the ordinary three-dimensional world) the most interesting case is $d=2$, which can also be directly studied experimentally. Qualitative differences with respect to $d=3$ can be seen from Eq. (12), which in fact is applicable for all dimensions provided f is redefined as $f=d(N-1)$.

The centrifugal barrier is still proportional to $(f-1)(f-3)/4$. This same barrier (same value of f) is found for different combinations of dimension and particle number, e.g., $f=6$ for $(d,N)=(2,4)$, $(3,3)$ and $f=30$ for $(d,N)=(2,16)$, $(3,11)$. When f is the decisive parameter for halo formation, the number of particles has to be larger in two dimensions than in three. In particular, the limit is $N\leqslant 4$ for $d=2$ compared to $N\leqslant 3$ for $d=3$.

For $N=3$ we have $f=2d$, and the centrifugal barrier is proportional to $(2d-1)(2d-3)/4$, as can be seen from Eqs. (12) and (13). The Efimov effect occurs when the effective radial potential is of the form in Eq. (3) with positive ν^2. Then the potential energy must contribute a term of the form $\hbar^2\lambda/(2\mu\rho^2)$ with a strength $\lambda<-(2d-1)(2d-3)/4-1/4=-(d-1)^2$. This only happens when $2.3<d<3.8$ (Nielsen *et al.*, 2001).

Thus the Efimov and Thomas effects do not occur for $d=2$. This is consistent with the general theorem that few-body systems with finite-range potentials in one and two dimensions can have only a finite number of bound states (Vugal'ter and Zhislin, 1983). Other authors have also argued that there are no Efimov and Thomas effects in $d=2$ dimensions (Adhikari *et al.*, 1988).

An especially interesting value is $f=2$, leading to a negative centrifugal barrier. This only occurs for two particles in two dimensions, namely, $(d,N)=(2,2)$. The lowest positive barrier in two dimensions is obtained for $N=3$. We shall concentrate on these cases in this section.

A. Two-body systems in *d* dimensions

The behavior of two-body systems in two dimensions is interesting in itself as a possible halo system. However, it is also a necessary component of halos with more than two particles. The full importance of the two-body component becomes evident when d is a parameter and $d=2$.

The s-wave (no angular dependence) scattering length a is defined for $d>2$ in terms of the asymptotic behavior of the wave function at large distances for zero energy,

$$\psi_0(r)\propto\left[1-\left(\frac{a}{r}\right)^{d-2}\right], \tag{27}$$

which shows that the scattering length a is the node in the zero-energy wave function outside the potential. For $d=2$ this behavior must be replaced by

$$\psi_0(r)\propto\ln\left(\frac{r}{a}\right), \tag{28}$$

where the scattering length must now be positive and still be the node of the wave function.

If a is larger than the effective range R_e, the zero-energy wave function has a node and the system must have at least one bound state of s-wave character. Thus, if the system does not have a bound state, the scattering length must be smaller than R_e.

The wave function at large distance outside the potential for a bound state of negative energy E is

$$\psi_0(r)=r^{(2-d)/2}K_{(d-2)/2}(\kappa r), \tag{29}$$

where K_ν is a modified Bessel function of the second kind and $\kappa=\sqrt{-2\mu E_d/\hbar^2}$. In the limit of very weak binding, $\kappa R_e\ll 1$, the logarithmic derivative at R_e of the bound-state wave function in Eq. (29) and the zero-energy wave function in Eqs. (27) and (28) must approximately be equal. Assuming equality we get

$$E_d=-\frac{4\hbar^2}{2\mu a^2}\left[\frac{\Gamma^2(d/2)\sin[\pi(d/2-1)]}{\pi(d/2-1)}\right]^{2/(d-2)}, \tag{30}$$

which for $d=2$ becomes

$$E_2=-4\exp(-2\gamma)\frac{\hbar^2}{2\mu a^2}, \tag{31}$$

where γ is Euler's constant. These expressions for the energy of the bound state are independent of R_e and thus exactly valid for zero-range potentials, where $R_e\equiv 0$.

The mean-square radius of a two-body system is then

$$\langle r^2\rangle = \frac{\int_0^\infty dr r^{d+1}[r^{(2-d)/2}K_{d/2-1}(\kappa r)]^2}{\int_0^\infty \int_0^\infty dr r^{d-1}[r^{(2-d)/2}K_{d/2-1}(\kappa r)]^2}$$
$$= \frac{(4-d)d}{6}\frac{\hbar^2}{2\mu(-E_d)} \tag{32}$$

in the zero-range approximation. This expression is valid in the limit of very weakly bound systems, where $2\mu(-E_d)\hbar^{-2}R_e^2 \ll 1$ implying that the mean-square radius is much larger than the effective range. The system is in a quantum halo state. For all E_d and μ the root-mean-square size has a maximum at $d=2$.

The relation in Eq. (32) between size and binding energy for weakly bound systems in d dimensions is a generalization of Eq. (1) for three dimensions. This expression is the same except for the dimension-dependent proportionality factor, and the previous discussion about quantum halos applies directly. Specifically, all weakly bound systems should appear on the universal curve deduced from Eq. (32), with both sides divided by the square of the classical turning point to use dimensionless quantities. When two-body systems do not obey this relation, either they are not effectively two-body systems or the mean-square radius is comparable to the range of the attractive interaction and the system is not a quantum halo.

A major difference between three and two dimensions is revealed by the behavior resulting from a zero-range attractive potential. For $d=2$ the number of bound states is finite (no Thomas effect). Even if an overall attractive potential is infinitesimally small, at least one bound state exists.

B. Three-body systems in two dimensions

For three particles in three dimensions one interesting limit is when the hyper-radius is much larger than the effective ranges and much smaller than the *s*-wave scattering lengths. Then the (Efimov) states characterized by Eq. (4) depend only on the shape of the two-body potentials through a cutoff at small distances, which must necessarily be present to define the energy of the lowest state of the series.

The occurrence of a halo state in three dimensions is based on the strength [multiplying $\hbar^2/(2\mu)$] arising from the potentials for three identical particles being $\lambda = -5.01$, while the centrifugal barrier is 15/4, producing an effective radial potential behaving as $-1.26/\rho^2$ in this ρ interval (Nielsen *et al.*, 2001).

In two dimensions, $d=2$, the strength of the radial potential arising from the two-body potentials is zero when ρ is much larger than the effective ranges. The repulsive centrifugal barrier $3/4\rho^{-2}$ then pushes the low-energy wave functions to distances outside the effective ranges, where the scattering lengths are the only decisive parameters. Therefore in the limit of large scattering lengths and low energy, the total bound-state wave function is independent of the shapes of the two-body potentials.

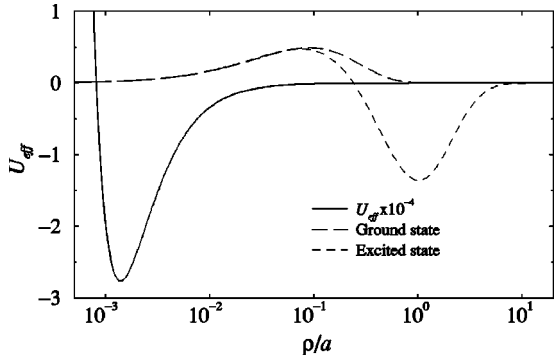

FIG. 6. The lowest diagonal hyper-radial effective potential $U_{\rm eff}$ [in units of $\hbar^2/(2ma^2)$] and the wave functions for the two bound states for three identical bosons in $d=2$ dimensions for zero-range two-body potentials. The total angular momentum is $L=0$ and the *s*-wave scattering length is a.

To illustrate we consider three identical bosons in two dimensions with total angular momentum zero. We use the zero-range approximation, i.e., we assume that $\rho \gg R_e$, and obtain a universal plot of the effective radial potential in Fig. 6. The small-distance repulsive behavior $+\frac{3}{4}\rho^{-2}$ is now dominant, in contrast to the $-1.26\rho^{-2}$ behavior in three dimensions.

With the potential in Fig. 6 we find two bound three-body states, ground state (g) and excited state (ex), with energies E and root-mean-square radii R,

$$E^{(g)} = 16.52E_2, \quad E^{(ex)} = 1.267E_2,$$
$$R^{(g)} = 0.111a, \quad R^{(ex)} = 0.927a, \tag{33}$$

expressed in terms of the scattering length a and the two-body energy in Eq. (31). Thus the properties of the weakly bound states depend only on a, in contrast to the Efimov states in three dimensions, where the range of the two-body potentials also enters in the length scale. In other words, potentials with the same scattering length produce approximately identical states in two dimensions.

The expressions in Eq. (33) are accurate as soon as a/R (R is the classical two-body turning point here assumed to be the effective range) is larger than one. The large or small proportionality factor between two- and three-body energy or root-mean-square radius is a residual resemblance to the Thomas effect for $d=3$, where the number is infinitely large or zero, respectively. Analogously the corresponding value for the excited state closely resembles those for the first Efimov state.

Using Eqs. (6) and (7) we find for three pointlike identical bosons that

$$\langle\rho^2\rangle/\rho_0^2 = \langle r_{12}^2\rangle/R_{12}^2 = 3\langle r^2\rangle/R^2 < 2, \tag{34}$$

where the index "12" refers to one two-body subsystem and the halo condition is the last inequality. From Eq. (33) we then get halos when $a \gtrsim 1.5R$ for the three-body excited state and $a > 12R$ for the ground states.

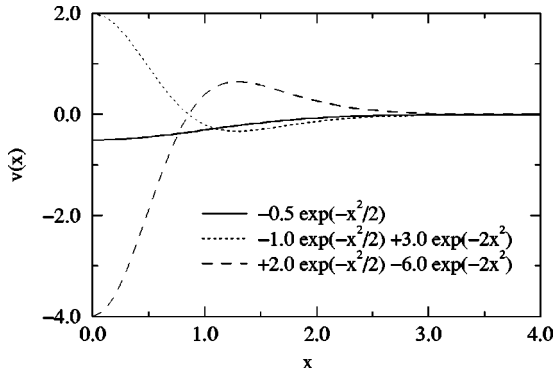

FIG. 7. Three two-body potentials of the form in Eq. (35) [in units of $\hbar^2/(2mb^2)$] as a function of $x=r/b$. The values of the parameters are given on the figure.

Thus the excited state is already a quantum halo for a relatively small a, whereas the ground state must have a much larger scattering length.

In contrast to the $3d$ case, here the scattering length completely determines the structure (both size and energy) for $d=2$. This model independence in two dimensions may be demonstrated in more detail by choosing a family of "double Gaussian" potentials of the simple form

$$V(r)=\frac{\hbar^2}{2m}\left[s_1\exp\left(-\frac{1}{2}r^2/b^2\right)+s_2\exp(-2r^2/b^2)\right]. \tag{35}$$

By construction, the signs of s_1 and s_2 determine the characteristic behavior of the potentials, i.e., purely attractive, with a repulsive core or with a repulsive barrier outside an attractive core. By adjusting the magnitude of one of the parameters s_i we can find systems with very large scattering length and therefore with two-body binding energy E_2 very close to 0. Three of these qualitatively different potentials are shown in Fig. 7.

The model independence is most efficiently illustrated by the use of dimensionless quantities in universal scaling plots. Therefore we show in Fig. 8 the combination $(E_3-E_2)/E_2$ (where E_3 is the three-body binding energy) for the calculated bound states of four series of potentials like those in Fig. 7. In the weak-binding limit $2m|E_2|b^2\hbar^{-2}\ll 1$, all the potentials have at least two bound states in which the energies are given by Eq. (33). This is in accordance with the conclusions of Bruch and Tjon (1979) and Adhikari *et al.* (1993), who, however, only discuss the ground state.

There is always a two-body bound state for the cases in Fig. 8. Furthermore, there are two three-body bound states in the limit of zero two-body binding. The energies of these two states are for all the potentials given by Eq. (33). For $s_1=+2$ an additional bound state appears near the threshold at $s_2=-5.80$, i.e., in total three bound states of which the ground-state binding remains finite across the threshold. This means that E_3/E_2 becomes infinite for the state of lowest energy corresponding to the diverging short-long dashed curve.

For potentials with a relatively high repulsive barrier,

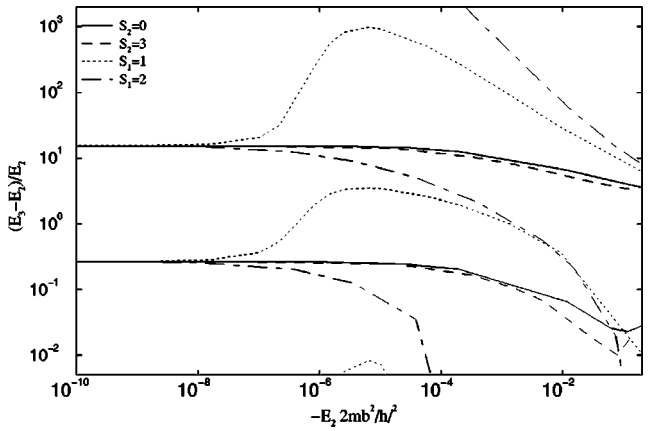

FIG. 8. Bound states of systems of three identical bosons in $d=2$ dimensions, with angular momentum $L=0$ obtained for two-body potentials of the type given in Eq. (35) and shown in Fig. 7. On the x axis we plot the two-body binding energy in dimensionless units, and on the y axis we plot the additional three-body binding below the two-body threshold relative to the two-body binding energy. The different curves correspond to different types of potentials: solid curve, $s_2=0$ and varying (negative) s_1 give a series of purely attractive potentials; dashed curves, $s_2=3$ and $s_1<-0.64$ give potentials with a repulsive core; dotted curve, $s_1=1$ or $s_1=2$ give potentials with a repulsive barrier; dot-dashed curve, $s_2<-3.33$ or $s_2=-5.80$, give a repulsive barrier but an attractive central part.

a third bound state is present. The energy of this state remains approximately constant, $E_3\simeq -0.34\hbar^2/(2mb^2)$ in the limit of vanishing two-body binding, and this state does indeed remain bound even though the attraction is so weak that no two-body bound state is present. The spatial extension of the state is limited to relatively small distances within the effective three-body potential, whereas the two other, far less bound states are placed far outside the potential.

All other types of short-range potentials (other than central attraction and outer repulsive barrier) produce no bound three-body state unless the corresponding two-body system also has a bound state. This demonstrates that it is very difficult to find bound three-body systems in two dimensions when all the two-body subsystems are unbound. Thus Borromean systems are difficult to construct and their properties differ markedly from those in three dimensions.

The generalization to systems with three different particles requires more parameters. However, a similar model independence still arises in the limit of weak binding, but the number of bound three-body states could now be either one or two. The three-body binding energies still depend only on the inverse square of a scattering length $\propto a^{-2}$, but the exact combination could be a complex function of the mass ratios and the ratios of the three scattering lengths. Details on the two-dimensional cases can be found in the work of Nielsen *et al.* (1999).

C. Molecular three-body examples

Examples could be constructed from systems in three dimensions by confining the systems to two dimensions

while maintaining the established interactions. We choose to investigate the atomic helium trimer systems in this way. The two-body interactions are strongly repulsive at short distances, and in three dimensions the $^4He_2$ dimer is extremely weakly bound, while both the ^{3}He-^{4}He and the $^3He_2$ dimer are unbound. We use the LM2M2 potential described by Aziz and Slaman (1991) in two dimensions, where all three dimers are bound in agreement with the universal results. Furthermore, when we treat the ^{3}He atoms as spin-0 bosons, we find that fully symmetric states exist for the $^3He_3$ trimer.

Note that this exercise, meant to illustrate the importance of mass dependence, clearly violates the fermionic nature of ^{3}He. The three-dimensional properties of these atomic dimers and trimers, as well as the corresponding interactions, have already been discussed in Sec. III.C.2.

The computed energies of the three-body bound states reveal that both $^4He_3$ and $^3He_3$ have two bound states in accordance with the general expectation. The ratios between the three-body binding energies and the two-body binding energies are smaller than predicted in Eq. (33). This tells us that the scattering lengths of ^{4}He^{4}He and ^{3}He^{3}He are not large enough to fall into the region where model-independent results are valid.

The asymmetric systems ^{3}He$^4He_2$ and ^{4}He$^3He_2$ each have only one bound state with $L^\pi=0^+$. When one of the atoms in $^4He_3$ is replaced by ^{3}He the kinetic energy is increased, whereas the potential energy is maintained unchanged. Therefore the very weakly bound excited state of $^4He_3$ must move to an energy above the unchanged two-body threshold. When an additional ^{4}He atom is replaced by a ^{3}He atom, the most strongly bound two-body subsystem is ^{3}He^{4}He, which is far less bound than $^4He_2$. Thus there is still room for a bound state in ^{4}He$^3He_2$ although it lies above the two-body breakup threshold in ^{3}He$^4He_2$.

The $^3He_3$ system is symmetric and indeed has two bound states. When one of the ^{3}He atoms is replaced by ^{4}He the two-body threshold decreases. The effective radial potential is then much lower at smaller distances, but receives asymptotically only contributions from the two configurations corresponding to the two identical ^{3}He-^{4}He subsystems. The last (symmetric) two-body configuration has a much higher energy and therefore no asymptotic contributions. In contrast a symmetric system receives contributions from all three components. Therefore the attractive pocket in the corresponding effective radial potential has to be shallower for asymmetric than for symmetric systems. This difference seems to be sufficient to eliminate the three-body excited state.

V. HIGH-ENERGY BREAKUP REACTIONS

An efficient way of probing the halo structure is to study scattering, reactions, or decay of the halo system. Scattering is very often only elastic, since excited (few-body) halo states are very fragile and excitations therefore cause fragmentation into the constituents of the halo. Elastic scattering, discussed in a recent review (Thompson and Suzuki, 2001), provides first of all information about the spatial extension, while forward scattering is especially sensitive to the matter distribution (Egelhof, 2001). It does not give information on the probability in the classical forbidden region. The sensitivity of computations for different halo wave functions can be seen in Fig. 9 by comparison with accurately measured cross sections. Inelastic reactions often involve breakup of the halo system, e.g., transfer processes like stripping of halo particles. Other reactions are possible, but these involve the nonhalo (intrinsic particle) degrees of freedom, which are much less informative reactions in connection with halo structure.

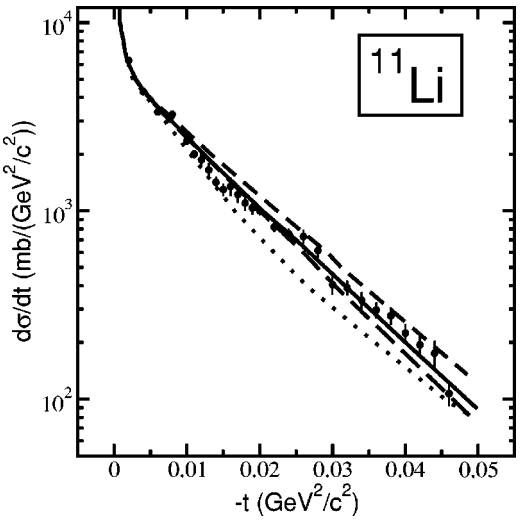

FIG. 9. Differential cross sections for elastic scattering of ^{11}Li on protons as a function of the square of the invariant four-momentum. The points are measured values and the curves are from various theoretical computations, each using extended density distributions for the halo nucleus. From Egelhof, 2001.

Breakup reactions carry information about the initial state (halo structure), the reaction mechanism, and the final state. These three ingredients are not easily disentangled. The importance of the reaction mechanism increases with decreasing relative collision energy, as more complicated reactions are possible at lower energies. High-energy reactions are best suited for studying initial and final states and thereby the halo degrees of freedom. This may seem strange because high energy is associated with small distances, and halos are spatially extended. However, high energies allow rapid transfer from initial to final state. The instantaneous structure is then probed for halos, since the time scale of the halo motion is much longer than the reaction process. The sudden approximation basically applies.

The methods can be applied to nuclear, atomic, and molecular halo systems, as the physics problems are similar. However, for molecules there is at least one interesting exception. The size of the atomic helium dimer is measured in a conceptually simple experiment that, in practice, is very difficult (Grisenti *et al.*, 2000). The intensity of the dimer beam is measured in transmission

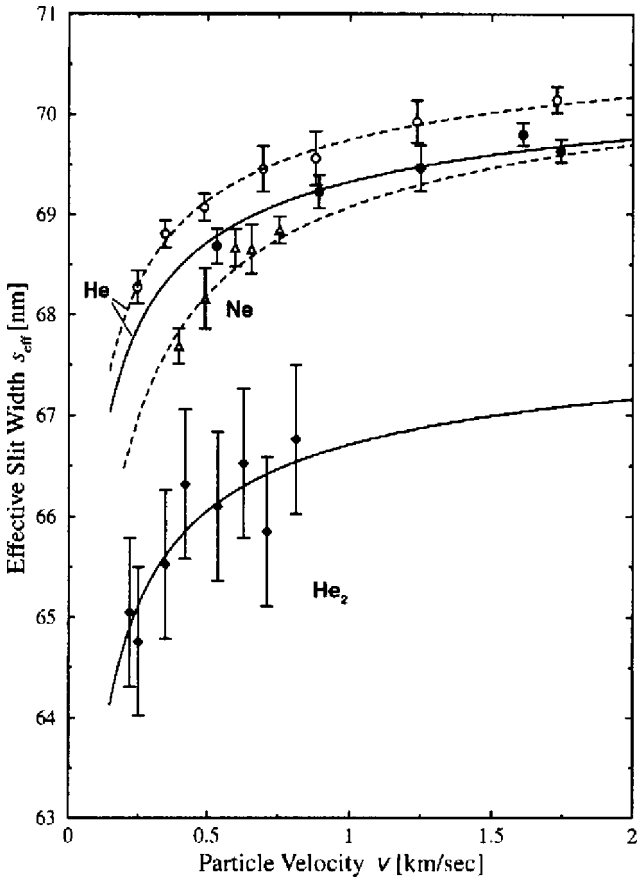

FIG. 10. Effective slit widths of He, Ne, and $^4He_2$ as a function of beam velocity. The points are obtained from measured intensities transmitted in diffraction through a 100-nm period grid. The solid curve is a best fit to $^4He_2$ for a size of $\langle r \rangle \approx 52$ Å. From Grisenti *et al.*, 2000.

through a lattice, where the size of the holes are varied. If the holes are too small, they do not allow transmission, and if they are too large, they do not disturb the dimer beam. At a grid size up to about an order of magnitude larger than the dimer size, transmission diffraction of the beam leaves an interference pattern with information about the size of the molecule. An analysis for atoms and molecules in terms of effective slit sizes is shown in Fig. 10, where the slit width difference between the atom and the molecule is approximately the extension of $^4He_2$ (Hegerfeldt and Köhler, 2000). Nuclei are too small for this type of measurement.

Another technique is used for the dipole-bound electron states in molecules first observed by photoexcitation and subsequent autodetachment (Lykke *et al.*, 1984). These states can be formed in cold collisions by direct electron capture or by electron exchange from laser-excited Rydberg atoms. Then the binding energy is determined by external electric-field detachment or by photodetachment (Desfrançois, 1995). This is a two-step process, like that for nuclei, in which the halo state is first created by fragmentation in a violent collision and afterwards studied in a collision experiment.

We shall not discuss any more examples from atoms and molecules, for which the analogous theoretical techniques, such as the impulse approximation carried out in the semiclassical impact-parameter picture, are well tested and well known. Electron scattering on neutral or charged atoms is briefly reviewed by Burke (1994), and ion-atom collisions with suitable few-body formulations involving a few active electrons are reviewed by Briggs and Macek (1990). Theoretical concepts suitable for knockout experiments on particles or clusters from solids, atoms, molecules, and nuclei are discussed by McCarthy and Weigold (1988, 1991).

Size information can also be obtained by the technique of intensity interferometry, originally used to determine sizes of astronomical objects. The method was recently applied to nuclear halos (Marques *et al.*, 2001). By taking proper account of the Pauli principle for identical fermions, one can determine the distance between two halo particles at the time of breakup. The analysis is intricate because both distances and emission times are involved. Furthermore, the reaction mechanism and final-state interactions may be intermixed in a nontransparent way, producing distorted signatures of resonance structures.

We shall from now on restrict ourselves to nuclear high-energy reactions substantially above the Fermi energy, although some of the considerations may also be valid at somewhat lower energies. We shall give qualitative and semiquantitative descriptions of recently studied reactions involving nuclear halos. For a detailed discussion of the accuracy and reliability of the experimental results, we refer the reader to Hansen *et al.* (1995), Tanihata (1996), Hansen and Sherill (2001), and Jonson (2004).

The theoretical formulation directly relevant for nuclear halos and the related examples are new, but several established models or computational schemes are also available. First, the early Glauber models can be used to relate the (large) measured reaction cross sections with the size of the system (Tanihata, 1996). Second, halo models have been employed in which the few-body wave function provides the density distribution and the constituent particles are pointlike (no internal excitations and describable by one point in space; Bertulani *et al.* (1993); Hansen (1996); Banerjee *et al.* (1998a, 1998b); Tostevin *et al.* (1998). Third, there are Glauber models in which both few-body granularity and spatial density distributions of the halo particles are incorporated.[1] Fourth, in some cluster models the finite size of the halo particles is treated by use of the optical model and the geometry in the impact-parameter formulation (Brooke *et al.*, 1999; Garrido *et al.*, 1999b; Garrido, Federov, and Jensen, 2001b). A comparison of different theoretical formulations for these models was recently attempted (Moro *et al.*, 2001).

[1]See, for example, Yabana *et al.*, 1992a, 1992b; Al-Khalili and Tostevin, 1996; Hencken *et al.*, 1996; Formanek and Lombard, 1997; Bertsch *et al.*, 1998; Thompson and Suzuki, 2001; Tostevin, 2001.

A. Qualitative description of the reaction mechanism

The crudest possible approximation is to assume that the observables directly reflect the structure of the wave function, e.g., momentum distributions are given by the Fourier transform of the halo wave function. Then the reaction mechanism must be an instantaneous release of the halo particles without disturbing their motion and without further mutual interactions. This might appear to be impossible, but statistical fragmentation models are able to describe the qualitative features of heavy-ion breakup reactions (Friedman, 1983). In the same way, the halo Fourier transform shows a very narrow momentum distribution, reflecting the spatial distribution and in qualitative agreement with measurements (Zhukov and Jonson, 1995; Aumann *et al.*, 2000).

The large-distance behavior of both two- and three-body halo wave functions is a Yukawa function. The Fourier transform is easily computed, and the length and momentum scales derived. The results are suggestive, but otherwise only useful for extreme halos, where only knockout processes contribute and the final-state interactions are negligible. These approximations are all not well fulfilled for nuclei generally, and representative examples accordingly cannot be found.

1. Dominant contribution

We first consider short-range interactions and breakup reactions for beam energies above 50 MeV/nucleon, taking the projectile to be the halo nucleus. At these energies the reaction time is much shorter than the time scale for the motion of the particles within the halo. Furthermore, when the halo is spatially extended, the halo particles interact with the target one at a time, and the total reaction can be described as an incoherent sum of individual two-body reaction cross sections (Bang and Pearson, 1967). Multiple scattering events are very rare. We shall first discuss the qualitative features using this participant-spectator model, in which a classification of reaction mechanism and reaction products is natural.

Inelastic features of two-body reactions can be described by introducing a phenomenological optical potential, which accounts for elastic scattering in detail, and an imaginary part which lumps together all other processes in an "absorption" cross section. Absorption now includes all inelastic processes, of which the most important are real absorption by the target and violent large-angle scattering leading to target's excitation or destruction.

This model allows classification of the breakup reactions according to the halo particles appearing in the final state (Barranco and Vigezzi, 1997), i.e., those reaching the narrow forward range of detectable angles. Some halo particles are absorbed and some continue their motion essentially undisturbed. The participant-spectator picture spells out the reaction mechanisms of the breakup processes—one halo particle is either absorbed or elastically scattered by the target in a two-body process, while all other halo particles remain undisturbed in their initial motion. The processes include fast removal or scattering of one particle and subsequent breakup of the remaining halo system. A number of experimental facts are in agreement with this description (see Zinser *et al.*, 1997; Aleksandrov *et al.*, 1998; Aumann *et al.*, 1999).

Clearly the two most important features are the initial structure of the halo system and the two-body differential cross sections. Quantitatively the resulting breakup cross sections must directly reflect these properties, e.g., the beam energy dependence and the ratio of elastic scattering to absorption where one particle is missing in the final state. Furthermore, large contributions to the breakup cross sections of a pronounced halo can be described in the participant-spectator model.

The dominant process for high energies can schematically be described as a one-particle knockout process that leaves all other halo particles essentially untouched, and the subsequent process is then shakeoff of the subsystem (without the knocked-out particle) as it existed initially within the halo. This remaining state is normally not an eigenstate, not the ground state, and not an excited state, but still the initial wave function with a well-defined time dependence. The procedure is then to expand this initial wave function on positive-energy distorted-wave eigenfunctions of the corresponding Schrödinger equation. These solutions are characterized by their relative energy when the particles are far apart and do not interact. The variation of the squared amplitudes with energy is the observable energy distribution.

A measured invariant-mass spectrum with resonance-like structures corresponding to positions and widths is obviously related to the remaining subsystem. However, for the well-defined knockout process an analysis in terms of the true resonances of the subsystem is conceptually wrong, since all continuum wave functions, not only resonances, are involved in the process. The energy dependence of the Breit-Wigner shape for a resonance is not obtained. However, such an analysis would often lead to reasonable numerical results, since the forces responsible for a possible resonance are precisely those forming the initial halo bound state. The subsystem remaining after knockout often has a large overlap with the resonance state of this subsystem. This does not make the procedure correct, only less transparent.

Analyses of invariant-mass spectra are easily confused with the procedure used in Dalitz plots, which refer to reactions or decays of particles as functions of their relative energy. This is analogous to reactions sweeping the energy of a resonance and revealing a large amplitude at small distance. This resonance behavior is not *a priori* present in the invariant-mass spectrum. Unfortunately, Dalitz plots image resonances directly only when the process proceeds via a resonance.

2. Multiple-collision corrections

The rather schematic knockout and shakeoff high-energy reaction mechanism does not give a full and accurate account of the breakup processes. Other processes, arising from the scattering of the halo particle,

also contribute significantly, and corrections are needed for a quantitative description. The most important modifications arise from simultaneous interaction with the target by more than one of the halo constituents. The assumption of incoherent contributions from the different particles is only correct when the halo particles (i) do not move during the reaction, (ii) are sufficiently far apart, and (iii) have sufficiently different impact parameters. The first assumption is valid for large beam energy. The second is valid for extreme halos, which, however, are not found in nuclei. The third assumption is violated when one halo particle first destroys the target and another geometrically is due to interact with that missing target. The participant-spectator picture is not valid for these parts of the initial wave function with a predominance of contributions from small distances between the two halo particles. This bias then eliminates large-momentum components resulting in more narrow distributions. This is often called the shadow effect (Esbensen, 1996; Hansen, 1996; Hencken *et al.*, 1996).

These corrections decrease with the size of the halo and increase with the size of the constituent halo particles. Both effects are related to the accuracy of the few-body cluster model, since an improved treatment of a few-body cluster reaction with a target should be matched by the accuracy of the structure model involved. Details on the reaction treatment for distances smaller than the particle radii cannot be expected when the few-body model assumes pointlike structures. On the other hand, the optical model treats the neglected intrinsic degrees of freedom and thereby extends the validity to lower energies than appropriate for Glauber models.

Another modification of this reaction model is necessary when long-range interactions are also present, since more than one halo particle then interacts simultaneously with the target at large distance. However, the important case of neutron halos in nuclei, where only one of the halo particles (the core) is charged, requires much less modification. We can then maintain the picture of incoherent individual contributions, since only the core-target interaction involves the Coulomb repulsion.

The modifications are then related to the two-body Coulomb reaction with the well-known divergence and the dominance of the large impact parameters. This reaction process is no longer fast compared to the halo motion, since the Coulomb interaction acts over large distances all the way out to the adiabatic distance, outside which elastic scattering is the only possibility. The Coulomb breakup process then occurs as a relatively gentle push of the core away from its neutral companions. This excites states in the low-energy few-body continuum, possibly but not necessarily resonances. The mechanism proceeds as for the knockout process, except that the final-state positive-energy distorted wave should describe the full halo system. The occupation probabilities of these continuum states are given by the momentum transfered in the Coulomb collision.

The reaction mechanisms are very different when Coulomb or short-range interactions dominate. For nuclear halos the Coulomb interaction dominates for heavy targets and is quite insignificant for light targets. For medium-heavy targets, short- and long-range contributions may be comparable and interference phenomena occur.

The participant-spectator model provides an intuitive description of the high-energy breakup reaction mechanisms. The many observables can be semiquantitatively explained within the same model, using only two-body interaction information. This reaction model only goes beyond the few-body structure model when required by the finite size of the halo particles. Other models have so far been exploited less in comprehensive simultaneous calculations of many different observables.

B. Reaction models

The simplest Glauber model for computing total interaction cross sections is based on individual nucleon-nucleon collisions arising when target and projectile nuclear density distributions, n_t and n_p, penetrate through each other in a high-energy nucleus-nucleus collision (Karoly, 1975; Al-Khalili and Tostevin, 1996). The cross section is given by

$$\sigma_I = 2\pi \int_0^\infty [1 - T(b)] b\, db, \tag{36}$$

where $T(b)$ is the probability for no interaction for the impact parameter b. A simple folding prescription gives

$$T(b) = \exp\left(-\overline{\sigma} \int \rho_p(|\mathbf{x}|)\rho_t(|\mathbf{b}-\mathbf{x}|) d^2\mathbf{x} \right), \tag{37}$$

where $\overline{\sigma}$ is a nucleon-nucleon interaction cross section averaged over the involved neutrons and protons at the corresponding relative energy, and

$$\rho_k(b) = \int n_k(\sqrt{\mathbf{b}^2 + \mathbf{z}^2}) dz \quad \text{with} \quad k = t,p. \tag{38}$$

Parametric forms of n_t and n_p with free radial scale parameters then allow extraction of the size by fitting computations to the measured cross sections.

This procedure, which is very simple and can certainly give a semiquantitative indication of anomalies in the cross sections, has a number of shortcomings. For neutron halos the outer part of the density distribution does not have the same isotopic mixture as the core and the average $\overline{\sigma}$ value entering in the exponent is a bad approximation. The shape of the distributions are different for core and tail parts. A better averaging procedure and parametrization could cure these problems.

A deeper problem is the neglect of the few-body nature of the halo density distribution in which only the single-particle density enters to accounts for both the halo and the finite size of the constituent particles (see Takigawa *et al.*, 1992; Yabana *et al.*, 1992a, 1992b; Al-Khalili and Tostevin, 1996). This excludes effects of the very same correlations as those forming the few-body

halo structure. Therefore Eq. (37) cannot account for details such as the shadow effect arising from correlations between halo particles. Incorporating these correlations leads to smaller cross sections and larger halo radii.

These few-body Glauber models are successful in descriptions of high-energy nuclei colliding with nuclear halo systems. Improvements beyond the eikonal approximation have also been attempted by allowing deviations from straight-line trajectories (Al-Khalili *et al.*, 1997). The other main assumption, slow internal motion of the halo particles, always seems well fulfilled at least for beam energies above about 30 MeV/nucleon.

An interesting development is reported by Brooke *et al.* (1999), who treated each halo particle-target interaction independently as a function of impact parameter. The two-body problem is then solved with optical potentials. Again the frozen internal halo motion is maintained. Sufficient accuracy is found down to about 10 MeV/nucleon.

This method is most accurate for spatially extended systems, for which simultaneous interactions between two halo particles and the target can be neglected. Therefore shadowing and similar finite-size effects are not treated. The method is conceptually similar to the participant-spectator model. Application to many-body halos is formally straightforward in both cases, but the smaller sizes of such systems make the methods less accurate.

Another few-body Glauber model has successfully been used to investigate neutron halo reactions (Hencken *et al.*, 1996; Bertsch *et al.*, 1998). The basis is again the eikonal approximation and the impact-parameter picture. The two-neutron halo wave function in its rest frame after interaction with the target is given as

$$\Psi(\mathbf{r},\mathbf{R}) = S_n(\mathbf{b}_{n1}) S_n(\mathbf{b}_{n2}) S_c(\mathbf{b}_c) \Psi_0(\mathbf{r_1},\mathbf{r_2}), \tag{39}$$

where Ψ_0 is the ground-state wave function, $\mathbf{r_1}$ and $\mathbf{r_2}$ are intrinsic halo coordinates, $\mathbf{R}$ is the halo center-of-mass coordinate, and $\mathbf{b}_c$ and $\mathbf{b}_{ni}$ are impact parameters of the core and the neutrons. The functions S_c and S_n are profile functions determined during the reaction with the target. They are expressed as

$$S(\mathbf{b}) = \exp\left(-\frac{i}{\hbar v} \int V(\mathbf{b} + \zeta \hat{\mathbf{z}}) d\zeta \right), \tag{40}$$

where v is the beam velocity, $\hat{\mathbf{z}}$ is a unit vector along the beam direction, and V is the optical potential including the imaginary part and the nondiverging part of the Coulomb interaction. The differential cross sections are now obtained by projecting onto the final state specified by relative momenta between the halo particles. Total cross sections, for example, for survival of one and only one neutron in the final state, are found by integration

$$\sigma_n = 2 \int \langle [1 - |S_n(\mathbf{b_{n1}})|^2][1 - |S_c(\mathbf{b_c})|^2] |S_n(\mathbf{b_{n2}})|^2 d^2\mathbf{b_{cm}} \rangle, \tag{41}$$

where $\langle\,\rangle$ denotes the expectation value of the ground state and $\mathbf{b_{cm}}$ is the impact parameter for the halo center of mass. The integration extends over directions of $\mathbf{b_{cm}}$ perpendicular to the beam. The factor 2 is due to the two identical neutrons. Other cross sections in which more halo particles are present in the final state can be obtained by changing the absorption probability $1 - |S|^2$ into the survival probability $|S|^2$. The numerical results are qualitatively similar to those obtained in the participant-spectator model.

The time-dependent Schrödinger equation is also used in calculations of nuclear breakup of one-neutron halos (Esbensen and Bertsch, 2001). It permits the study of how important higher-order effects are and tests the eikonal approximation. Similar calculations and tests are carried out when both Coulomb and nuclear interactions contribute (Esbensen and Bertsch, 2002). The conclusion is that deviations from the eikonal approximation increase with decreasing beam energy and especially the Coulomb contribution has to be treated with care for energies below 50 MeV/nucleon.

Many more details can be found in the review of few-body reaction theories by Thompson and Suzuki (2001).

C. Participant-spectator model

The participant-spectator model provides both an intuitive geometric description of halo reactions and a number of different observables computed systematically with the same set of parameters. It is not much discussed in previous reviews and we shall therefore briefly sketch the model and its predictions. Such a sketch was given earlier by Bang and Pearson (1967). More details can be found in Garrido *et al.* (1997, 1999b). The fundamental assumption is that each halo particle interacts independently with the target. The general validity conditions are that (i) the system must be spatially extended with little overlap between the constituent particles and (ii) the reaction time must be small compared to the time scale for the relative motion. Thus the model is well suited for high-energy reactions of quantum halos when only short-range interactions are important. Furthermore, although violating (ii), the basic condition of independent two-body reactions also applies when long-range interactions only contribute significantly to one of the two-body reactions.

Let us consider three-body halos colliding with an ordinary nuclear target or with an electron. The cross section is given in Fig. 11 by the incoherent sum of the partial cross sections corresponding to all the possible scenarios. The impact parameter b separates processes in which different numbers of halo particles participate in the reaction. If b is smaller than the sum of halo particle and target radii, the corresponding two-body reaction contributes to the cross section. For larger b as in Fig. 11(d) only the long-range interaction contributes. The momentum transfer q connected to b is often more conveniently used.

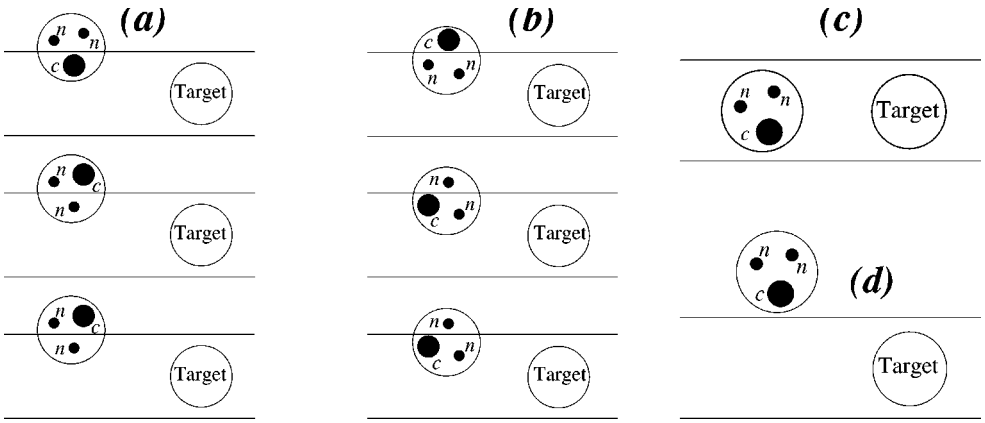

FIG. 11. The impact-parameter scenario for three-body halo collisions. The three particles labeled "n," "n," and "c" are encircled to indicate a two-neutron halo bound state. The horizontal lines indicate the interaction cylinder around the target. The particles within this cylinder are going to interact strongly with the target, e.g., in the upper left corner the core and the target collide. The number of particles within the interaction cylinder is 0, 1, 2, 3. For a core and two neutrons, either of the indistinguishable neutrons can be inside the cylinder and the two lowest sketches in columns (a) and (b) are therefore identical.

1. Model description

Let us start with collisions in which the momentum transfer to the halo is relatively large and the particles only interact pairwise in the final state after the interaction region [see Figs. 11(a) and 12]. Then the participant i can be elastically scattered or absorbed by the target, whereas j and k are the spectators continuing undisturbed in the final state. The transition amplitude $T^{(i)}$ for elastic scattering is in the center-of-mass system of the projectile given by (Garrido, Federov, and Jensen, 2001b)

$$T^{(i)}=\langle \phi^{(0i-)}_{\boldsymbol{p}'_{0i}}\phi^{(jk-)}_{\boldsymbol{p}'_{jk}}e^{i\boldsymbol{P}'\cdot\boldsymbol{R}'}|V_{0i}|\Psi e^{i\boldsymbol{P}\cdot\boldsymbol{R}}\rangle, \tag{42}$$

where Ψ is the initial three-body halo state, $\phi^{(0i-)}_{\boldsymbol{p}'_{0i}}$ and $\phi^{(jk-)}_{\boldsymbol{p}'_{jk}}$ are the distorted-wave functions of the two independent final-state two-body subsystems, and V_{0i} is the participant-target optical potential. The conjugate momenta corresponding to the relative radial coordinates specified in Fig. 12 are denoted by $\boldsymbol{p}$'s with the same indexes. The final-state momenta are denoted with primes.

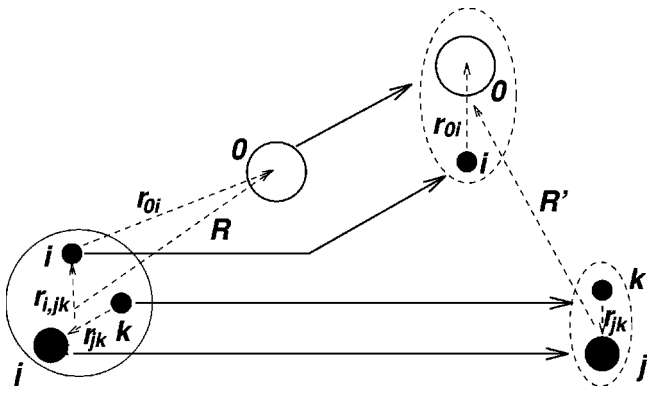

FIG. 12. The reaction scenario with two halo particles in the final state and the related coordinates.

The differential diffraction (elastic scattering) cross section is then given by (Garrido *et al.*, 1999b)

$$d^9\sigma^{(i)}_{el}=\frac{2\pi}{\hbar}\frac{1}{v}\frac{\delta(E'_{0i}-E_{0i})}{2J+1}\sum|T^{(i)}|^2 d\nu^{(i)}_f, \tag{43}$$

where $d\nu^{(i)}_f$ is the density of final states, v is the velocity of the target seen from the projectile rest frame, and $E_{0i}=p^2_{0i}/2\mu_{0i}$ and $E'_{0i}=p'^2_{0i}/2\mu_{0i}$ are the relative energies of particle i and the target in the initial and final states. When the target has spin 0 or 1/2, Eq. (43) leads to (Garrido *et al.*, 1999b)

$$\frac{d^9\sigma^{(i)}_{el}(\boldsymbol{p}'_{0i,jk},\boldsymbol{p}'_{jk},\boldsymbol{q})}{d\boldsymbol{p}'_{0i,jk}d\boldsymbol{p}'_{jk}d\boldsymbol{q}}$$
$$=\frac{d^3\sigma^{(0i)}_{el}(\boldsymbol{p}_{0i}\to\boldsymbol{p}'_{0i})}{d\boldsymbol{q}}[1-|\langle\Psi|\exp(i\,\delta\boldsymbol{q}\cdot\boldsymbol{r}_{i,jk})|\Psi\rangle|^2]$$
$$\times|M_s(\boldsymbol{p}_{i,jk},\boldsymbol{p}'_{jk})|^2, \tag{44}$$

where $\delta\boldsymbol{q}=(\boldsymbol{p}'_{i,jk}-\boldsymbol{p}_{i,jk})(m_j+m_k)/(m_i+m_j+m_k)$ is the momentum transfer into the relative motion of the interacting particle and the other two halo particles. In this expression the factor $d^3\sigma^{(0i)}_{el}(\boldsymbol{p}_{0i}\to\boldsymbol{p}'_{0i})/d\boldsymbol{q}$ is the differential cross section for elastic scattering of particle i. The second factor is the probability for excitation of the halo after transfer of the momentum $\delta\boldsymbol{q}$, introduced to remove the probability of elastic scattering of the three-body system as a whole arising from the nonorthogonality between initial and final states in Eq. (42). The third factor, $M_s(\boldsymbol{p}_{i,jk},\boldsymbol{p}'_{jk})$, is the normalized overlap between the initial three-body halo ground state and the distorted two-body final state of particles j and k.

Similarly, when particle i is absorbed by the target we obtain, in analogy to Eq. (44),

$$\frac{d^6\sigma^{(i)}_{abs}(\boldsymbol{p}'_{0i,jk},\boldsymbol{p}'_{jk})}{d\boldsymbol{p}'_{0i,jk}d\boldsymbol{p}'_{jk}}=\sigma^{(0i)}_{abs}(p0i)|M_s(\boldsymbol{p}_{i,jk},\boldsymbol{p}'_{jk})|^2, \tag{45}$$

where $\sigma^{(0i)}_{abs}$ is the absorption cross section of particle i.

When more than one halo particle simultaneously interacts, one is selected as the participant while the others are treated in the black-disk model, i.e., absorbed inside and left untouched outside the interaction cylinder. In practice this is approximated by computing the overlap function $M_s(\boldsymbol{p}_{i,jk},\boldsymbol{p}'_{jk})$ including only those parts of the initial three-body wave function in which the distances between the halo particles are consistent with the geometries of the different reactions (Garrido, Federov, and Jensen, 2001b).

The total cross sections for the processes are obtained after integration of Eqs. (44) and (45) over momentum transfer corresponding to distances smaller than the short-range interaction radii. It is important to emphasize that the participant should be chosen as the charged particle in the halo. Then nuclear and Coulomb participant-target interactions as well as interference between the particles are simultaneously included. If the charged particle is treated in the black-disk (short-range) approximation, all long-range features are omitted.

Let us now discuss small momentum transfer or large impact parameters caused by the Coulomb interaction. These cause the halo to be excited very gently and the breakup process proceeds via the three-body halo continuum states. This does not imply that three-body resonance states are the doorway states, although they very well may be. The final-state wave function is now the continuum three-body distorted wave function populated by the momentum transfer to the participant (charged halo particle) in the initial halo ground state.

For impact parameters outside the adiabatic distance b_a, only elastic scattering is possible. For this limiting distance the reaction time is comparable to the period of the relative motion of the halo particles. Furthermore, the energy transferred from target to the charged particle has to be sufficiently large to allow breakup. This corresponds to another limiting momentum transfer. In the calculation of the cross section corresponding to the reaction in Fig. 11(d) only momentum transfer larger than the largest of these two momenta should be included.

The cross section σ_C for Coulomb breakup of a two-body halo is then

$$\sigma_C=\int_{q_a}^{q_{\max}} dq\,\frac{d\sigma}{dq}P(\boldsymbol{q}m_n/m_c), \tag{46}$$

where $q_{\max}$ corresponds to the short-range interaction distance and m_n and m_c are the two masses. The probability P for breakup of the only bound state and the differential cross section are given by

$$P(\boldsymbol{k})=1-|\langle\Psi|\exp(i\boldsymbol{r}\cdot\boldsymbol{k}/\hbar)|\Psi\rangle|^2, \tag{47}$$

$$\frac{d\sigma}{dq}=\frac{8\pi}{v^2}\frac{(Z_0Z_ce^2)^2}{q^3}, \tag{48}$$

where Ψ is the halo ground-state wave function and Z_0e and Z_ce are target and core charges. The momentum $\boldsymbol{q}m_n/m_c$ is the neutral-particle momentum after collision in the center of mass of the halo system. Assuming small momentum transfer, we can expand the exponential in Eq. (47) to second order and find that

$$\sigma_C=\frac{16\pi}{3}\frac{c^2}{v^2}\frac{m_c^2}{m_n^2}\langle r^2\rangle Z_0Z_c\left(\frac{e^2}{\hbar c}\right)^2\ln\left(\frac{q_{\max}}{q_a}\right), \tag{49}$$

which is proportional to the mean-square radius of the halo. Thus a large halo implies a large Coulomb dissociation cross section (Hansen and Jonson, 1987). This Coulomb dissociation process is the dominating breakup mechanism for heavy targets. The largest contribution is from large impact parameters.

Replacing a nuclear target by electrons has the important advantage that the interaction between the electron and the nucleus is very well established. Therefore structure and reaction features are much easier to separate from each other. However, the experimental challenge is to achieve sufficient in-flight collisions of electrons and the unstable radioactive halo nuclei. These kinds of experiments are expected to be feasible in the near future.

The assumptions in the theoretical description are now better fulfilled since the electron is a pointlike particle and therefore much less likely to interact with two halo particles in the same process. For a sufficiently large momentum transfer the reaction scenario is as shown in Fig. 12, where the interaction between the electron and the participant takes place through the exchange of a virtual photon carrying the energy and momentum transfer $(\omega,\boldsymbol{q})$. This impulse approximation is especially good around the quasielastic peak, where the energy transfer is approximately equal to $q^2/2m_N$ (where m_N is the nucleon mass; Frullani and Mougey, 1984). The nine-dimensional differential electron breakup cross section is again given by Eq. (44). The corresponding differential cross section $d^3\sigma^{(0i)}/d\boldsymbol{p}'_{0i}$ has been computed assuming ultrarelativistic electrons (Garrido and Moya de Guerra, 1999, 2000).

2. Numerical results

The participant-spectator model predicts absolute values for a large number of cross sections. We use ^{6}He (^{4}He$+n+n$) and ^{11}Li (^{9}Li$+n+n$) as illustrative examples. The three-body projectile wave functions are computed with two-body interactions that reproduce the available two-body low-energy scattering data for neutron-neutron, neutron-^{4}He, and neutron-^{9}Li. The small underbinding of the three-body system is corrected by a short-range three-body interaction accounting for polarization beyond that of the two-body interactions. This fine-tuning is necessary since the correct binding energy often is decisive. Global parameters are used for the optical potentials describing the interaction between halo particles and targets (Garrido, Federov, and Jensen, 2001b).

Different processes can lead to the same reaction product, which is denoted by σ labeled by the number of surviving halo particles. The reactions can first be divided into absorption and scattering of particle i and then into small or large impact parameters for the other two particles. Small impact parameter (inside the cylin-

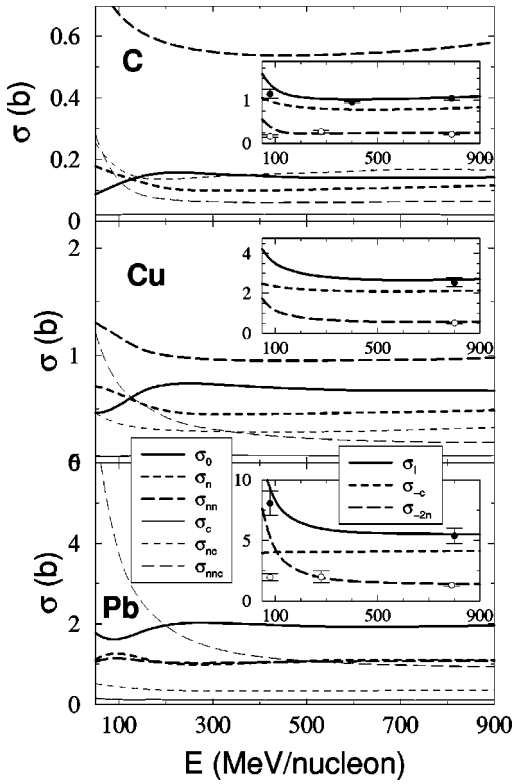

FIG. 13. Breakup cross sections as a function of beam energy for ^{11}Li breakup on C, Cu, and Pb. The inset shows $\sigma_{-2n}=\sigma_c+\sigma_{nc}+\sigma_{nnc}$, $\sigma_{-c}=\sigma_0+\sigma_n+\sigma_{nn}$, $\sigma_I=\sigma_{-2n}+\sigma_{-c}$. The experimental data are from Tanihata (1988), Kobayashi *et al.* (1989), Blank *et al.* (1993), Suzuki *et al.* (1994), Zinser *et al.* (1997), and Aumann *et al.* (1999).

der) means absorption in the black-disk model, while use of optical model probabilities also allows scattering (Garrido, Federov, and Jensen, 2001b). In this way, absorption of particle i and large or small impact parameters for both particles j and k contributes to σ_{jk} or σ_0, while one small and one large impact parameter contribute to σ_j or σ_k. Similarly, scattering of particle i contributes to σ_{ijk} (σ_i) when j and k are outside (inside) the cylinder or to σ_{ij} or σ_{ik} when one of j or k is inside and the other is outside the cylinder.

The results carry the signature of the reaction mechanisms. For light targets the nuclear interactions are dominant, while for heavy targets the Coulomb interactions predominate. Each contribution as well as the nuclear-Coulomb interference term can be computed. The cross sections for reaching the different final states consisting of the nonabsorbed particles vary with target, projectile, and beam energy (Garrido *et al.*, 2000a, 2001a); see Fig. 13. For light targets, two surviving neutrons and core absorption is most probable, while survival of all three halo particles or the core alone is least probable. For heavy targets, absorption of all three particles is most probable except at low beam energies, where simultaneous survival of all three halo particles is most probable. The smallest probability is found for survival either of the core alone or of the core and one neutron.

In the insets of Fig. 13 we observe that core destruction or absorption is more probable than two-neutron removal for all energies and targets. Core destruction receives the largest contribution for heavy targets when all halo particles are absorbed, while for light targets the noninteracting two-neutron contribution is dominant for core destruction (heavy long-dashed line in the upper part of the figure). Two-neutron removal receives for heavy targets the largest contributions from the core participant, while for light targets the largest contribution is from the noninteracting core spectator. The relative sizes of these cross sections reflect the reaction mechanisms, which in this way are open for experimental tests.

The momentum distributions are much more accurately and systematically measured than absolute cross sections. The core and neutron momentum distributions differ significantly. The final-state interactions reduce the widths of the distributions, more for the neutron than for the core because of the mass. The transverse distributions are broader than the longitudinal by 6–12 MeV/c.

The high-energy reaction mechanisms described here imply that the dominant contribution to the two-neutron removal cross section (σ_{-2n}) on a light target is absorption of one neutron, leaving the final-state neutron core system undisturbed. The reaction time is too short to allow this system to adjust its relative state during the reaction. An analysis of momentum distributions as arising from the decays of low-lying resonance states is therefore inappropriate (Garrido, Federov, Jensen, and Riisager, 2001). However, the difference can hardly be detected for ^{6}He; see Fig. 14. For ^{11}Li the resonances and virtual states used in the analysis allow good fits but with very different parameters.

The computed participant-spectator-model result reproduces the measurements as well as these fits. Nevertheless, measurement of the neutron-neutron invariant-mass spectrum arising from breakup of both ^{6}He and ^{11}Li could distinguish between the two reaction mechanisms, decay through the resonances or decay of the wave packet formed instantaneously. The decay through final-state resonances would produce the same spectrum for both halos, while the participant-spectator model would produce very different spectra; see Fig. 14.

The electron breakup processes have not yet been measured, but predictions may still be useful. The inclusive differential cross sections are again obtained by integrating over the nonmeasured variables. Leaving only the energy E_0' and momentum direction Ω_0' of the electron in the final state, we show in Fig. 15 an example of electron breakup of ^{6}He as a function of the energy transfer ω.

The longitudinal contribution is mainly due to α knockout $(e,e'\alpha)$, while the transverse component is from neutron knockout $(e,e'n)$. The total cross sections are then at forward scattering angles [Fig. 15(a), $\theta_e=60°$] and backward scattering angles [Fig. 15(b), $\theta_e=170°$] in practice fully given by the longitudinal $(e,e'\alpha)$ and the transverse $(e,e'n)$ processes, respec-

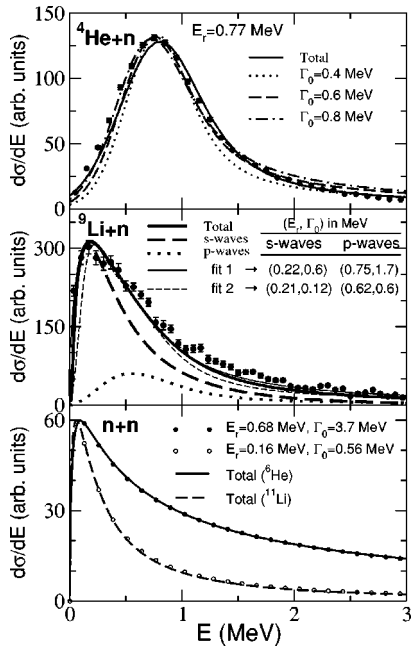

FIG. 14. Invariant-mass spectra from 300 MeV/nucleon ^{6}He and ^{11}Li on carbon. Upper part is n-^{4}He, middle part is n-^{9}Li, and bottom is n-n. The solid curves are computed and the broken lines are R-matrix fits to the data from Zinser *et al.* (1997) and Aleksandrov *et al.* (1998).

tively. In contrast to nuclear breakup, where the cross sections are fractions of barns, the absolute values are now fractions of nanobarns. Thus high-intensity beams are needed.

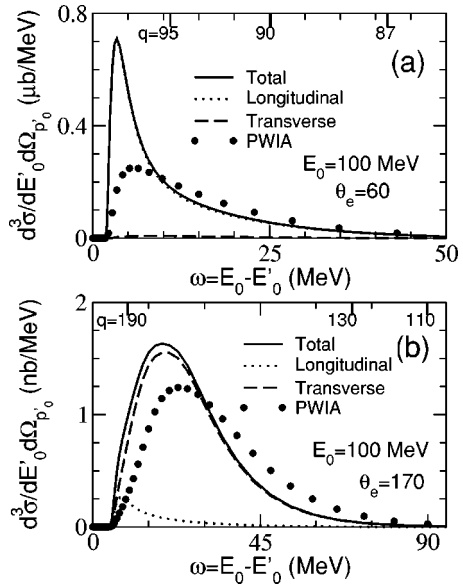

FIG. 15. Differential breakup cross section for electrons of energy $E_0 = 100$ MeV colliding with ^{6}He for (a) forward and (b) backward scattering angles: solid lines, the total cross section; fine dotted lines, the longitudinal contribution; long-dashed lines, the transverse contribution; large-dotted lines full plane-wave impulse approximation (PWIA) calculation. The momentum transfer q corresponding to different values of ω are given in MeV/c along the x axis at the top of the figure.

These results in Fig. 15 are in qualitative agreement with those of the plane-wave impulse approximation (PWIA), in which the interaction is neglected between the two halo constituents (spectators) in the final state. The differences are in general less than a factor of 3.

VI. ELECTROWEAK PROBES

The electromagnetic and weak interactions in nuclei have been studied in great detail and can for our purpose be regarded as well-understood probes of nuclear structure. This section gives an overview of how these probes are used to provide information about halo structures. For the case of electromagnetic interactions, information comes from observations of static moments of the nucleus, of electromagnetic transitions between discrete nuclear states, and of radiative capture reactions. (The important role of Coulomb dissociation in breakup reactions is treated in Sec. V, since these processes also involve the strong interactions.) For the case of weak interactions we shall consider decays involving halo states.

Well-known operators and interaction mechanisms allow one to focus more directly on the structure of the initial state and on potential uncertainties in the final-state interactions. Some disadvantages must also be mentioned: beta decay and electromagnetic transitions and moments provide only partial information on the structure, and some of the interesting information must be sought elsewhere, for instance, extracted from high-energy nuclear reactions. Still, these probes give independent and quite reliable tests of the structure and are therefore of great value.

A. Beta decay

The topic of beta decay of (or into) halo states has been reviewed recently (Nilsson *et al.*, 2000; Jonson and Riisager, 2001). We therefore refer the reader to these papers for details and concentrate on the main physics points here. The question of isospin, which often enters in connection with beta decay, is also discussed in Secs. III.B.1 and III.C.1.

Halo nuclei mainly occur close to the neutron dripline, and their beta decays will therefore typically take place on time scales below 10 ms and with Q_β values of 15–20 MeV. Beta-delayed particle emission is a prominent feature in these nuclei (Jonson and Riisager, 2001) and will complicate the experimental investigations. One of these channels, beta-delayed deuteron emission from two-neutron halo nuclei, is believed to be better described by decays directly to continuum states than by decay through intermediate states in the daughter; this process is therefore of specific interest. In essence, the two halo neutrons beta decay into a deuteron with the core as a spectator. (This picture might be developed further to include core decays; see Nilsson *et al.*, 2000.) The pattern seen in several light dripline nuclei (Borge *et al.*, 1991) with strong feeding to a state a few MeV

below the mother nucleus could be a related phenomenon; see also Jeppesen *et al.* (2002) and references therein.

As usual, the structure of the beta-decaying state can be tested through the transition strength to states of well-known structure. The overlap between the spatially extended halo wave function and a daughter state of normal size is of high interest. However, the size of the signal here is typically moderate (Riisager *et al.*, 1992) and therefore requires reliable structure calculations. An overlap effect might be seen not only in individual transitions, but also in the total half-life. That individual transitions can also give other types of information is shown by the decay of ^{11}Li to the first excited state in ^{11}Be, from which the amount of $(p_{1/2})^2$ configuration in the ^{11}Li halo can be deduced to be about 50% (see Suzuki and Otsuka, 1994 and the references in Nilsson *et al.*, 2000).

B. Electromagnetic moments and transitions

It is instructive to consider the electric multipole operator of order λ for a two-body halo system with mass numbers A_c and A for the core and the total system, and charges Z_c and Z_h for the core and halo part (Riisager *et al.*, 1992):

$$\mathcal{M}(E\lambda,\mu)=\left[Z_c e\left(\frac{A-A_c}{A}\right)^{\lambda} + (-1)^{\lambda} Z_h e\left(\frac{A_c}{A}\right)^{\lambda}\right] r^{\lambda} Y_{\lambda\mu}. \quad (50)$$

Here r is the core-halo distance. The factor r^{λ} enhances the large-distance parts, and the charge Z_h implies that electric moments and transitions are good probes for proton halos. For neutron halos the dipole moment still gives a large signal, whereas sensitivity is lost rapidly for higher moments. A similar situation holds for magnetic multipoles, the main difference being that the radial factor here is $r^{\lambda-1}$. The classic example of a halo seen in this way is ^{11}Be (Millener *et al.*, 1983), although this was not fully realized until several years later. See also the discussion by Riisager *et al.* (1992) and the following section.

The static electromagnetic moments can give important information on halo structures in an indirect way, through a comparison of their values for a two-neutron halo nucleus and the corresponding core nucleus. Since the two neutrons should couple to 0^+, the values should be the same for the two nuclei provided the halo structure really is present. One example of this is the nucleus ^{11}Li in which β-NMR spectroscopy could be used to measure the magnetic moment as well as the electric quadrupole moment (Arnold *et al.*, 1992, 1994). Measurements for one-neutron halo states are also of interest, as shown by the recent (Geithner *et al.*, 1999) measurement of the magnetic moment of ^{11}Be, which is sensitive to the detailed structure of the state.

C. Proton and neutron capture reactions

A special type of electromagnetic transition connects continuum and bound states. Radiative proton capture has been known since the early 1960s to be sensitive mainly to the outer parts of the nuclear wave function (see, for example, the references in the article of Riisager *et al.*, 1992). A very clear example is given by proton capture into the excited state in ^{17}F, treated in detail by Rolfs (1973). Radiative capture into the ground state of ^{8}B is also relevant in this respect.

Radiative neutron capture could be even more affected than proton captures. However, the corresponding experiments are much harder to do directly, and one might have to rely on Coulomb dissociation experiments instead. Although direct neutron capture reactions are relevant for the astrophysical *r* process, or rapid process, of neutron capture (Goriely, 1998), it is unlikely that halo effects play an important role there (Jensen *et al.*, 2001).

D. Multipole response

The large spatial size of halo structures goes along with an enhanced dipole response at low excitation energies. This is particularly noteworthy for nuclei in which such strength normally is found in collective states. It was noted already by Hansen and Jonson (1987) that the electric dipole energy-weighted sum rule reveals a very soft dipole mode in nuclei such as ^{11}Li. The question of electromagnetic dipole response and the closely related Coulomb dissociation reactions were reviewed earlier (Hansen *et al.*, 1995; Tanihata, 1996). Here we therefore restrict ourselves to a few references to the recent literature.

The results for electric dipole strength were soon generalized to other multipoles both through use of random-phase approximation (RPA) calculations (Fayans, 1991) and through the use of sum-rule techniques (Sagawa *et al.*, 1992). This line of theoretical work has been successfully extended to include other unstable nuclei and has been reviewed recently (Sagawa, 2001; Sagawa and Esbensen, 2001). At early stages there was some discussion of the nature of the soft dipole mode. It is now clear that it is a few-body effect not indicative of any collective features. See Catara *et al.* (1996) for a transparent explanation.

Experimentally only the E1 strength has been probed so far. The challenge is to measure the breakup into continuum states with energy resolution sufficient to resolve the soft dipole mode and with sufficient statistics. This task has only been partially accomplished. References to the recent experimental literature can be found in the articles of Meister *et al.* (2002) and Jonson (2004).

VII. SUMMARY AND CONCLUSIONS

We first gave a short history of the development leading to the by now established concept of halos. The discussion stressed the importance of the *a priori* assumption of cluster division or equivalently of the definition

of active degrees of freedom. The wave function must contain a substantial amount of this cluster structure. As soon as the principles were clarified, we formulated definitions of quantum halos and discussed the conditions under which they occur. The basic condition is that the cluster wave function extend substantially into the classically forbidden region where it essentially depends only on the cluster binding energy. This structure is universal, and scaling properties arise allowing dimensionless relations between size and energy. The halo concept thereby becomes useful in several subfields of physics.

A halo is not defined by the value of a specific discrete quantum number like strangeness. A continuum of structures from none to pronounced halos exists. The possible transitions and the intermediate structures are also interesting. In particular, the intermediate structures are sometimes rather special, like the Borromean systems and the extreme Efimov states.

After a discussion of the general properties, we presented some examples. We listed the established nuclear cases and discussed a number of halo candidates, most but not all are two- and three-body structures at the driplines. Some combinations involving strange Λ particles were seen to produce novel structures, restructuring of known systems, and extension of ordinary driplines by addition of one or more Λ particles. The energy scale allowing halos in nuclei is fractions of a MeV.

In atomic and molecular systems many combinations are possible. Clusterization is more natural for molecules than for nuclei and the structures are more pure. We discussed a number of examples characterized by the asymptotic behavior of their effective two-body interactions. The most important were the Coulomb-like $1/r$ potentials, the $1/r^2$ potentials generating Efimov states, and the $1/r^6$-induced dipole-dipole interactions. The molecular energy scale for halos is fractions of a μeV. When an electron is involved the energy scale is meV and the size remains as for molecules larger than about 10 Å.

The properties of weakly bound structures in two dimensions are different from those discussed in three dimensions. Since these geometries can be realized in both molecular and solid-state physics, we briefly reviewed the possibilities. In two dimensions traces of the three-dimensional structures remain, but the extreme Efimov states and the Thomas collapse are not present. Borromean systems are very difficult to construct, since a surface repulsive barrier seems to be required. Thus there may be many very large halos, but the extreme divergences which exist in three dimensions cannot occur.

Halo structures can be probed by reactions. Currently available high-energy beams are well suited for such investigations, because the interaction time is short compared to the intrinsic motion of the nuclear halo. Thus a snapshot can be obtained with minimal reaction dynamics involved. Still experimentally the separation of structural effects from dynamics is not complete, and reliable models are necessary. We concentrated on nuclear reactions for which many new data have become available in the last decade. We used the rather efficient geometric impact-parameter picture. This allowed a rough classification of the different breakup processes and reaction mechanisms appropriate for short-range and Coulomb long-range potentials. Similar methods for the theoretical treatment of high-energy atomic and molecular collisions are well advanced and described elsewhere.

The entanglement of initial state, reaction mechanism, and final state can to some extent be circumvented by studying decays of halo states. In decays, the quantum number of the initial state is precisely given, and the final state can be selected experimentally. Furthermore, the operator responsible for the decays is known, for example, for allowed beta decay. This cleaner mechanism offers a complementary method for the study of halos.

In conclusion, we have discussed an overall framework for descriptions of halo properties. The established facts are incorporated into a consistent picture. The formulations extract the universal features, allowing application in different subfields of physics ranging from quantum chemistry to atomic, molecular, nuclear, and particle physics. Structure and high-energy reactions are considered. Many pieces of information are still lacking and significant experimental and theoretical effort is underway to obtain more details. Large facilities around the world are being upgraded or under construction, which will contribute to an improved picture. In some cases the future directions can be predicted. Knowledge of the neutron dripline is only available for light nuclei. Heavier systems, also closer to beta stability than the dripline, are completely unexplored experimentally. It is necessary to better understand the various transitions between two-, three- and many-body structures and between independent-particle and cluster descriptions. In particular, unambiguous examples of Efimov states have still to be found. Low-energy reactions are more sensitive to the reaction mechanism and have so far not been studied. The recent availability of low-energy beams is an opportunity to study the dynamics of halo reactions. Other unexplored directions are molecular halos, two-dimensional structures, few-body (halo) effects within N-body systems, for example, in Bose-Einstein condensates, and more speculatively, the possible implications for catalysts arising from reactions within a medium and mediated by long-distance halo correlations.

REFERENCES

Abdoul-Carime, H., J. P. Schermann, and C. Desfrancois, 2002, Few-Body Syst. **31**, 183.
Adhikari, S. K., A. Delfino, T. Frederico, I. D. Goldman, and L. Tomio, 1988, Phys. Rev. A **37**, 3666.
Adhikari, S. K., A. Delfino, T. Frederico, and L. Tomio, 1993, Phys. Rev. A **47**, 1093.
Adhikari, S. K., T. Frederico, and I. D. Goldman, 1995, Phys. Rev. Lett. **74**, 487.
Ajzenberg-Selove, F., 1990, Nucl. Phys. A **506**, 1.
Ajzenberg-Selove, F., 1991, Nucl. Phys. A **523**, 1.
Aleksandrov, D., *et al.*, 1998, Nucl. Phys. A **633**, 234.

Al-Khalili, J. S., and J. A. Tostevin, 1996, Phys. Rev. Lett. **76**, 3903.
Al-Khalili, J. S., J. A. Tolstevin, and J. M. Brooke, 1997, Phys. Rev. C **55**, R1018.
Allen, B. J., and A. R. de L. Musgrove, 1978, Adv. Nucl. Phys. **10**, 129.
Amorim, A. E. A., L. Tomio, and T. Frederico, 1997, Phys. Rev. C **56**, R2378.
Andersen, L. H., D. Mathur, H. T. Schmidt, and L. Vejby-Christensen, 1995, Phys. Rev. Lett. **74**, 892.
Andersen, T., H. H. Andersen, P. Balling, P. Kristensen, and V. V. Petrunin, 1997, J. Phys. B **30**, 3317.
Arai, K., Y. Ogawa, Y. Suzuki, and K. Varga, 2001, Prog. Theor. Phys. Suppl. **142**, 97.
Arai, K., Y. Suzuki, and R. G. Lovas, 1999, Phys. Rev. C **59**, 1432.
Arai, K., Y. Suzuki, and K. Varga, 1995, Phys. Rev. C **51**, 2488.
Arnold, E., J. Bonn, A. Klein, P. Lievens, R. Neugart, M. Neuroth, E. W. Otten, H. Reich, and W. Widdra, 1994, Z. Phys. A **349**, 337.
Arnold, E., J. Bonn, A. Klein, R. Neugart, M. Neuroth, E. W. Otten, P. Lievens, H. Reich, and W. Widdra, 1992, Phys. Lett. B **281**, 16.
Audi, G., and A. H. Wapstra, 1995, Nucl. Phys. A **595**, 409.
Aumann, T., *et al.*, 1999, Phys. Rev. C **59**, 1252.
Aumann, T., *et al.*, 2000, Phys. Rev. Lett. **84**, 35.
Aziz, R. A., and M. J. Slaman, 1991, J. Chem. Phys. **94**, 8047.
Balling, P., H. H. Andersen, C. A. Brodie, U. V. Pedersen, V. V. Petrunin, M. K. Raarup, P. Steiner, and T. Andersen, 2000, Phys. Rev. A **61**, 022702.
Banerjee, P., I. J. Thompson, and J. A. Tostevin, 1998a, Phys. Rev. C **58**, 1042.
Banerjee, P., J. A. Tostevin, and I. J. Thompson, 1998b, Phys. Rev. C **58**, 1337.
Bang, J., and C. A. Pearson, 1967, Nucl. Phys. A **100**, 1.
Barranco, F., R. A. Broglia, G. Colo, and E. Vigezzi, 2001, Eur. Phys. J. A **11**, 385.
Barranco, F., R. A. Broglia, G. Gori, E. Vigezzi, P. F. Bortignon, and J. Terasaki, 1999, Phys. Rev. Lett. **83**, 2147.
Barranco, F., and E. Vigezzi, 1997, in *Proceedings of 4th Course of the International School of Heavy Ion Physics. Exotic Nuclei*, edited by R. A. Broglia and P. G. Hansen (World Scientific, Singapore), pp. 217–254.
Barnea, N., 1999a, Phys. Lett. B **446**, 185.
Barnea, N., 1999b, Phys. Rev. A **59**, 1135.
Baye, D., 1987, J. Phys. A **20**, 5529.
Baym, G., and C. Pethick, 1978, in *The Physics of Liquid and Solid Helium*, edited by K. H. Bennemann and J. B. Ketterson (Wiley, New York), Vol. II.
Bayman, B. F., S. Fricke, and Y. C. Tang, 1985, Phys. Rev. C **31**, 679.
Baz', A. I., V. I. Gol'danskiĭ, and Ya. B. Zel'dovich, 1960, Usp. Fiz. Nauk **72**, 211 [Sov. Phys. Usp. **3**, 729 (1960)].
Bedaque, P. F., H-W. Hammer, and U. van Kolck, 1999, Phys. Rev. Lett. **82**, 463.
Belyaev, V. B., A. K. Motovilov, M. B. Miller, A. V. Semyagin, I. V. Kuznetzov, Yu. G. Sobolev, A. A. Smolnikov, A. A. Klimenko, S. B. Osetrov, and S. I. Vasiliev, 2001, Phys. Lett. B **522**, 222.
Bendazzoli, G. L., S. Evangelisti, and F. Passarini, 1997, Chem. Phys. **215**, 217.
Bennaceur, K., J. Dobaczewski, and M. Ploszajczak, 2000, Phys. Lett. B **496**, 154.
Bertsch, G. F., B. A. Brown, and H. Sagawa, 1988, Phys. Rev. C **39**, 1154.
Bertsch, G. F., and H. Esbensen, 1991, Ann. Phys. (N.Y.) **209**, 327.
Bertsch, G. F., K. Hencken, and H. Esbensen, 1998, Phys. Rev. C **57**, 1366.
Bertulani, C. A., L. F. Canto, and M. Hussein, 1993, Phys. Rep. **163**, 281.
Blank, B., *et al.*, 1993, Nucl. Phys. A **555**, 408.
Bohr, A., and B. R. Mottelson, 1969, *Nuclear Structure* (Benjamin, Reading, MA), Vol. I.
Bohr, A., and B. R. Mottelson, 1975, *Nuclear Structure* (Benjamin, Reading, MA), Vol. II.
Borge, M. J. G., P. G. Hansen, L. Johannsen, B. Jonson, T. Nilsson, G. Nyman, A. Richter, K. Riisager, O. Tengblad, and K. Wilhelmsen, 1991, Z. Phys. A **340**, 255.
Bressanini, D., G. Morosi, L. Bertini, and M. Mella, 2002, Few-Body Syst. **31**, 199.
Briggs, J. S., and J. H. Macek, 1990, Adv. At., Mol., Opt. Phys. **28**, 1.
Brooke, J. M., J. S. Al-Khalili, and J. A. Tolstevin, 1999, Phys. Rev. C **59**, 1560.
Brown, B. A., 2001, Prog. Part. Nucl. Phys. **47**, 517.
Brown, B. A., P. G. Hansen, B. M. Sherrill, and J. A. Tostevin, 2002, Phys. Rev. C **65**, 061601.
Bruch, L. W., and J. A. Tjon, 1979, Phys. Rev. A **19**, 425.
Burke, P. G., 1994, Adv. At., Mol., Opt. Phys. **32**, 39.
Carlson, J., and R. Schiavilla, 1998, Rev. Mod. Phys. **70**, 743.
Catara, F., C. H. Dasso, and A. Vitturi, 1996, Nucl. Phys. A **602**, 181.
Christy, R. F., and I. Duck, 1961, Nucl. Phys. **24**, 89.
Clary, D. C., 1988, J. Phys. Chem. **92**, 3173.
Cobis, A., D. V. Fedorov, and A. S. Jensen, 1997, J. Phys. G **23**, 401.
Cobis, A., D. V. Fedorov, and A. S. Jensen, 1998, Phys. Rev. C **58**, 1403.
Cornelius, T., and W. Glöckle, 1986, J. Phys. Chem. **85**, 3906.
Cornish, S. L., N. R. Claussen, J. L. Roberts, E. A. Cornell, and C. E. Wieman, 2000, Phys. Rev. Lett. **85**, 1795.
Csótó, A., 1993, Phys. Rev. C **48**, 165.
Davids, B., S. M. Austin, D. Bazin, H. Esbensen, B. M. Sherrill, I. J. Thompson, and J. A. Tostevin, 2001, Phys. Rev. C **63**, 065806.
Demkov, Yu. N., and V. N. Ostrovskii, 1988, *Zero Range Potentials and their Applications in Atomic Physics* (Plenum, New York).
Descouvemont, P., 1995, Phys. Rev. C **52**, 704.
Desfrançois, C., 1995, Phys. Rev. A **51**, 3667.
Dobaczewski, J., I. Hamamoto, W. Nazarewicz, and J. A. Sheikh, 1994, Phys. Rev. Lett. **72**, 981.
Dobaczewski, J., W. Nazarewicz, T. R. Werner, J. F. Berger, C. R. Chinn, and J. Dechargé, 1996, Phys. Rev. C **53**, 2809.
Efimov, V. M., 1970, Phys. Lett. B **33**, 563.
Efimov, V. M., 1990, Comments Nucl. Part. Phys. **19**, 271.
Egelhof, P., for the IKAR Collaboration, 2001, Prog. Part. Nucl. Phys. **46**, 307.
Ellis, P. J., and Y. C. Tang, 1986, Phys. Rev. Lett. **56**, 1309.
Enders, J., *et al.*, 2002, Phys. Rev. C **65**, 034318.
Endt, P. M., 1990, Nucl. Phys. A **521**, 1.
Esbensen, H., 1996, Phys. Rev. C **53**, 2007.
Esbensen, H., and G. F. Bertsch, 2001, Phys. Rev. C **64**, 014608.
Esbensen, H., and G. F. Bertsch, 2002, Nucl. Phys. A **706**, 383.

Esbensen, H., G. F. Bertsch, and K. Hencken, 1997, Phys. Rev. C **56**, 3054.
Faddeev, L. D., 1961, Zh. Eksp. Teor. Fiz. **39**, 1459 [Sov. Phys. JETP **12**, 1014].
Fayans, S. A., 1991, Phys. Lett. B **267**, 443.
Fedorov, D. V., E. Garrido, and A. S. Jensen, 1995, Phys. Rev. C **51**, 3052.
Fedorov, D. V., and A. S. Jensen, 1993, Phys. Rev. Lett. **71**, 4103.
Fedorov, D. V., and A. S. Jensen, 2001a, Phys. Rev. A **63**, 063608.
Fedorov, D. V., and A. S. Jensen, 2001b, J. Phys. A **34**, 6003.
Fedorov, D. V., and A. S. Jensen, 2002, Nucl. Phys. A **697**, 783.
Fedorov, D. V., A. S. Jensen, and K. Riisager, 1993, Phys. Lett. B **312**, 1.
Fedorov, D. V., A. S. Jensen, and K. Riisager, 1994a, Phys. Rev. Lett. **73**, 2817.
Fedorov, D. V., A. S. Jensen, and K. Riisager, 1994b, Phys. Rev. C **49**, 201.
Fedorov, D. V., A. S. Jensen, and K. Riisager, 1994c, Phys. Rev. C **50**, 2372.
Fermi, E., and E. Teller, 1947, Phys. Rev. **72**, 399.
Feshbach, H., M. S. Hussein, A. K. Kerman, and O. K. Vorov, 2000, Adv. Nucl. Phys. **25**, 207.
Formanek, J., and R. J. Lombard, 1997, J. Phys. G **23**, 423.
Frederico, T., L. Tomio, A. Delfino, and A. E. A. Amorim, 1999, Phys. Rev. A **60**, R9.
Friedman, W. A., 1983, Phys. Rev. C **27**, 569.
Frullani, S., and J. Mougey, 1984, Adv. Nucl. Phys. **14**, 1.
Gadioli, E., and P. E. Hodgson, 1992, *Pre-Equilibrium Nuclear Reactions* (Oxford University, Oxford, England).
Gao, B., 1999, Phys. Rev. Lett. **83**, 4225.
Garrido, E., D. V. Fedorov, and A. S. Jensen, 1997, Phys. Rev. C **55**, 1327.
Garrido, E., D. V. Fedorov, and A. S. Jensen, 1999a, Nucl. Phys. A **650**, 247.
Garrido, E., D. V. Fedorov, and A. S. Jensen, 1999b, Phys. Rev. C **59**, 1272.
Garrido, E., D. V. Fedorov, and A. S. Jensen, 2000a, Phys. Lett. B **480**, 32.
Garrido, E., D. V. Fedorov, and A. S. Jensen, 2000b, Europhys. Lett. **50**, 735.
Garrido, E., D. V. Fedorov, and A. S. Jensen, 2001a, Phys. Lett. B **499**, 109.
Garrido, E., D. V. Fedorov, and A. S. Jensen, 2001b, Nucl. Phys. A **695**, 109.
Garrido, E., D. V. Fedorov, and A. S. Jensen, 2002, Nucl. Phys. A **700**, 117.
Garrido, E., D. V. Fedorov, A. S. Jensen, and K. Riisager, 2001, Phys. Rev. Lett. **86**, 1986.
Garrido, E., and E. Moya de Guerra, 1999, Nucl. Phys. A **650**, 387.
Garrido, E., and E. Moya de Guerra, 2000, Phys. Lett. B **488**, 68.
Geithner, W., *et al.*, 1999, Phys. Rev. Lett. **83**, 3792.
Gibson, B. F., 2001, Nucl. Phys. A **689**, 57c.
Glöckle, W., H. Witala, D. Hüber, H. Kamada, and J. Golak, 1996, Phys. Rep. **274**, 107.
Goriely, S., 1998, Phys. Lett. B **436**, 10.
Goy, J., J.-M. Richard, and S. Fleck, 1995, Phys. Rev. A **52**, 3511.
Grigorenko, L. V., B. V. Danilin, V. D. Efros, N. V. Shul'gina, and M. V. Zhukov, 1999, Phys. Rev. C **60**, 044312.
Grisenti, R. E., W. Schöllkopf, J. P. Toennies, G. C. Hegerfeldt, T. Köhler, and M. Stoll, 2000, Phys. Rev. Lett. **85**, 2284.
Guardiola, R., and J. Navarro, 2000, Phys. Rev. Lett. **84**, 1144.
Gutowski, M., K. D. Jordan, and P. Skurski, 1998, J. Phys. Chem. A **102**, 2624.
Gutowski, M., and P. Skurski, 1999, Chem. Phys. Lett. **303**, 65.
Hamamoto, I., 2001, RIKEN Rev. **39**, 129.
Hamamoto, I., S. V. Lukyanov, and X. Z. Zhang, 2001, Nucl. Phys. A **683**, 255.
Hansen, P. G., 1996, Phys. Rev. Lett. **77**, 1016.
Hansen, P. G., A. S. Jensen, and B. Jonson, 1995, Annu. Rev. Nucl. Part. Sci. **45**, 591.
Hansen, P. G., A. S. Jensen, and K. Riisager, 1993, Nucl. Phys. A **560**, 85.
Hansen, P. G., and B. Jonson, 1987, Europhys. Lett. **4**, 409.
Hansen, P. G., and B. M. Sherill, 2001, Nucl. Phys. A **693**, 133.
Hegerfeldt, G. C., and T. Köhler, 2000, Phys. Rev. A **61**, 023606.
Heller, E. J., 1996, Phys. Rev. Lett. **77**, 4122.
Hencken, K., H. Esbensen, and G. F. Bertsch, 1996, Phys. Rev. C **54**, 3043.
Hiyama, E., 1996, Phys. Rev. C **53**, 2075.
Hiyama, E., 2001, Nucl. Phys. A **691**, 107c.
Itagaki, N., S. Okabe, and K. Ikeda, 2001, Prog. Theor. Phys. Suppl. **142**, 297.
Jensen, A. S., and D. V. Fedorov, 2003, Europhys. Lett. **62**, 336.
Jensen, A. S., E. Garrido, and D. V. Fedorov, 1997, Few-Body Syst. **22**, 193.
Jensen, A. S., and K. Riisager, 1991, Phys. Lett. B **264**, 238.
Jensen, A. S., and K. Riisager, 1992, Nucl. Phys. A **537**, 45.
Jensen, A. S., and K. Riisager, 2000, Phys. Lett. B **480**, 39.
Jensen, A. S., K. Riisager, and D. V. Fedorov, 2001, Nucl. Phys. A **688**, 563c.
Jensen, A. S., K. Riisager, D. V. Fedorov, and E. Garrido, 2003, Europhys. Lett. **61**, 320.
Jensen, A. S., and M. V. Zhukov, 2001, Nucl. Phys. A **693**, 411.
Jeppesen, H., *et al.*, 2002, Nucl. Phys. A **709**, 119.
Jeukenne, J. P., A. Lejeune, and C. Mahaux, 1976, Phys. Rep. **25**, 83.
Johannsen, L., A. S. Jensen, and P. G. Hansen, 1990, Phys. Lett. B **244**, 357.
Jonson, B., and K. Riisager, 1998, Philos. Trans. R. Soc. London, Ser. A **356**, 2063.
Jonson, B., and K. Riisager, 2001, Nucl. Phys. A **693**, 77.
Jonson, B., 2004, Phys. Rep. **389**, 1.
Kanada-En'yo, Y., and H. Horiuchi, 2001, Prog. Theor. Phys. Suppl. **142**, 205.
Kanada-En'yo, Y., H. Horiuchi, and A. Ono, 1995, Phys. Rev. C **52**, 628.
Kanungo, R., I. Tanihata, and A. Ozawa, 2001, Phys. Lett. B **512**, 261.
Karoly, P. J., 1975, Phys. Rev. C **11**, 1203.
Kleinekathöfer, U., M. Lewerenz, and M. Mladenović, 1999, Phys. Rev. Lett. **83**, 4717.
Kobayashi, T., O. Yamakawa, K. Omata, K. Sugimoto, T. Shimoda, N. Takahashi, and I. Tanihata, 1988, Phys. Rev. Lett. **60**, 2599.
Kobayashi, T., *et al.*, 1989, Phys. Lett. B **232**, 51.
Koester, L., H. Rauc, and E. Seymann, 1991, At. Data Nucl. Data Tables **49**, 65.
Koonin, S. E., D. J. Dean, and K. Langanke, 1997, Phys. Rep. **278**, 1.
Korsheninnikov, A. A., *et al.*, 1994, Phys. Lett. B **326**, 31.

Landau, L. D., and E. M. Lifshitz, 1958, *Quantum Mechanics* (Pergamon, London).
Langanke, K., and G. Martínez-Pinedo, 2003, Rev. Mod. Phys. **75**, 819.
Lassaut, M., and R. J. Lombard, 1997, J. Phys. A **30**, 2467.
Lassaut, M., and R. J. Lombard, 1999, Eur. Phys. J. A **4**, 111.
LeRoy, R. J., and R. B. Bernstein, 1969, Phys. Rev. **52**, 3869.
Li, Y., and C. D. Lin, 1999, Phys. Rev. A **60**, 2009.
Li, Zhihong, Weiping Liu, Xixiang Bai, Youbao Wang, Gang Lian, Zhichang Li, and Sheng Zeng, 2002, Phys. Lett. B **527**, 50.
Lombard, R. J., 2001a, Yad. Fiz. **64**, 1315 [Phys. At. Nucl. **64**, 1240].
Lombard, R. J., 2001b, "Comparing two kinds of extended objects," preprint.
Lombard, R. J., and C. Volpe, 2002, Phys. Rev. Lett. **88**, 190402.
Lukyanov, S. M., *et al.*, 2002, J. Phys. G **28**, L41.
Lykke, K. R., R. D. Mead, and W. C. Lineberger, 1984, Phys. Rev. Lett. **52**, 2221.
Lynn, J. E., 1968, *The Theory of Neutron Resonance Reactions* (Clarendon, Oxford, England).
Marqués, F. M., *et al.*, 2001, Phys. Rev. C **64**, 061301.
McCarthy, I. E., and E. Weigold, 1988, Rep. Prog. Phys. **51**, 299.
McCarthy, I. E., and E. Weigold, 1991, Rep. Prog. Phys. **54**, 789.
Meister, M., *et al.*, 2002, Nucl. Phys. A **700**, 3.
Meng, J., and P. Ring, 1996, Phys. Rev. Lett. **77**, 3963.
Meng, J., and P. Ring, 1998, Phys. Rev. Lett. **80**, 460.
Merkuriev, S. P., 1974, Yad. Fiz. **19**, 447 [Sov. J. Nucl. Phys. **19**, 222].
Mezei, J. Zs., J. Mitroy, R. G. Lovas, and K. Varga, 2001, Phys. Rev. A **64**, 032501.
Middleton, R., and J. Klein, 1999, Phys. Rev. A **60**, 3515.
Migdal, A. B., 1972, Yad. Fiz. **16**, 427 [Sov. J. Nucl. Phys. **16**, 238].
Millener, D. J., 1997, Phys. Rev. C **55**, R1633.
Millener, D. J., J. W. Olness, E. K. Warburton, and S. S. Hanna, 1983, Phys. Rev. C **28**, 497.
Misu, T., W. Nazarewicz, and S. Åberg, 1997, Nucl. Phys. A **614**, 44.
Mitchell, G. E., J. D. Bowman, S. I. Penttilä, and E. I. Sharapov, 2001, Phys. Rep. **354**, 157.
Mitchell, G. E., J. D. Bowman, and H. A. Weidenmüller, 1999, Rev. Mod. Phys. **71**, 445.
Miyagawa, K., and W. Glöckle, 1993, Phys. Rev. C **48**, 2576.
Miyagawa, K., and W. Glöckle, 1995, Nucl. Phys. A **585**, 169c.
Mizutori, S., J. Dobaczewski, G. A. Lalazissis, W. Nazarewicz, and P. G. Reinhard, 2000, Phys. Rev. C **61**, 044326.
Moro, A. M., J. A. Caballero, and J. Gómez-Camacho, 2001, Nucl. Phys. A **695**, 143.
Moszkowski, S., S. Fleck, A. Krikeb, L. Theussl, J.-M. Richard, and K. Varga, 2000, Phys. Rev. A **62**, 032504.
Myers, W. D., and W. J. Swiatecki, 1969, Ann. Phys. (N.Y.) **55**, 395.
Myers, W. D., and W. J. Swiatecki, 1974, Ann. Phys. (N.Y.) **84**, 186.
Nakamura, T., *et al.*, 1999, Phys. Rev. Lett. **83**, 1112.
Nielsen, E., D. V. Fedorov, and A. S. Jensen, 1998a, Phys. Rev. Lett. **82**, 2844.
Nielsen, E., D. V. Fedorov, and A. S. Jensen, 1998b, J. Phys. B **31**, 4085.
Nielsen, E., D. V. Fedorov, and A. S. Jensen, 1999, Few-Body Syst. **27**, 15.
Nielsen, E., D. V. Fedorov, A. S. Jensen, and E. Garrido, 2001, Phys. Rep. **347**, 373.
Nielsen, E., H. Suno, and B. D. Esry, 2002, Phys. Rev. A **66**, 012705.
Nilsson, T., G. Nyman, and K. Riisager, 2000, Hyperfine Interact. **129**, 67.
Notani, M., *et al.*, 2002, Phys. Lett. B **542**, 49.
Nunes, F. M., A. Christley, I. J. Thompson, R. C. Johnson, V. D. Efros, 1996, Nucl. Phys. A **609**, 43.
Ostrowski, A. N., *et al.*, 1994, Phys. Lett. B **338**, 13.
Otsuka, T., N. Fukunishi, and H. Sagawa, 1993, Phys. Rev. Lett. **70**, 1385.
Otsuka, T., Y. Utsuno, R. Fujimoto, B. A. Brown, M. Honma, and T. Mizusaki, 2001, Eur. Phys. J. A **13**, 69.
Pen'kov, F. M., 1999, Phys. Rev. A **60**, 3756.
Pieper, S. C., 2002, Eur. Phys. J. A **13**, 75.
Richard, J.-M., and S. Fleck, 1994, Phys. Rev. Lett. **73**, 1464.
Riisager, K., 1994, Rev. Mod. Phys. **66**, 1105.
Riisager, K., D. V. Fedorov, and A. S. Jensen, 2000, Europhys. Lett. **49**, 547.
Riisager, K., and A. S. Jensen, 1993, Phys. Lett. B **301**, 6.
Riisager, K., A. S. Jensen, and P. Møller, 1992, Nucl. Phys. A **548**, 393.
Ring, P., 1996, Prog. Part. Nucl. Phys. **37**, 193.
Roberts, J. L., N. R. Claussen, S. L. Cornish, E. A. Donley, E. A. Cornell, and C. E. Wieman, 2001, Phys. Rev. Lett. **86**, 4211.
Robicheaux, F., 1999, Phys. Rev. A **60**, 1706.
Rolfs, C., 1973, Nucl. Phys. A **217**, 29.
Rotter, I., 1991, Rep. Prog. Phys. **54**, 635.
Sagawa, H., 2001, Prog. Theor. Phys. Suppl. **142**, 1.
Sagawa, H., and H. Esbensen, 2001, Nucl. Phys. A **693**, 448.
Sagawa, H., N. Takigawa, and N. van Giai, 1992, Nucl. Phys. A **543**, 575.
Sakurai, H., 2002, Eur. Phys. J. A **13**, 49.
Sakurai, H., *et al.*, 1997, Nucl. Phys. A **616**, 311c.
Sakurai, H., *et al.*, 1999, Phys. Lett. B **448**, 180.
Satchler, G. R., 1983, *Direct Nuclear Reactions* (Oxford University, New York), p. 58.
Schöllkopf, W., and J. P. Toennies, 1994, Science **266**, 1345.
Schöllkopf, W., and J. P. Toennies, 1996, J. Chem. Phys. **104**, 1155.
Sharma, M. M., G. A. Lalazissis, W. Hillebrandt, and P. Ring, 1994, Phys. Rev. Lett. **72**, 1431.
Siemens, P. J., and A. S. Jensen, 1987, *Elements of Nuclei* (Addison-Wesley, Redwood City, CA), Chaps. 3, 4, and 8.
Skurski, P., M. Gutowski, and J. Simons, 2000, Int. J. Quantum Chem. **80**, 1024.
Stahlhofen, A. A., 1996, J. Phys. A **29**, L581.
Sørensen, O., D. V. Fedorov, and A. S. Jensen, 2002a, Phys. Rev. Lett. **89**, 173002.
Sørensen, O., D. V. Federov, and A. S. Jensen, 2002b, Phys. Rev. A **66**, 032507.
Sugawa, Y., M. Kimura, and H. Horiuchi, 2001, Prog. Theor. Phys. **107**, 1129.
Suzuki, T., and T. Otsuka, 1994, Phys. Rev. C **50**, R555.
Suzuki, Y., T. Kido, Y. Ogawa, K. Yabana, and D. Baye, 1994, Nucl. Phys. A **567**, 957.
Takigawa, N., M. Ueda, M. Kuratani, and H. Sagawa, 1992, Phys. Lett. B **288**, 244.
Tamura, H., 2002, Eur. Phys. J. A **13**, 181.

Tanihata, I., 1988, Nucl. Phys. A **488**, 113c.
Tanihata, I., 1996, J. Phys. G **22**, 157.
Tanihata, I., H. Hamagaki, D. Hashimoto, Y. Shida, N. Yoshikawa, K. Sugimoto, O. Yamakawa, T. Kobayashi, and N. Takahashi, 1985a, Phys. Rev. Lett. **55**, 2676.
Tanihata, I., *et al.*, 1985b, Phys. Lett. B **160**, 380.
Thomas, G. C., and N. W. Tanner, 1963, Nucl. Phys. **44**, 647.
Thomas, L. H., 1935, Phys. Rev. **47**, 903.
Thompson, I. J., and Y. Suzuki, 2001, Nucl. Phys. A **693**, 424.
Tilley, D. R., H. R. Weller, and C. M. Cheves, 1993, Nucl. Phys. A **565**, 1.
Tilley, D. R., H. R. Weller, C. M. Cheves, and R. M. Chasteler, 1995, Nucl. Phys. A **595**, 1.
Tilley, D. R., H. R. Weller, and G. M. Hale, 1992, Nucl. Phys. A **541**, 1.
Tostevin, J. A., 2001, Nucl. Phys. A **682**, 320c.
Tostevin, J. A., S. Rugmai, and R. C. Johnson, 1998, Phys. Rev. C **57**, 3225.
Tosaka, Y., and Y. Suzuki, 1990, Nucl. Phys. A **512**, 46.
Tosaka, Y., Y. Suzuki, and K. Ikeda, 1990, Prog. Theor. Phys. **83**, 1140.
Utsuno, Y., T. Otsuka, T. Mizusaki, and M. Honma, 1999, Phys. Rev. C **60**, 054315.
Vallet, V., G. L. Bendazzoli, and S. Evangelisti, 2001, Chem. Phys. **263**, 33.
Vogt, E., 2002, preprint.
von Oertzen, W., 1997, Z. Phys. A **357**, 355.
Vugal'ter, S. A., and G. M. Zhislin, 1983, Teor. Mat. Fiz. **55**, 269 [Theor. Math. Phys. **55**, 493].
Weikert, H.-G., and L. S. Cederbaum, 1993, J. Chem. Phys. **99**, 8877.
Wilkinson, D. H., 1986, Nucl. Phys. A **452**, 296.
Wiringa, R. B., S. C. Pieper, J. Carlson, and V. R. Pandharipande, 2000, Phys. Rev. C **62**, 014001.
Yabana, K., Y. Ogawa, and Y. Suzuki, 1992a, Nucl. Phys. A **539**, 295.
Yabana, K., Y. Ogawa, and Y. Suzuki, 1992b, Phys. Rev. C **45**, 2909.
Young, B. M., W. Benenson, M. Fauerbach, J. H. Kelley, R. Pfaff, B. M. Sherrill, M. Steiner, and J. S. Winfield, 1993, Phys. Rev. Lett. **71**, 4124.
Yuan, J., and C. D. Lin, 1998, J. Phys. B **31**, L637.
Zelevinsky, V., 1996, Annu. Rev. Nucl. Part. Sci. **46**, 237.
Zhukov, M. V., B. V. Danilin, D. V. Fedorov, J. M. Bang, I. J. Thompson, and J. S. Vaagen, 1993, Phys. Rep. **231**, 151.
Zhukov, M. V., B. V. Danilin, L. V. Grigorenko, and J. S. Vaagen, 1995, Phys. Rev. C **52**, 2461.
Zhukov, M. V., and B. Jonson, 1995, Nucl. Phys. A **589**, 1.
Zinser, M., *et al.*, 1997, Nucl. Phys. A **619**, 151.